UNIVERSITÀ
DI PAVIA

Dipartimento di Biologia e Biotecnologie
"L. Spallanzani"

Functional characterization of Tribbles pseudokinases in gastric cancer

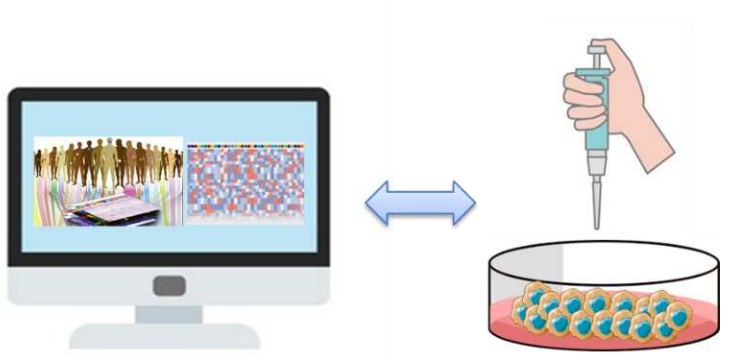

Alessia Foscarini

Dottorato di Ricerca in

Genetica, Biologia Molecolare e Cellulare

Ciclo XXXIV– A.A. 2018-2021

Table of contents

Abstract

Introduction: Gastric cancer (GC) is the fifth most common cancer and the fourth leading cause of cancer-related deaths worldwide. It is often diagnosed at advanced stages and is mostly resistant to conventional chemotherapy. To help GC management, there is a need to develop new biomarkers: they are needed to improve diagnosis, as well as novel therapeutic targets that may lead to the development of effective therapies.
TRIB2 belongs to the Tribbles family of serine/threonine pseudokinases, scaffold proteins involved in several cellular processes. In cancer, *TRIB2* can act either as an oncogene or a tumor suppressor gene, depending on the cellular context. TRIB2 also promotes drug resistance in different cancer types. Since this protein has never been investigated in GC, our study aimed at addressing the significance of TRIB2 in this tumor.

Material & Methods: We performed data mining of The Cancer Genome Atlas (TCGA) Stomach Adenocarcinoma (STAD) dataset and of the Broad Institute Cancer Cell Line Encyclopedia (CCLE) GC dataset. Based on *in silico* results, we then investigated the impact of lentiviral-mediated TRIB2 overexpression (OE) in four GC cell lines (MKN45, KATO-III, MKN74 and NCI-N87) with chromosomal instability phenotype (CIN). The impact of TRIB2 OE was evaluated by different functional assays, including cell proliferation, migration, colony formation and cell cycle analysis. Moreover, we investigated the mitogen-activated protein kinase (MAPK) downstream pathway and the possible involvement of TRIB2 in drug response, following cell treatments with two agents commonly used in GC chemotherapy (5-fluorouracil and doxorubicin).

Results: Data mining of the TCGA STAD dataset and of the CCLE dataset revealed a limited number of genetic and genomic alterations and a wide range of mRNA expression levels of *TRIBs* in GC tissues, and in GC cell lines, respectively. The analysis of *TRIBs* expression of STAD cases sorted by molecular phenotypes showed that a lower *TRIB2* mRNA expression was statistically significantly associated with tumors characterized by chromosomal instability (CIN) compared to tumors characterized by microsatellite instability (MSI). In addition, T4 stage in CIN tumors was statistically significantly associated with low *TRIB2* expression. *In vitro*, TRIB2 OE was able to reduce proliferation and colony formation ability in MKN45 and NCI-N87 cells. Furthermore, TRIB2 OE induced cell cycle arrest in G2/M phase in MKN45 cells and reduced migration ability in NCI-N87 compared to the control cells. On the other side, TRIB2 OE did not affect the MAPK pathway and no differences were detected between TRIB2-overexpressing cells and control cells treated both with 5-fluorouracil and doxorubicin.

Conclusions: Taken together, our results point to a tumor suppressor function of TRIB2 in GC with CIN phenotype. Therefore, TRIB2 may represent a novel putative biomarker in GCs characterized by chromosomal instability. Ongoing studies are assessing the expression of the TRIB2 protein in human GC samples to evaluate its potential implications for patients' stratification.

Abbreviations

GC: Gastric cancer

H. Pylori: Helicobacter Pylori

EBV: Epstein-Barr virus

IARC: International Agency for Research on Cancer

CagA: cytotoxin associated gene A

VacA: vacuolating cytotoxin A

NDMA: *N*-nitrosodimethylamine

NSAIDs: nonsteroidal anti-inflammatory drugs

SGCs: Sporadic gastric cancer

FGC: Familial gastric cancers

HGC: Hereditary gastric cancers

HDGC: Hereditary Diffuse Gastric Cancer

IGC: intestinal type gastric cancer

DGC: diffuse type gastric cancer

WHO: World Health Organization

TCGA: The Cancer Genome Atlas

CIN: chromosomal instability

SCNAs: somatic copy-number aberrations

EGFR: epidermal growth factor receptor

RTKs receptor tyrosine kinases

MSI: Microsatellite instability

MMR: Mismatch Repair

CIMP: CpG island methylator phenotype

GS: genomically stable

MSS: Microsatellite stability

SNVs: Somatic Single Nucleotide Variants

AJCC/UICC: American Joint Committee on Cancer

TNM: tumor, node, metastasis

EGD: esophagogastroduodenoscopy

EUS: Endoscopic ultrasound

MRI: magnetic resonance imaging

CT: Computed tomography

PET: position emission tomography

ESD: endoscopic mucosal dissection

ECF: epirubicin, cisplatin and fluorouracil

5FU: 5-Fluorouracil

FP: 5-Fluorouracil and cisplatin

MOC: chemoresistance

CEA: carcinoembryonic antigen

CA19-9: carbohydrate antigen 19-9

CA 72-4: carbohydrate antigen 72-4

ECS: embryonic stem cells

AML: acute myeloid leukemia

CRC: colorectal cancer

EMT: epithelial-mesenchymal transition

MET: mesenchymal-epithelial transition

ER: endoplasmic reticulum

STAD: Stomach Adenocarcinoma

CCLE: Cancer Cell Line Encyclopedia

RSEM: RNA-Seq by Expectation Maximization

TPM: transcript per million

SD: standard deviation

ACC: Adrenocortical carcinoma

BLCA: Bladder Urothelial Carcinoma

BRCA: Breast invasive carcinoma

CESC: Cervical squamous cell carcinoma and endocervical adenocarcinoma

CHOL: Cholangiocarcinoma

COAD: Colon adenocarcinoma

DLBC: Lymphoid Neoplasm Diffuse Large B-cell Lymphoma

ESCA: Esophageal carcinoma

GMB: Glioblastoma multiforme

HNSC: Head and Neck squamous cell carcinoma

KICH: Kidney Chromophobe

KIRC: Kidney renal clear cell carcinoma

KIRP: Kidney renal papillary cell carcinoma

AML: Acute Myeloid Leukemia

LGG: Brain Lower Grade Glioma

LIHC: Liver hepatocellular carcinoma

LUAD: Lung adenocarcinoma

LUSC: Lung squamous cell carcinoma

MESO: Mesothelioma

OV: Ovarian serous cystadenocarcinoma

PAAD: Pancreatic adenocarcinoma

PCPG: Pheochromocytoma and Paraganglioma

PRAD: Prostate adenocarcinoma

READ: Rectum adenocarcinoma

SARC: Sarcoma

SKCM: Skin Cutaneous Melanoma

STAD: Stomach adenocarcinoma

TGCT: Testicular Germ Cell Tumors

THCA: Thyroid carcinoma

THYM: Thymoma

UCEC: Uterine Corpus Endometrial Carcinoma

UCS: Uterine Carcinosarcoma

UVM: Uveal Melanoma

WB: western blot

GFP OE: GFP overexpression

TRIB2 OE: TRIB2 overexpression

CDC25C: Cell Division Cycle 25C

Introduction

1. Gastric cancer (GC)

The human stomach is a muscular organ responsible for the temporary storage of food and for the initial part of the digestion process. It can be divided into four sections: **the *fundus***, the upper part directly connected to the cardiac opening from the oesophagus; **the body**, or intermediate region, which is the largest portion; **the *antrum***, the lower region, directly connected to **the *pylorus***, where the stomach joins the small intestine through the pyloric sphincter.

The gastric wall is composed of 4 layers, which are, from the inside to outside (Fig. 1):

- **the *mucosa***: a mucous membrane layer, densely packed with gastric glands, which is responsible to produce the digestive enzymes. The *mucosa* contains the glands and the gastric pits, constituted by the *lamina propria* (thin layer of connective tissue) and the *muscularis mucosae* (thin layer of muscle);
- **the *submucosa***: a thin layer of dense irregular connective tissue that supports the *mucosa*;
- **the *muscularis externa***: a region of muscle adjacent to the *submucosa*;
- **the *serosa***: a smooth tissue membrane consisting of two layers of *mesothelium*, which secretes serous fluid and is separated from the *muscularis externa* by a thin layer of connective tissue (***subserosa***).

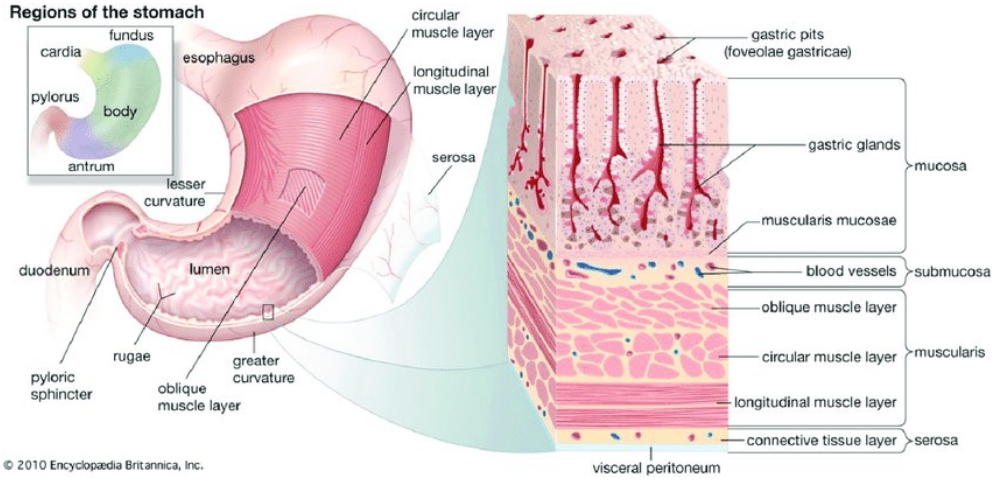

Figure 1. Human stomach anatomy: on the left, the regions of the stomach are indicated with different colors; on the right, the detailed view of the four layers that constitute the stomach wall.

Based on the tissue of origin there are four types of GC:

- **adenocarcinomas** (90-95% of cases) originate from the glandular epithelium of the gastric *mucosa*;
- **lymphomas** (5% of cases) originate from the lymphoid tissue;
- **stromal tumors** (2% of cases) originate from the connective tissue;
- **carcinoid tumors** (1% of cases) originate from the neuroendocrine system.

Given the rarity of lymphomas, stromal and carcinoid tumors, in this thesis GC refers to adenocarcinomas.

GC is a multifactorial disease, where both environmental and genetic factors can influence the insurgence and the development of the disease. Correa's model of human gastric carcinogenesis, describes the phenotypic markers, the etiological factors and the sequential stages of carcinogenesis. According to this model, the process initiates with **active chronic gastritis** due to exogenous factors (about two-thirds to three-quarters of cases are associated with the presence of *Helicobacter pylori*). The resulting gastric mucosal inflammation may lead to **chronic atrophic gastritis**. Then, the atrophy progresses to **intestinal metaplasia**, followed by **dysplasia**, and ultimately by **invasive carcinoma** (Correa, 1992).

GC is a highly aggressive malignancy with a heterogeneous clinical behavior, which represents a global health problem.

1.1 Epidemiology of GC

GC is the fifth most common cancer world-wide, with an incidence of about one million new cases every year and with 1'089'103 new cases in 2020. GC incidence rates increase with increasing age and are two-fold higher in men *versus* women (in 2020, males: 719'523, females: 369'580). Moreover, GC is the fourth most common cause of cancer mortality in both sexes worldwide, with 768'793 estimated deaths worldwide in 2020 (Sung *et al*., 2021). Globally, GC incidence and mortality are highly variable: most cases occur in Eastern Asia, Central-Eastern Europe, and South America, while a lower incidence is reported in North America and many African regions (Fig. 2A-B). Environmental factors can explain this geographic variation, including *Helicobacter pylori (H. pylori)* infection, which is the main risk factor for GC. Of relevance, highly virulent strains of *H. pylori* are found in Eastern and South-eastern Asia. However, high-income countries in these areas (Thrift & Nguyen, 2021) have shown a decline in incidence and mortality rates of the disease over the past years, possibly due to improved living conditions associated with economic development.

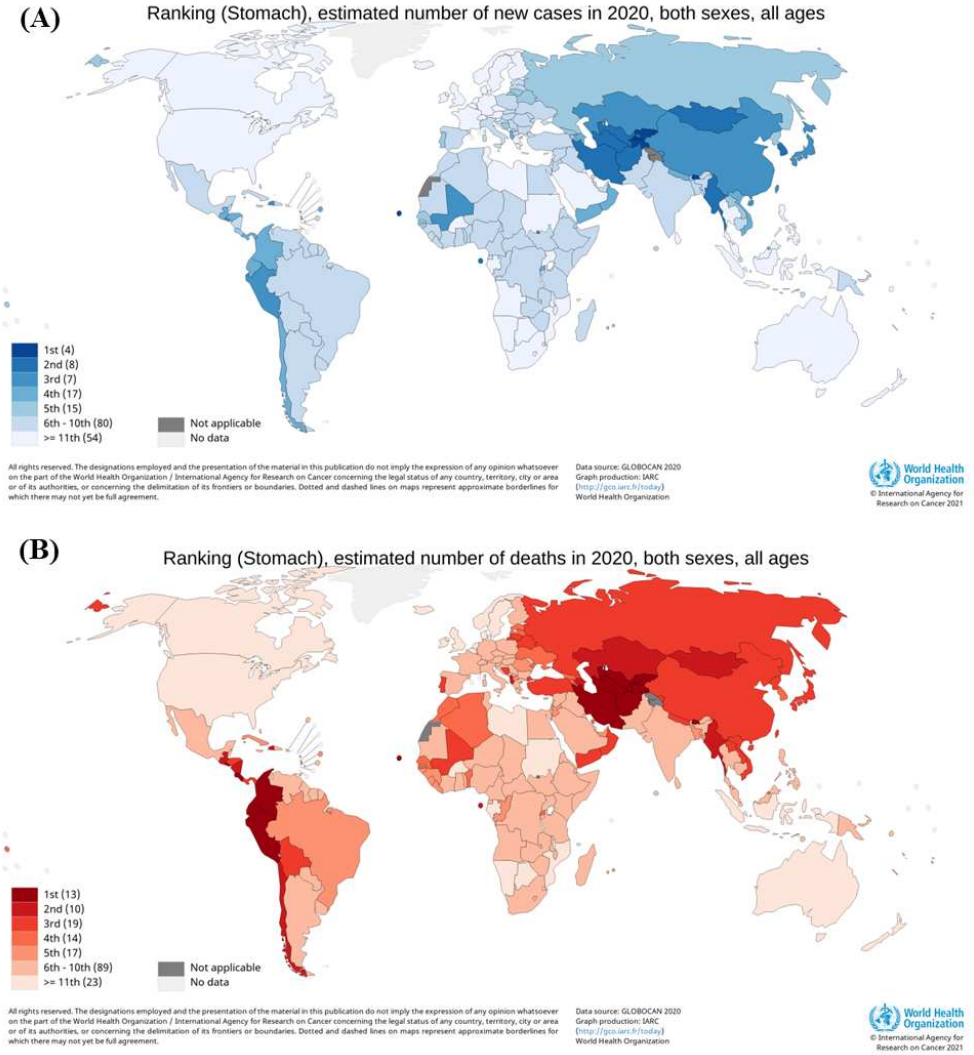

Figure 2. (A) Map shows the geographic distribution of stomach cancer incidence worldwide in 2020. **(B)** Map shows the geographic distribution of stomach cancer mortality worldwide in 2020. Data source: GLOBOCAN 2020, Graph production: IARC (http://gco.iarc.fr/today), World Health Organization.

1.2 GC risk factors

GC is a multifactorial disease, where both environmental and genetic factors can impact on the occurrence and development. *H. pylori*, Epstein-Barr virus (EBV), tobacco smoking, alcohol consumption, excess body weight and dietary factors increase the disease risk (Forman & Burley, 2006).

The association between *H. pylori* and GC was first demonstrated by Warren and Marshal in 1983, while in 1994, this Gram-negative bacterium was classified as class I carcinogen by the IARC (International Agency for Research on Cancer) Working Group on the Evaluation of Carcinogenic Risks to Humans. Afterwards, many studies confirmed that *H. pylori* is the causative agent of GC; in particular, in 2015, Plummer and collaborators, demonstrated that *H. pylori* chronic infection accounts for 89% of distal gastric cancer cases. *H. pylori* infection impairs the gastric tissue microenvironment, promoting epithelial-mesenchymal transition (ETM) and leading to GC development (Baj *et al*., 2020). The bacterial virulence factor CagA (cytotoxin associated gene A) is a well-known oncoprotein that contributes to the development of the disease, while the other major virulence factor VacA (vacuolating cytotoxin A) disrupts endolysosomal vesicular trafficking and impairs the autophagy pathway (Khatoon *et al*., 2016). Since CagA and VacA proteins have been associated with GC carcinogenesis, *H. pylori* eradication by early treatment is one of the main goals of cancer prevention.

Another risk factor is EBV, one of the most common human herpes viruses. In 1994, Imai and collaborators found a strong association between a significant proportion of GCs and EBV. The virus was then proven to be directly responsible for the tumor growth, starting from a single infected cell that proliferates and forms the tumor (Takada, 2000). On the whole, approximately 8% of GC cases harbor EBV, with 100% of carcinoma cells being EBV-positive (Thrift & Nguyen, 2021).

Many studies have shown that tobacco smoking predisposes to GC. A recent analysis of 10’290 GC cases and 26’145 controls from the Stomach Cancer Pooling Project (StoP) revealed that current smokers have 25% higher risk of GC compared with never smokers, and that increasing number of cigarettes and duration of smoking correlate with an increased risk of GC. Interestingly, GC risk is reduced with increased years of smoking cessation (Praud *et al*., 2018).

High alcohol consumption also increases the risk of GC. A meta-analysis of 56 case-control and 17 cohort studies showed that high consumption of beer and liquor, but not wine, increases GC insurgence, as demonstrated by the subgroup analysis of type of alcohol (Wang *et al*., 2017).

As reviewed by Thrift and Nguyen (2021), also obesity is associated with a modest increased risk for GC, and in particular with cardia GC. Generally, studies on dietary factors produced conflicting results: heterogeneity might reflect the influences of hereditary factors combined with dietary habits, but might also depend on whether *H. pylori* infection was considered in the study or not. For example, only certain studies demonstrated that red meat is associated with an increased risk, based on the epidemiological design of the study. The same applies to white meat, which is not significantly associated with a reduced risk in all published studies. There is, however, stronger evidence for the association between processed meat and GC risk; specifically, high processed meat consumption is associated with an increased risk for non-cardia GC. This association can be explained by the presence of *N*-nitrosodimethylamine (NDMA), a nitrosamine produced by chemical reactions of nitrates and nitrites. NDMA is used as food additive in processed meat and it is classified as potential carcinogen. Furthermore, high salt intake promotes gastric mucosa damage, hypergastrinemia and cell proliferation, and has been associate with a higher GC risk. Nevertheless, not all studies take into account the possible positive association of high prevalence of *H. pylori* infection and diets high in salt with ethnicities (Thrift & Nguyen, 2021).

On the contrary, medications, healthy dietary habits including high intake of fresh fruits and vegetables, Mediterranean diet, low-sodium diet, salt-preserved food, red and cured meat consuming, sensible alcohol drinking and maintaining a proper weight, might be associated with a reduced risk of GC (Sitarz *et al*., 2018). In addition, nonsteroidal anti-inflammatory drugs (NSAIDs) like aspirin, and statins have been proposed as possible chemiopreventive therapy (Niikura *et al*., 2020; Singh & Singh, 2013); however there are conflicting opinions regarding these drugs since their long-term use can cause severe side effects.

Overall, there are significant differences in GC incidence across the world and within ethnic/racial subgroups also in developed countries where GC incidence has significantly declined in the last decades. The cause of this decline is multifactorial and related to higher standard hygiene levels, *H. pylori* eradication, improved food conservation, and increased attention for healthy dietary habits.

1.3 Genetic classification

From a genetic point of view, GC can be divided into three groups: sporadic, familial and hereditary (Fig. 3).

Sporadic gastric cancers (SGCs): most GCs (about 90% of cases) occur sporadically, *i.e.,* they are due to a combination of factors, such as age, lifestyle, environmental triggers (including *H. pylori* or EBV infections), and multiple gene changes over time, without evidence of constitutive genetic predisposition. SGCs have a late onset (60-80 years of age) and they are mainly of the intestinal histotype.

Familial gastric cancers (FGCs) represent about 10% of all GC cases. They cluster in families, without a well-defined pattern of inheritance. FGCs are due to different combinations of low/medium-penetrance variants and environmental factors: affected members of a given family are likely to share both genetic and environmental risk factors.

Hereditary gastric cancers (HGCs) represent 1-3% of all GC cases and are due to a germline mutation in a high penetrance gene. Most HGC cases are juvenile (<40 years of age), cancers are mainly of the diffuse histotype, and the disease shows a mendelian transmission pattern. Different susceptibility genes have been reported to be associated with GC. The most common inherited condition is the Hereditary Diffuse Gastric Cancer (HDGC) syndrome which is caused by germline inactivating mutations in *CDH1* gene (OMIM *192090) encoding the E-caderine (UniProtKB - P12830) protein. E-cadherin is a homodimeric calcium-dependent transmembrane glycoprotein involved in the formation of cell-cell junctions in epithelial tissues, and in signal transduction pathways regulating cell survival and differentiation (Berx *et al*., 1995). Mutations in a second adherents junction protein, alpha-catenin (*CTNNA1* gene), have also been found in a small minority of hereditary cases (Majewski *et al*., 2013), while rare mutations in genes with high and moderate penetrance have emerged from recent NGS studies, including *BRCA2, STK11, SDHB, PRSS1, ATM, MSR1*, and *PALB2* genes (Hansford *et al*., 2015).

The HDGC syndrome associated with *CDH1* is an autosomal dominant condition, characterized by incomplete penetrance, that causes diffuse, poorly differentiated GCs with typical microscopic foci of signet ring cells. Heterozygous *CDH1* mutation carriers have 80% lifetime risk of developing diffuse GC. In addition to GC, up to 60% of female mutation carriers develop lobular carcinoma of the breast, and some carriers also develop colorectal cancer. The diffuse type stomach cancer associated with HDGC usually involves the *submucosa* and infiltrates into the stomach wall leading to the thickening of the wall, usually without producing an evident mass. For this reason, the cancer is not visible on routine upper endoscopy screening, and it is difficult to diagnose. Therefore, most cases are diagnosed at late stages, when they are advanced with a poor prognosis (Fitzgerald *et al*., 2010).

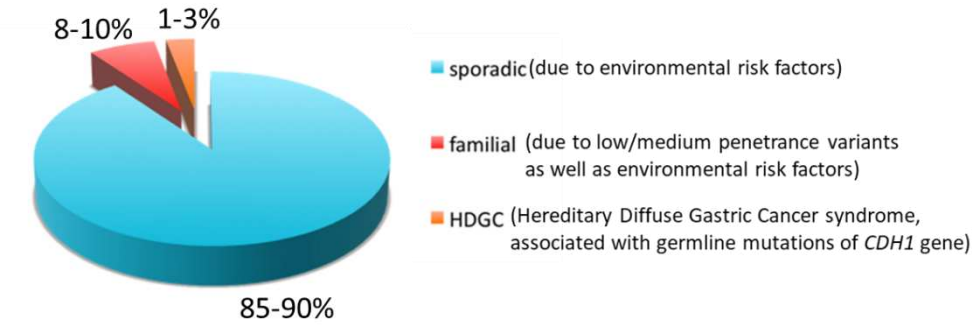

Figure 3. Genetic classification of GCs.

1.3.1 Histopathological classification

Different histopathological classifications of GC have been developed over time. The most commonly used is the one developed by Lauren in 1965 which identifies two GC subtypes (plus indeterminate type as uncommon variant) based on the structural cellular components (Lauren, 1965):

- **intestinal type gastric cancer (IGC):** is characterized by visible glands and cohesive cells. It is well-differentiated with cells describing irregular tubular structures with multiple lumens and reduced stroma (Fig. 4A). IGC is the most common type (54%), often related to *H. pylori* infection and associated with the metaplasia of the gastric mucosa;
- **diffuse type gastric cancer (DGC):** is characterized by poorly cohesive cells, diffuse and infiltrating in the gastric wall without gland formation. Discohesive cells produce mucin droplets which push the nucleus to the periphery, giving them a "signet ring" shape (Fig. 4B). DGC is less frequent than IGC (32%), and is more common among females and younger patients;
- **indeterminate-type gastric cancer**: was defined later with the aim of including also tumors with unusual histology (15%) (Hu *et al*., 2012; Machlowska *et al*., 2020).

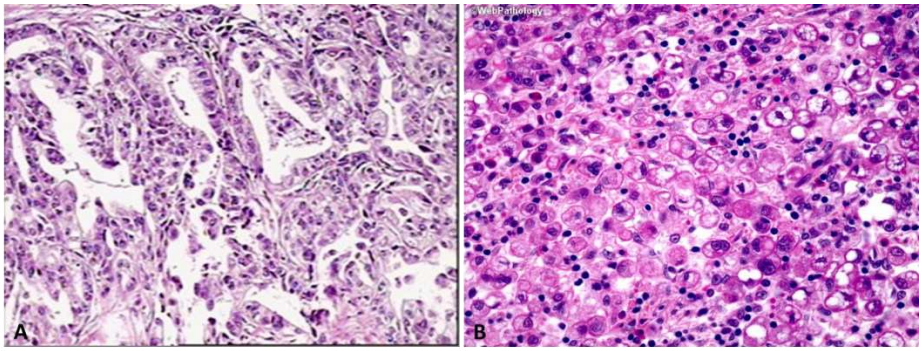

Figure 4. (A) Haematoxylin-eosin staining showing intestinal GC subtype. **(B)** Haematoxylin-eosin staining showing diffuse GC subtype.

In 2010, the World Health Organization (WHO) established a new classification, which is the most detailed among classification systems. The WHO criteria, apart from stomach adenocarcinomas, also include other types of gastric tumors (Flejou, 2011):

- **tubular adenocarcinoma:** the cancer tends to form polypoid or fungating masses and is composed of fused or branching tubules of various sizes, often with intraluminal mucus, nuclear and inflammatory debris;
- **papillary adenocarcinoma:** the cancer grows outward from the stomach wall and is characterized by epithelial projections scaffolded by a central fibrovascular core;
- **mucinous adenocarcinoma:** the cancer cells form glandular architecture and irregular cell clusters and are characterized by extracellular mucinous pools in which occasional scattered signet ring cells are floating;
- **signet ring cell carcinoma and other poorly cohesive carcinomas:** these cancers are often composed of a mixture of signet ring cells and non-signet ring cells, that can form irregular microtrabeculae or lace-like abortive glands, often accompanied by marked desmoplasia in the gastric wall and with a depressed or ulcerated surface;
- **mixed carcinoma:** the cancer is a mix of different types of adenocarcinomas.

According to the WHO classification, the most common GC subtype is tubular adenocarcinoma, followed by papillary and mucinous types. The signet ring cell carcinoma accounts for 10% of GCs and is characterized by the occurrence of signet ring cells in over 50% of the tumor. In addition to the above subtypes, this

classification also considers a series of rare histologic variants (Fig. 5) (Hu *et al*., 2012).

Table 1 Gastric adenocarcinoma classification systems

WHO (2010)	Lauren (1965)
Papillary adenocarcinoma Tubular adenocarcinoma Mucinous adenocarcinoma	Intestinal type
Signet-ring cell carcinoma And other poorly cohesive carcinoma	Diffuse type
Mixed carcinoma	Indeterminate type
Adenosquamous carcinoma	
Squamous cell carcinoma	
Hepatoid adenocarcinoma	
Carcinoma with lymphoid stroma	
Choriocarcinoma	
Carcinosarcoma	
Parietal cell carcinoma	
Malignant rhabdoid tumor	
Mucoepidermoid carcinoma	
Paneth cell carcinoma	
Undifferentiated carcinoma	
Mixed adeno-neuroendocrine carcinoma	
Endodermal sinus tumor	
Embryonal carcinoma	
Pure gastric yolk sac tumor	
Oncocytic adenocarcinoma	

Figure 5. WHO and Lauren's classifications of GCs (from Hu *et al*, 2012).

1.3.2 Molecular classification

In the past years, several molecular classifications have been proposed attempting to relate GC molecular characteristics to histological phenotypes and clinical features.

In 2014, The Cancer Genome Atlas Research Network described a comprehensive molecular evaluation of 295 primary gastric adenocarcinomas as part of The Cancer Genome Atlas (TCGA) project. With the purpose to define molecular subgroups of GCs, a molecular characterization was performed with different approaches including whole exome sequencing, array-based somatic copy number analysis,

array-based DNA methylation profiling, messenger RNA sequencing, microRNA sequencing and reverse-phase protein array analysis. Based on the results obtained, the following four subtypes can be distinguished (Cancer Genome Atlas Research, 2014):

tumors with chromosomal instability (CIN): they account for 50% of all cases, they often occur in the gastroesophageal junction/cardia, and are characterized by extended aneuploidy and chromosomal instability. These cancers show extensive somatic copy-number aberrations (SCNAs) and high frequency of *TP53* gene mutations (71%). Phosphorylation at specific residues of the epidermal growth factor receptor (EGFR) is significantly increased, together with the expression of p53 protein, consistent with a critical role of changes in EGFR and p53 mediated signaling. In addition, receptor tyrosine kinases (RTKs) amplification is also frequently observed;

tumors with microsatellite instability (**MSI)**: they represent 22% of cases and are characterized by the MSI-H status, hereafter indicated as MSI. MSI stands for microsatellite instability (*i.e*. insertions/deletions along repeated sequences), while H means that there is a high amount of instability in the tumor (*i.e.* involving a number of repeated sequences throughout the genome). MSI is the hallmark of a defective DNA Mismatch Repair (MMR) system. Accordingly, MSI tumors also show a high mutation rate and lesions in genes encoding targetable oncogenic signaling proteins, such as *PIK3CA*, *ERBB3*, *ERBB2* and *EGFR*. The epigenetic profile can display hypermethylation at the *MLH1* gene promoter and, in some cases, a specific CpG island methylator phenotype (CIMP). MSI tumors are commonly diagnosed in patients at an old age (median age of 72 years) and most often they affect women (56% of cases);

genomically stable tumors (GS) represent 20% of GC cases and are more commonly of the diffuse type. They are characterized by the absence of aneuploidy, DNA hypermethylation and sequence hypermutation, and by the presence of somatic mutations in *CDH1*, *ARID1A* and *RHOA* genes. GS tumors are commonly diagnosed at an earlier age compared to the other GC types (median age of 59 years);

Epstein–Barr virus (EBV+) positive tumors represent 9% of all GCs. EBV+ tumors exhibit extreme CIMP phenotype and are characterized by *CDKN2A* promoter hypermethylation, presence of *PIK3CA, ARID1A* and *BCOR* mutations, and recurrent amplification of the 9p24.1 locus. This region contains genes that encode proteins involved in anti-tumor immune response (PD-L1 and PD-L2). Most

EBV+ tumors develop in the gastric-fundus or body. The majority of EBV+ cases are male (81%).

Fig. 6 shows the histology and the main molecular lesions of the above subtypes and their localization in the stomach areas.

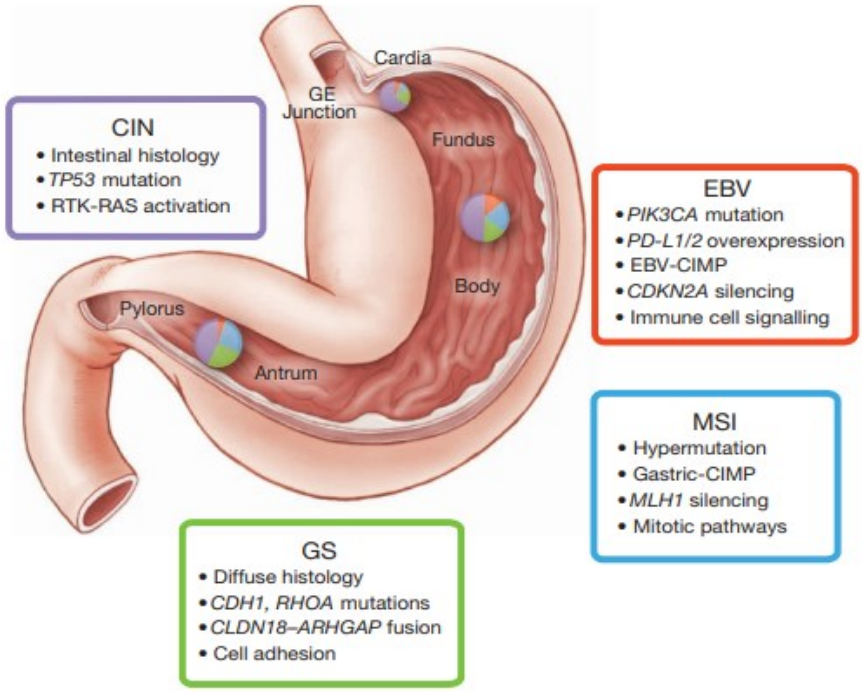

Figure 6. Key features of the four molecular subtypes of gastric cancer. Pie charts in the stomach show the relative distribution of molecular patterns with respect to cancer localization. EBV: Epstein-Barr virus; GS: genomically stable; MSI: microsatellite instability; CIN: chromosomal instability (from Cancer Genome Atlas Research, 2014).

In 2014, Wang and collaborators performed a whole-genome sequencing in 100 GCs and paired normal samples, along with DNA copy number analysis, gene expression and methylation profiling. This comprehensive analysis identified subtype-specific genetic and epigenetic lesions and unique mutational signatures. The results are summarized in Fig. 7 where circos plots show specific genetic and epigenetic lesions of the different subtypes: GCs without microsatellite instability (MSS: microsatellite stable) show a CIN phenotype with heterogeneous chromosomal rearrangements and extensive DNA demethylation; GCs with MSI

phenotype are chromosomal stable with extensive hypermethylation at different loci and a large number of somatic single nucleotide variants (SNVs); EBV-associated GCs are chromosomal stable with extensive hypermethylation.

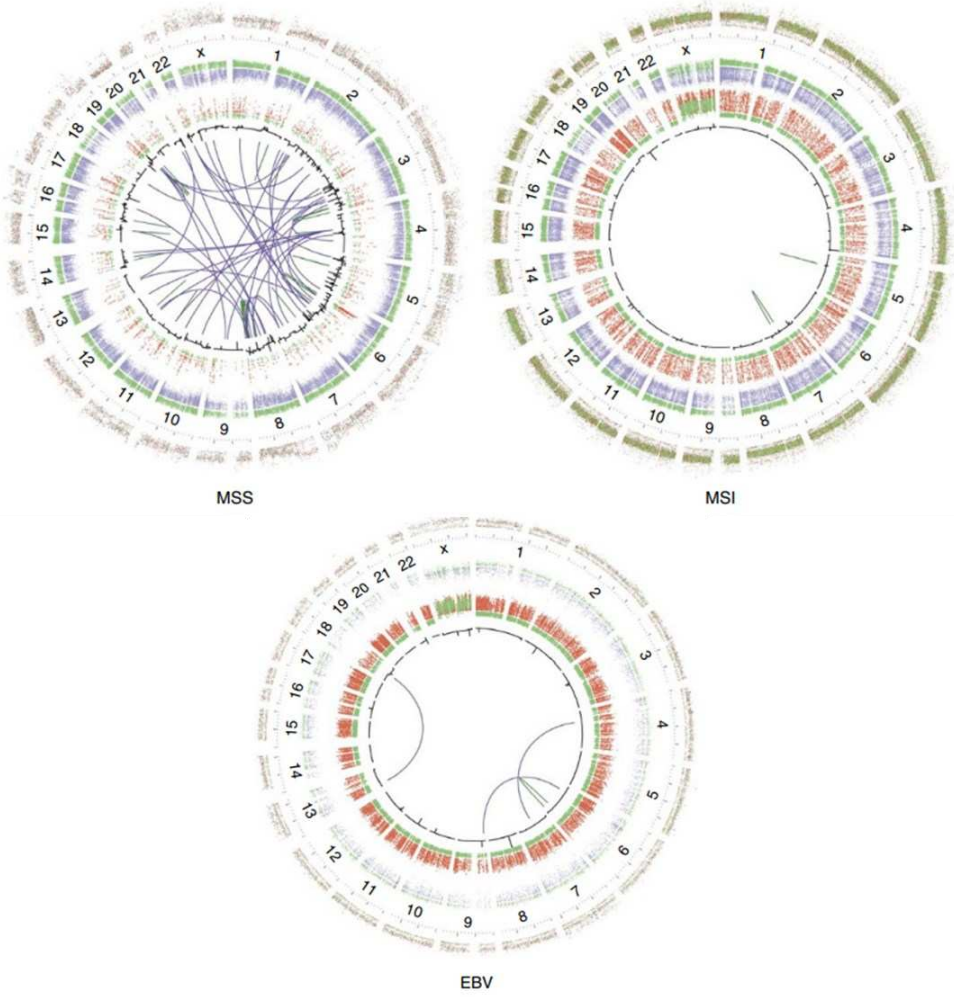

Figure 7. Genetic and epigenetic lesions in MSS, MSI and EBV GCs. The inner circle denotes somatic copy number change and chromosomal translocation; in the second circle, red dots denote the values of hypermethylated loci in tumors, and green dots denote the corresponding values in normal samples; in the third circle, blue dots denote the values of demethylated loci in tumors, and green dots denote the corresponding values in normal samples; and in the outer circle, each dot denotes one somatic SNV, colored according to the different mutation types. MSS: microsatellite stability; MSI: microsatellite instability; EBV: Epstein-Barr virus (modified from Wang *et al*., 2014).

The overlapping classifications of GCs depicted in Fig. 8 highlights that the great majority of CIN (MSS) and GS tumors are of the intestinal type (*WHO: tubular or papillary*) and of the diffuse type (*WHO: poorly cohesive or signet ring*), respectively; on the contrary, MSI and EBV+ tumors are more frequent among indeterminate-unclassifiable cases (Laurén classification).

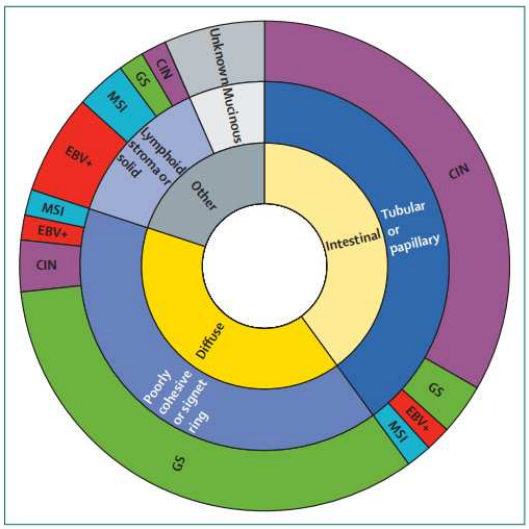

Figure 8. Graphical depiction of overlapping classifications. CIN: chromosomal unstable; GS: genomically stable; MSI: microsatellite unstable; EBV+: Epstein-Barr virus positive (from Smyth *et al.*, 2020).

1.3.3 Clinical classification

During tumor development, GC tends to invade the gastric wall and then spread to regional lymph nodes, finally generating metastases in distant organs. **Staging** is a critical step in cancer diagnosis, able to guide therapy. The most widely accepted staging follows the American Joint Committee on Cancer and International Union Against Cancer (AJCC/UICC) system which considers tumor, node and metastasis to classify the anatomic extent of disease (Amin *et al*., 2010). The **TNM** (tumor, node and metastasis) classification, that measures the extent of cancer spread, is based on the combination of three factors:

- **T** (**tumor**) describes the size of the primary tumor and the invasion of nearby tissues. It ranges from **T0**, with no evidence of primary tumor, **Tis** for the

carcinoma *in situ*, **T1** to **T4** depending on the layers invaded by the tumor [**T1** (*lamina propria* or *muscularis mucosae*), **T2** (*muscularis externa*), **T3** (*subserosa*), **T4** (*sierosa*), **TX** (*size and invasion of the primary tumor cannot be assessed*)];

- **N** (**node**) describes the involvement of the regional lymph nodes. It ranges from **N0**, when there are no metastases, to **N1, N2** and **N3** with the presence of metastases in different regional lymph nodes. **NX**: the presence of metastases in the regional lymph nodes cannot be assessed;

- **M** (**metastasis**) describes the presence of distant metastases. It ranges from **M0**, no distant metastases to **M1** where distant metastases are present. **MX**: the presence of metastases cannot be assessed.

Staging is established based on size and cancer spread.

The different stages (**0, IA, IB, IIA, IIB, IIIA, IIIB, IIIC, IV**) are assigned following the TNM classification, based on the tumor grown no further than the lining of the stomach or through the nearby lymph nodes, into the muscle of the stomach wall or within the nearby tissues and organs. The correspondence between Cancer Staging and TNM classification is reported in the following table:

STAGE	TNM
Stage 0	Tis N0 M0
Stage IA	T1 N0 M0
Stage IB	T2 N0 M0 T1 N1 M0
Stage IIA	T3 N0 M0 T2 N1 M0 T1 N2 M0
Stage IIB	T4a N0 M0 T3 N1 M0 T2 N2 M0 T1 N3 M0
Stage IIIA	T4a N1 M0 T3 N2 M0 T2 N3 M0
Stage IIIB	T4b N0-1 M0 T4a N2 M0 T3 N3 M0
Stage IIIC	T4a N3 M0 T4b N2-3 M0
Stage IV	any T any N M1

Table 1: Correspondence between Cancer Staging and TNM classification.

Tumor grading, also called Broder's classification, is a measure of cell differentiation degree. It is an indicator of how the tumor cells differ from the cells of the normal tissue they have originated from. "Well-differentiated" tumor tends to grow and spread at a lower rate than tumors that are "undifferentiated" or "poorly differentiated", which have abnormal-looking cells. Accordingly, it is a measure of tumor aggressiveness, a parameter which is different from staging, a measure of tumor spread. The most commonly grade score, recommended by the American Joint Commission on Cancer, includes 4 possible grades:

- **G1:** well-differentiated (low grade) with less than 25% undifferentiated cells;
- **G2:** moderately differentiated (intermediate grade) with less than 50% undifferentiated cells;
- **G3:** poorly differentiated (high grade) with 50-75% undifferentiated cells;
- **G4:** undifferentiated (anaplastic) with more than 75% undifferentiated cells;
- **GX:** the grade cannot be assessed.

Tumor grading, together with cancer staging, are used to evaluate each cancer patient, in order to optimize the treatment strategy and to predict prognosis.

1.4 GC diagnosis

The signs and symptoms associated with GCs include weight loss, nausea, emesis, anorexia, early satiety, dyspepsia, and epigastric pain. However, in early stages, GC is often asymptomatic; otherwise, the symptoms are vague, non-specific, consistent with gastritis or gastric ulcer disease, and often they only occur in the late stages of the disease. Physical examination is largely unrevealing in early stages since in late stages only, abdominal masses can be present. Therefore, the diagnosis of GC is usually performed by gastroscopy, with esophagogastroduodenoscopy (EGD) being the gold standard procedure. Early cancers can be detected thorough evaluation of the gastric mucosa by EGD and biopsy of suspicious lesions. Endoscopic ultrasound (EUS) can assess the depth of primary tumor invasion and identify suspected nodal metastases. Moreover, endoscopic ultrasound or magnetic resonance imaging (MRI) or radiological investigation of the abdomen are widely used to evaluate cancer penetration of the gastric wall and distant metastasis (Huo *et al*., 2014; Mocellin & Pasquali, 2015). Computed tomography (CT) scan, in

combination with position emission tomography (PET), may be useful for cancer staging in patient with advanced tumors (Rosenbaum *et al*., 2006).

Although there are several methods of analysis, GC remains one of the most difficult cancers to diagnose at an early stage. In Eastern countries, where GC is quite frequent, population-based screening programs are "affordable" in terms of cost-benefit and effective in detecting early GC cases, while in Western countries, where GC incidence is relatively low and screenings are considered too expensive, GCs are usually diagnosed at advanced stages (Johnston & Beckman, 2019).

1.5 GC therapy

GC therapy depends on the tumor stage and a multidisciplinary approach is generally required. The main treatment and the only curative option is surgery, in combination with chemotherapy, radiation therapy or immunotherapy to prevent adverse events.

The standard surgical treatment for GC is the D2 lymphadenectomy, a complete resection of the whole stomach (gastrectomy) and of the regional lymph nodes. In recent years, two new methods of minimally invasive endoscopic resection had an important impact in the surgical treatment of GC. They are: endoscopic mucosal resection and endoscopic mucosal dissection (ESD), both having lower rates of postoperative complications (Gholami *et al*., 2017). Prophylactic gastrectomy is strongly recommended for individuals at high risk of GC, such as *CDH1* gene mutation carriers. For patient with advanced GC and distant metastases, who are usually incurable, palliative resection may improve the quality of life, but it is not curative and not recommended in asymptomatic patients (Scheidbach *et al*., 2010).

Chemotherapy is performed in combination with surgery as adjuvant chemotherapy or as elective therapy when surgery is not possible, *e.g.* in presence of metastatic lesions. Neoadjuvant chemotherapy is performed before radical surgery to reduce the tumor size, while adjuvant treatment is performed after radical surgery to improve the progression free-survival. Palliative chemotherapy is recommended in patients with metastases. The most common treatment regiments in European countries are based on the MAGIC and FFCD9703 randomized trials. In the first trial, a perioperative regimen of **epirubicin**, **cisplatin** and infused **fluorouracil** (**ECF**) administrated to patients with operable gastric or lower oesophageal adenocarcinoma caused a decrease in tumor size, stage and, importantly, improved progression-free and overall survival (Cunningham *et al*., 2006). In the second trial, a combination of **5-Fluorouracil** (5FU) and **cisplatin** (**FP**) improved the disease-

free and overall survival of patients with advanced adenocarcinoma of the stomach and lower esophagus (Boige *et al*., 2007).

The most common mechanism responsible for the treatment failure is the acquisition of resistance to chemotherapy agents. There are different mechanisms of chemoresistance (MOC) that are responsible for poor response of GC to chemotherapy and consequently for lack of therapy response (Marin *et al*., 2016).

Radiation therapy uses high-energy X-rays to kill cancer cells. In the majority of cases, radiation therapy is administrated with chemotherapy (chemo-radiation) in adjuvant setting. The combination therapy improves the resectability of the tumor.

Immunotherapy is an innovative therapeutic approach that uses immune checkpoint blockade drugs that block proteins responsible for immune system escape (antiPD-1 therapy). It is now an established treatment for chemorefractory GC (cancer which has progressed after two or more lines of chemotherapy) or is indicated to treat GC cases with mismatch repair deficiency (MSI cases).

1.6 Molecular biomarkers

As above mentioned, GCs are often diagnosed at advanced stages. Furthermore, drug resistance to conventional chemotherapy can occur, leading to treatment failure. Therefore, molecular biomarkers are needed to improve a timely diagnosis, as well as novel therapeutic targets that may lead to the development of effective therapies.

To date, the traditional cancer markers for GC detection are the serum carcinoembryonic antigen (CEA), the serum carbohydrate antigen 19-9 (CA19-9) and carbohydrate antigen 72-4 (CA 72-4). Blood tests can be performed to detect tumor markers for monitor tumor growth or regression and for earlier detection of malignancies. However, the above GC markers are inadequate in terms of specificity and sensitivity, and are only beneficial in detection of late stage GC and as monitoring and prognostic tools (Kotzev & Draganov, 2018). Therefore, the identification of new biomarkers is mandatory for GC prevention and for early-diagnosis and treatment. The investigation of GC genetic signatures might represent a new approach to identify biomarkers and the studies aimed at assessing the role of new genes in GC tumorigenesis might unveil molecular targets for innovative therapies.

2. Tribbles gene family

The *Tribbles* (*TRIB*) gene family encodes a group of highly conserved serine/threonine pseudokinase proteins, which act as signalling mediators or scaffold subunits to regulate the degradation of target proteins and to modulate multiple signalling pathways. The family derives its name from the *Tribbles* gene (*Trbl*) originally identified in *Drosophila melanogaster,* where it plays a crucial role as regulator of morphogenesis, cell division, cell proliferation, cell cycle and cell migration (Grosshans & Wieschaus, 2000; Mata *et al*., 2000). Later, homologues of *Tribbles* were also found in different mammalian species, including humans (Mayumi-Matsuda *et al*., 1999; Tang *et al*., 2000; Wilkin *et al*., 1997). Three human genes were isolated by independent investigators, and they were called *TRIB1*, *TRIB2* and *TRIB3* encoding for three proteins that share the same names of the genes: TRIB1, TRIB2 and TRIB3 (Hegedus *et al*., 2007). As shown in Fig. 9, the three human *TRIB* pseudokinases are homologous to the *Drosophila Tribbles* pseudokinase, they are highly conserved and share a high percentage of identity. This is likely due to the evolution of the three mammalian genes that originated from an ancestor *TRIB2* gene by duplication events, thus leading to the acquisition of specialized protein functions and non-redundant biological roles. Of relevance, a high homology across species also exists, suggesting conserved interactions between TRIB proteins and their partners (Eyers *et al*., 2017).

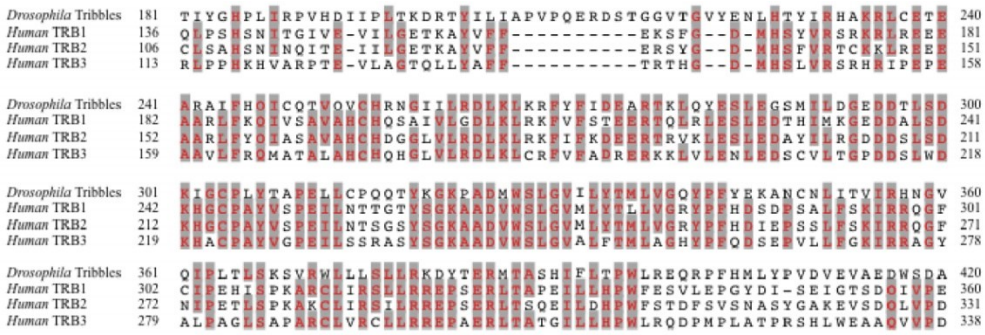

Figure 9. Drosophila *Tribbles* and its human homologs *Tribbles* family members: *TRIB1*, *TRIB2* and *TRIB3*, indicated as *TRB* (from Sakai *et al*., 2016).

2.1 TRIB proteins

TRIB proteins are classified as serine/threonine pseudokinases since they contain the substrate binding-domain of protein kinases, but they do not contain any ATP-binding site or catalytic motif essential for kinase activity (Fig. 10). Accordingly,

TRIBs play different roles in various cellular processes as scaffold or adaptor proteins, regulating the degradation of target proteins and consequently signal transduction pathways.

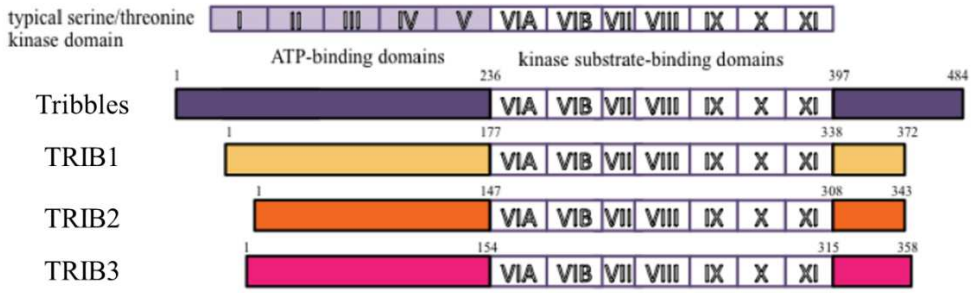

Figure 10. Schematic structure of a typical serine/threonine kinase domain and TRIB proteins domains: TRIB1, TRIB2 and TRIB3 have high homology to serine/threonine kinases but they lack ATP-binding domains and kinase-activation domains (modified from Sakai *et al*., 2016).

2.1.1 Structure of TRIB proteins

Mammalian TRIBs are three-domain proteins containing an N-terminal region, an atypical bilobed pseudokinase core and a C-terminal tail (Fig. 11).

The N-terminal region (PEST) is a predicted nuclear localization signal; this sequence varies among TRIBs (Hegedus *et al*., 2007), with slight differences being responsible for cellular localization. Indeed, TRIB1 and TRIB3 are localized in the nucleus, while TRIB2 is expressed in the cytoplasm (Bisoffi *et al*., 2004; Kiss-Toth *et al*., 2006; Wu *et al*., 2003).

The central pseudokinase domain, which lacks the canonical metal-binding amino acids (the DFG motif), is associated with a scaffold-adaptor function and is critical for cellular signalling regulation (Hua *et al*., 2011; Imajo & Nishida, 2010; Wei *et al*., 2012).

The C-terminal domain contains two conserved sequences: the ILLHPW motif, also named MEK1, targets the MEK family members and through this interaction modules the MAPK/ERK signal transduction pathway via increased ERK phosphorylation (Yokoyama *et al*., 2010); the DQLVP motif, also named COP1, drives the association with E3 ubiquitin ligase by anchoring target proteins in close

proximity to the E3 ligase for their degradation (Keeshan *et al*., 2010; Qi *et al*., 2006).

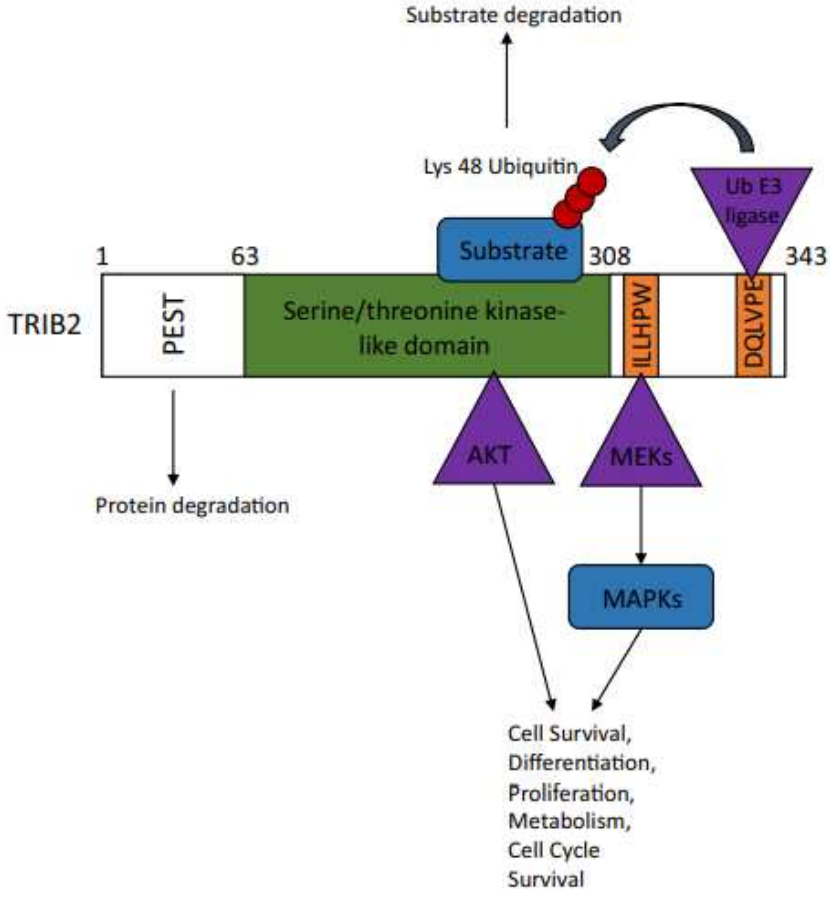

Figure 11. Structure and function of TRIB2: example of TRIB proteins (from Richmond and Keeshan, 2020).

2.1.2 Tribbles' function

As mentioned above, TRIB proteins regulate intracellular signalling through two major mechanisms. The first is to bring the substrates in close proximity to the E3 ubiquitin ligase and to control their ubiquitination, likely through a switch-like pseudokinase mechanism. The second involves a scaffolding function, which integrates and modulates signals through canonical MAPK and AKT pathways. By regulating the activity and the degradation of transcription factors, like C/EBPα, or other proteins including the MAPK family members, AKT, CDC25 or WNT/β-catenin, TRIBs exert their function as regulators of cell cycle, differentiation, cell growth, metabolism, proliferation and cell stress, with a role in both physiological and pathological conditions (Eyers *et al*., 2017; Lohan & Keeshan, 2013; Yokoyama & Nakamura, 2011).

It has been reported that the physiological functions of TRIBs include: hepatic lipogenesis (Bauer *et al*., 2015), immunoglobulin production (Simoni *et al*., 2018), pluripotency of embryonic stem cells (ECS) (Do *et al*., 2017), thermogenesis (Nakayama & Iwamoto, 2017), adipogenesis (Bezy *et al*., 2007), glucose regulation (Du *et al*., 2003), neuronal apoptosis/autophagy (Saleem & Biswas, 2017) and lipid metabolism (Qi *et al*., 2006). Among these processes, haematopoiesis is an interesting example of the multifaceted function of Tribbles: different expression of the three proteins have been observed in the various haematopoietic cell lineages, highlighting a non-redundant and lineage-specific function for each TRIB protein during the normal hematopoietic cell differentiation (Salome *et al*., 2018). Of relevance, Sung and collaborator (2006) reported that the expression of all members of the human gene family is dynamically controlled and cell-type dependent in response to inflammatory stimulation, suggesting that regulation of TRIB levels plays an important role in cell-type specific cellular responses.

Considering many physiological processes in which TRIB proteins take part, it is not surprising that their dysregulation is involved in different pathological processes. Several studies have demonstrated the association of TRIB proteins with a series of human diseases, including diabetes (Prudente *et al*., 2009), lipid disorders (Kathiresan *et al*., 2008), cardiovascular diseases (Willer *et al*., 2008), autoimmune pathology (Zhang *et al*., 2005), neurological disorders (Aime *et al*., 2015) and cancer (Richmond & Keeshan, 2020).

2.2 Tribbles in cancer

In last years, many studies demonstrated that Tribbles play a role in several types of cancers. In particular, their expression varies among cancer subtypes and current knowledge indicates that TRIBs behave either as oncogenes or tumor-suppressors, depending on the cellular context (Richmond & Keeshan, 2020). For instance, TRIB2 confers resistance to anti-cancer therapy in melanoma via direct interaction with AKT, a key signalling protein in cell proliferation, survival and metabolism. Moreover, TRIB2 expression is significantly increased in tumor tissues from melanoma patients correlating with a poor clinical outcome (Hill *et al*., 2017). In contrast, TRIB3 has been reported to have a tumor-suppressive role: its loss promotes AKT-driven tumorigenesis via FOXO inactivation, and associates with a more aggressive tumor phenotype *in vitro* and *in vivo* (Salazar *et al.,* 2015). In general, the three proteins can play different roles in several cancers: TRIB1 is involved in prostate cancer (Lin *et al*., 2014), glioma (Tang *et al*., 2015), ovarian (Puiffe *et al*., 2007) and thyroid cancers (Puskas *et al*., 2005); TRIB2 in melanoma (Hill *et al*., 2015), lung (Grandinetti *et al*., 2011), and liver cancers (Wang *et al*., 2013), acute leukaemia (Keeshan *et al*., 2006) and glioblastoma (Wang *et al*., 2020); and TRIB3 in lung (Zhou *et al*., 2013), breast (Wennemers *et al*., 2011), renal (Hong *et al*., 2019), liver (Wang *et al*., 2020), and ovarian cancers (Wang *et al*., 2020), retinoblastoma (Bao *et al*., 2021), and glioblastoma (Tang *et al*., 2015). Interestingly, all TRIB members have a role in gastrointestinal tumors, including colorectal cancer (CRC) and GC.

TRIB protein expression has been proposed as biomarker in different types of cancers. In particular, advances in knowledge of the role of Tribbles in cancer have established these proteins as valuable biomarkers for diagnosis, prognosis, and prediction of therapeutic response. The best-known example is TRIB2 in acute myeloid leukemia (AML): O'Connor and collaborators (2018) demonstrated that in AML cell lines an elevated TRIB2 protein expression correlates with a high expression of the anti-apoptotic BCL-2 protein, which drives tumor survival and chemoresistance. These cells were highly sensitive to BCL-2 inhibitors and there was a synergistic effect between high TRIB2 and BCL-2 expression and treatment with chemotherapy agents. Interestingly, the co-expression of TRIB2 and BCL-2 was directly found in ~ 25% of primary patient samples, suggesting that TRIB2 expression has clinical and biological relevance, helping to stratify AML patients in view of specific treatments.

2.2.1 Tribbles in gastrointestinal tumors: novel findings

From 2003 to date, an increasing number of papers have been published on CRC describing different functions of TRIB proteins in this cancer type. Ferreira and collaborators (2021) presented a comprehensive timeline describing what is known about the putative role of each TRIB protein in CRC: as is evident from their scheme (Fig. 12), most of the studies have been published in the last six years and the majority of papers are focused on TRIB3.

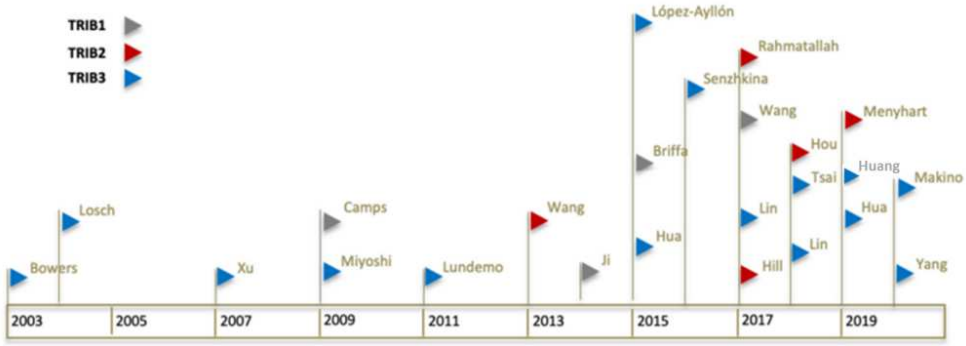

Figure 12. Chronological representation of significant publications on Tribbles in CRC, from 2003 to 2020. Each publication is represented by the first author last name and a colored flag symbol. Each TRIB protein is represented by a different color (modified from Ferreira *et al*., 2021).

The most recent papers identify *TRIB2* as a potentially druggable gene in CRC, where its mRNA levels correlate with worse survival outcome (Menyhart *et al*., 2019). High *TRIB3* expression levels also correlate with low overall survival and represent a potential prognostic biomarker (Huang & Pan, 2019). In addition, Hua and collaborators (2019) demonstrated that, in colorectal cancer cells, TRIB3 interacts with β-catenin and TCF4, and increases the expression of genes that are associated with cancer stem cell proliferation. It is well known that the constitutive activation of the Wnt signalling pathway through β-catenin accumulation is crucial for CRC development. Accordingly, high *TRIB3* expression levels correlate with lower survival rates and poor outcomes of CRC patients. The epithelial to mesenchymal transition (EMT) is associated with a more invasive or metastatic CRC phenotype: interestingly, Makino and collaborators (2020) showed that the down-regulation of *TRIB3* in colorectal cancer cell lines lead to the reverse mesenchymal-epithelial transition (MET) phenotype. On the whole, the analysis of the association between gene expression and clinical features in CRC cases from the TCGA (The Cancer Genome Atlas) dataset, allowed *TRIB3* and immune-related genes to be classified as a biomarker for CRC prognosis (Yang *et al*., 2020).

GC has been less investigated than CRC in relation to TRIB proteins expression, and there are a few studies on this topic. Wu and collaborators (2013) in an attempt to evaluate the effect of Clopidogrel on GC cells, found that *CHOP* and *TRIB3* were up-regulated in a concentration and time-dependent manner following drug treatment and this was related to the induction of cell stress and apoptosis. Moreover, in human GC cells, upon endoplasmic reticulum (ER) stress, TRIB3 is triggered by VacA (the *H. pylori* vacuolating cytotoxin) and TRIB3 knockdown decreases VacA induced cell death (Zhu *et al*., 2017). In GC samples, TRIB3 overexpression appears to be associated with tumor angiogenesis and poor prognosis: accordingly, TRIB3 can be considered a potential target for anti-angiogenic therapy (Dong *et al*., 2016). TRIB3 also plays an anti-apoptotic role in doxorubicin-treated GC cell lines and its downregulation promotes cell death and enhances doxorubicin-induced apoptosis: this correlation between TRIB3 expression and response to anticancer drugs indicates that the protein is relevant in predicting therapy efficacy (Wu *et al*., 2017). Recently, based on information in TCGA, *TRIB3*, together with nine other genes, has been selected to form a risk assessment panel for GC prognosis, to improve patients' stratification, when combined with other clinical indicators (Sun *et al*., 2020).

So far, there is one only study on TRIB2 in GC, reporting that the protein level in MGC-803 cells is downregulated following treatment with the Dioscin anti-cancer agent (Zhao *et al*., 2016).

Aim of the work

Aim of the work

Gastric cancer (GC) is a high aggressive malignancy that represents a major health problem. The main issue of GC is late diagnosis: tumors are often asymptomatic or with non-specific symptoms and the presence of an abdominal mass is usually diagnosed during late stage of the disease. Moreover, no effective therapies have been found for GC and drug resistance to conventional chemotherapy is the main cause for treatment failure. The currently used GC biomarkers are inadequate in terms of specificity and sensitivity, and are only beneficial in detection of late stage GC and as monitoring and prognostic tools. Therefore, the identification of new biomarkers is mandatory for cancer prevention and early diagnosis, as well as the identification of new molecular targets for innovative therapies.

The *Tribbles (TRIBs)* gene family encodes a group of highly conserved psuedokinase proteins named TRIB1, TRIB2 and TRIB3, which act as scaffold or adaptor proteins, regulating the degradation of target proteins involved in signal transduction pathways. In cancer, TRIBs pseudokinases have been shown to play multifactorial roles and current knowledge indicates both oncogenic and tumor suppressive functions, depending on family member and on cellular context. Some studies investigated their function in gastrointestinal tumors: in colorectal cancer, TRIBs have been extensively studied and defined as novel markers for this tumor type; on the contrary, their relevance and their role in GC remain largely unexplored.

First aim of this work was to investigate the pattern of genetic and genomic alterations and the mRNA expression profile of *TRIB* genes in GC tissues and cell lines by an ***in silico*** approach. For this purpose, we performed data mining of the Stomach Adenocarcinoma (STAD) TCGA dataset and the Broad Institute Cancer Cell Line Encyclopedia GC dataset.

Second aim of this work was to investigate the possible involvement of *TRIB2* in gastric cancer by using an ***in vitro*** model of GC. To achieve this goal, we investigated the impact of lentiviral-mediated TRIB2 overexpression in four GC cell lines (MKN45, KATO-III, MKN74 and NCI-N87) by performing different functional assays (cell proliferation, migration and colony formation assays, and cell cycle analysis). This *in vitro* approach also offered the opportunity to explore downstream pathways that are possibly perturbated by changes in TRIB2 protein expression and to investigate the role of TRIB2 in drug response, following cells treatment with chemotherapeutic agents.

Materials and methods

1. Bioinformatics analysis

For the *in silico* analysis, we performed the data mining of The Cancer Genome Atlas (TCGA) dataset - Stomach Adenocarcinoma (STAD) dataset publicly available on the cBio Cancer Genomics Portal (v3.6.9; 03/21) and on the UALCAN web resource. We also investigated the transcriptomic profiles of a panel of gastric cancer cell lines available on the Cancer Cell Line Encyclopedia (CCLE, update 25/03/21) database.

1.1 cBio Cancer Genomics Portal

The cBio Cancer Genomics Portal (cBioPortal, *http://cbioportal.org*) is an open-source software system that provides intuitive visualization, download and analysis of public large-scale cancer genomics datasets in the context of clinical data and biologic pathways (Fig. 1). The software was developed by the Dana-Farber Cancer Institute, the Memorial Sloan-Kettering Cancer Center, the Princess Margaret Cancer Centre, the Children's Hospital of Philadelphia and the Hyve in 2012 (Cerami *et al*., 2012; Gao *et al*., 2013).

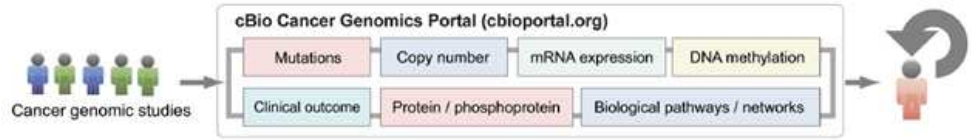

Figure 1: The cBioPortal: an open platform for interactively exploring multidimensional cancer genomics datasets in the context of clinical data and biologic pathways (from Cerami *et al*, 2012).

In particular, cBioPortal provides access to the most comprehensive catalogue of genetic, epigenetic, transcriptomic, proteomic and clinical data including the TCGA *Pan-Cancer Atlas (PanCanAtlas)* program data (*https://www.cancer.gov/about-nci/organization/ccg/research/structural-genomics/tcga*). Briefly, the TCGA is a landmark cancer genomics program launched in 2006 by the National Cancer Institute and the National Human Genome Research Institute with the aim to provide an accurate molecular and clinical characterization of over 20,000 primary cancers and matched normal samples for 33 cancer types.

First, we performed a cross-cancer query to evaluate the type and frequency of the genetic and genomic alterations of the *Tribbles* genes in 10976 patients across 33

tumor types included in the TCGA *PanCanAtlas.* The data mining was performed according to the below options:

- select "TCGA *PanCancer Atlas studies"* from the *quick select menu*;
- select "*Query by genes*" and enter the HUGO gene symbol of *TRIB1, TRIB2* and *TRIB3* in the query box;
- select "*mutations*", "*structural variant*" and "*copy number alterations"* from the "*Select Molecular Profiles*" menu;
- enter the HUGO gene symbol of the gene set of interest: *TRIB1, TRIB2* and *TRIB3* in the "*User-defined List*" box.

We also evaluated the type and frequency of the genetic and genomic alterations of the *Tribbles* in the stomach cancer dataset, following the procedure describe above and selecting the "*Stomach Adenocarcinoma (STAD, PanCancer Atlas)*" from the *quick select menu*. Next, we generate a series of reports, including a graphical summary, called OncoPrint, showing the genetic and genomic alterations across all the patients included in the dataset selected (*e.g.* TCGA *PanCancer Atlas studies* or *STAD, PanCancer Atlas*) and a graph showing the distribution of point mutations across TRIBs protein domains from the Pfam database (Mistry *et al*., 2020).

Second, we downloaded and investigated the gene expression data (RNA-seq, RSEM) of *Tribbles* genes in 412 patients from the TCGA STAD *PanCanAtlas* dataset according to the below options:

- select the study of interest from the *query menu*: "*Stomach Adenocarcinoma (TCGA, PanCanAtlas)"*;
- select the genes of interest (*TRIB1, TRIB2* and *TRIB3)* from the "*Query by genes*" box ;
- select *"Samples with mRNA data (RNA Seq V2*)" from the *"Patient/Case Set"* menu*;*
- select "*mRNA Expression"* from the "*Select Molecular Profiles*" menu;
- select the reference populations to normalize the mRNA expression data:
    - *mRNA expression z-scores relative to all samples (log RNA Seq V2 RSEM)*
    - *mRNA expression z-scores relative to normal samples (log RNA Seq V2 RSEM)*

The RNASeqV2 is processed and normalized using RSEM (RNA-Seq by Expectation Maximization), an user-friendly software package for quantifying gene and isoform abundances from single-end or paired-end RNA-Seq data (Li &

Dewey, 2011). cBioPortal computes the relative mRNA expression of an individual gene in a tumor sample to the gene's expression distribution in a reference population of samples (*e.g.* all profiled tumor samples or normal samples). The value obtained from this computation is expressed in z-score of mRNA expression which indicates the number of standard deviations away from the mean of expression in the reference population (z-score). The z-score can be calculated as:

$$Z = \frac{r - \mu}{\sigma}$$

where r corresponds to the value of the raw data, μ corresponds to the mean and σ corresponds to the standard deviation of all samples in the reference population.

For a gene of interest, the z-score value is 0 at the mean; a z-score above the mean indicates an over-expression; a z-score below the mean indicates an under-expression.

In this study, we normalize the mRNA expression of *Tribbles* to all samples or to normal samples. For each *TRIB*, the 412 STAD samples were divided in quartiles based on the expression levels (log RNA Seq V2 RSEM) using the *INC.QUARTILE* function of the Excel software. We indicated with "high-25" the top quartile which includes the cases with highest *TRIBs* expression; with "low-25" the bottom quartile which contains the cases with lowest *TRIB*s expression. "Others" indicates the cases with an intermediate and low *TRIB*s expression and included the second, third and fourth quartiles. For each gene, we performed the two comparisons: a) "high-25" *versus* "low-25"; b) "high-25" *versus* "others". The cut-off for "high-25", "low-25" and "others" were defined for each normalized dataset (Table 1):

GENE	QUARTILE	mRNA EXPRESSION: z-score relative to all samples	mRNA EXPRESSION: z- score relative to normal samples
TRIB1	high-25	≥ 0.6	≥ 0.8
	low-25	< -0.6	< -0.2
	others	< 0.6	< 0.8
TRIB2	high-25	≥ 0.6	≥ 1.9
	low-25	< -0.6	< 0.2
	others	< 0.6	< 1.9
TRIB3	high-25	≥ 0.7	≥ 2.3
	low-25	<-0.7	< 0.4
	others	< 0.7	< 2.3

Table 1: z-scores values for *TRIB1*, *TRIB2* and *TRIB3* of "high-25", "low-25" and "others" subsets relative to all samples and relative to normal samples.

Finally, we explored the correlations between *Tribbles* gene expression (normalized to all samples) in the "high-25" and the "others" groups, and molecular and clinico-pathological parameters, including molecular subtypes (CIN: chromosomal instability, MSI: microsatellite instability, GS: genomically stable and EBV: Epstein-Barr virus), stage (American Joint Committee on Cancer Tumor Stage Code), histological grade (Neoplasm Histologic Grade), sex and overall survival.

1.2 UALCAN

We compared the level of *TRIBs* gene expression (RNASeq, TPM: transcript per million) in STAD samples and their matched normal tissue using the UALCAN database (*http://ualcan.path.uab.edu/index.html*). UALCAN is a web resource, developed by the Comprehensive Cancer Center at the University of Alabama in 2017, that provide easy access to publicly available TCGA omics and clinical data from 31 cancer types and their matched normal tissues (Chandrashekart *et al*., 2017).

1.3 Broad Institute Cancer Cell Line Encyclopedia (CCLE)

We downloaded the gene expression data (RNA-seq, RSEM) and explored the *Tribbles* levels of expression in 37 gastric cancer cell lines from the Cancer Cell Line Encyclopedia (CCLE, *https://sites.broadinstitute.org/ccle/*). The CCLE is a project initiated in 2008 by a collaboration between the Broad Institute and the Novartis Biomedical Research Institutes, with the goal to provide detailed genetic and pharmacological characterization of a large panel of cell lines used as human tumor models (Barretina *et al*., 2012).

2. *In vitro* data

2.1 Gastric cancer cell lines

The human gastric cancer (GC) cell lines MKN45, derived from a liver metastasis of poorly differentiated gastric adenocarcinoma (diffuse histotype), and KATO-III, obtained from a signet ring carcinoma (diffuse histotype), were purchased from the Cell Bank RIKEN BioResource Center (Tsukuba, Japan). MKN74 cells, derived

from a liver metastasis of moderately differentiated gastric adenocarcinoma (intestinal histotype), were kindly provided by Prof. V. Ricci (Department of Molecular Medicine, University of Pavia-Italy) and NCI-N87 cells, derived from a liver metastasis of a well-differentiated carcinoma of the stomach (intestinal histotype), were kindly provided by Dr. D. Calistri (Laboratorio di Bioscienze IRST-IRCCS, Meldola FC-Italy). The four selected cell lines are microsatellite stable (MSS). MKN74, KATO-III, MKN45 and NCI-N87 were cultured in RPMI1640 media (Gibco-Thermo Fisher Scientific, USA) supplemented with 10% FBS. HEK293T cells (derived from human embryonic kidney) where used to produce lentiviruses and were cultured in DMEM (Gibco-Thermo Fisher Scientific, USA) supplemented with 10% FBS. All media were supplemented with 100 units/ml penicillin-streptomycin (Thermo Fisher Scientific, USA) and 1 mg/ml of Primocin (Invivogen. CA, USA) and cells were grown at 37°C in a humidified 5% CO2 incubator. Cell lines were mycoplasma tested regularly by PCR (PCR Mycoplasma Test Kit I/C, Promocell, Germany).

2.2 Lentiviral mediated gene modulation

Stable GC cell lines have been produced by lentiviral-mediated transduction to obtain cells with stable overexpression of TRIB2. The vector for TRIB2 overexpression (pLenti-C-mGFP-P2A-Puro-TRIB2) was purchased from OriGene Technologies GmbH (32052 Herford-Germany). This vector was used as transfer vector in combination with the envelop vector (pmD2.G) and the packaging vector (psPAX2) to produce TRIB2-overexpression lentivirus in the HEK293T cells, as shown in the scheme on the left.

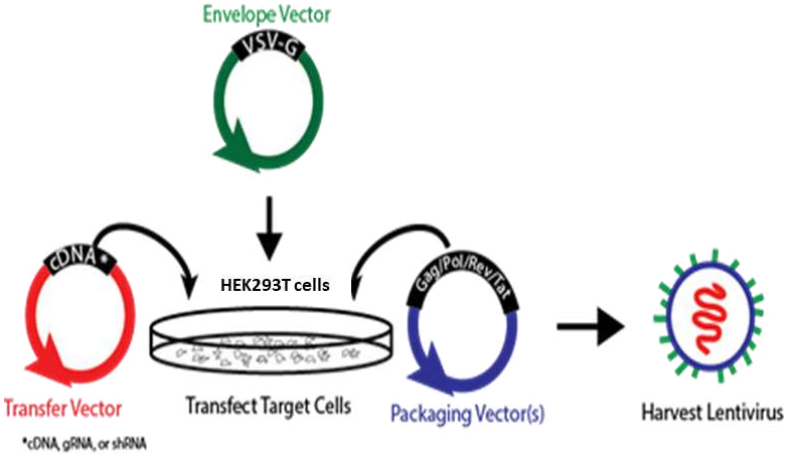

HEK293T cells were seeded in a 10-cm culture dishes at a density of 1×10^6 cells/plate, and the calcium phosphate transfection was performed after 24h, when cells reached about 80% confluence. Transfection complex solution

comprising 6 µg psPAX2 and pmD2.G packaging vectors, 5 µg lentiplasmid, CaP (calcium phosphate), HBS (HEPES buffered saline) buffer and H2O, was added to the culture dish with HEK293T cells, according to the manufacturer's protocol. After 24h, the culture medium was replaced with DMEM containing 10% FBS. The supernatant of HEK293T cells was collected 48h after the transfection and the lentiviruses were filtered by 0.45µm filter. Lenti-X GoStix Plus (Takara Bio, USA) was used to determine the titer of the lentiviruses. The obtained lentiviral vectors allowed me to deliver and stably express TRIB2 as a fluorescent fusion protein in the different cell lines.

GC cell lines were seeded at 5×10^5 cells/well in 6-well plates. After 24h, 2 ml of lentivirus and 1 µg/ml of Polybrene (Sigma-Aldrich, USA) were added into each well. After 6h, the culture medium was replaced with RPMI-1640 medium containing 10% FBS. After 72h, culture medium containing 1 µg/ml Puromycin was used to select the cells for about 2 weeks to obtain stable transfected cell lines.

All four cell lines were transduced with the TRIB2-overexpression lentivirus; a lentiviral vector for GFP-overexpression (pLenti-C-mGFP-P2A-Puro) was used as positive control. The overexpression of TRIB2 in the stable cell lines was confirmed by western blot analysis.

2.3 Western blotting

The cells were harvested and lysed in RIPA lysis buffer (Sigma Aldrich, USA) supplemented with the protease and phosphatase inhibitor cocktail purchased from Sigma Aldrich. The protein extracts were run on 10% SDS-polyacrylamide gel electrophoresis and transferred to nitrocellulose membranes by voltage gradient transfer. The blots were blocked 1h at room temperature in 5% non-fat dry milk. The membranes were then incubated overnight at 4 °C with the primary antibodies for TRIB2 (ATLAS ANTIBODIES, Sweden), for AKT, Phospho-Akt (Ser473), ERK and Phospho-ERK (137F5) (Cell Signaling Technology, USA) diluted 1:1000, and then incubated with an anti-rabbit secondary antibody (Sigma-Aldrich). The visualization of TRIB2 protein bands was obtained by using the horseradish peroxidase (HRP) development system.

2.4 Cell proliferation assay

Cells were seeded into a 96-well plate with 5,000 cells/well for MKN45 and MKN74 and 10,000 cells/well for NCI-N87and KATO-III cells. The cell viability was measured using the Cell Proliferation Reagent WST-1 (Roche, Switzerland): at different time point, 10 µl WST-1 (water-soluble tetrazolium salt) were added into each well and the absorbance was measured at 440-450 nm every 30 minutes, every day for 4 days. Each time point had six replicates.

2.5 Colony formation assay

The ability of the cells to form colony was tested by seeding in 6 well-plate 1000 cells/well incubated for ten days. At this time point, the colonies in each well were stained by Crystal violet and then counted with countPHICS program.

2.6 Cell cycle analysis

Cell cycle analysis was carried out by comparing parental cells with control cells and with the stably infected cells. For each cell line $5x10^5$ cells were seeded in a medium flask (75 cm^2) and after 24h of starvation, the FBS-free medium was replaced with normal medium for 24h, 48h or 72h. At each time point, the cells were harvested and resuspended in 75% cold ethanol, treated with 10 µg/ml RNAse at 37 °C for 15min and stained with 50 µg/ml Propidium iodide (PI) solution for 1h. Then, samples were analysed by MACSQuant Analyzer Flow Cytometry (Miltenyi Biotec) and the obtained data were analysed by FloJo program.

2.7 Migration assay

The cell migration was determined with Twin Certs-TC inserts with a size of pore of 8 µm (Greiner Bio-One, Austria). $1.5×10^4$ cells were seeded without serum in the upper part of the Twin Certs-TC inserts. After 24h, the lower insert was placed in complete medium with 10% FBS. Cells were then incubated for 24h and 48h. At the different time points, cells were stained by haematoxylin and cell count was performed using FIJI program.

2.8 Drugs treatment

Doxorubicin and 5-Fluorouracil (5-FU) were purchased from Sigma-Aldrich (USA). Cells were seeded into a 96-well plate with 5,000 cells/well for MKN45 and 10,000 cells/well for NCI-N87 cells. After 24h incubation, cells were treated with various concentrations of 5-FU (50, 100, 200, 400 µM) and of Doxorubicin (50, 100, 200, 400 mM/50, 100, 150 µM) for 72h. The cytotoxicity was evaluated by cell viability assay as described above. Determination of drug concentration to inhibit cell proliferation by 50% (IC 50) was calculated for each cell lines with the parental cells.

2.9 Statistical analysis

P values were calculated with Mann-Whitney statistical test, Welch's test and multiple T test with GraphPadPrism v8.0 software. Statistical significance was defined as *P <0 .05; **P<0.01; ***P<0.001; **** P ≤ 0.0001. Each graph is representative of multiple independent experiments. Data are shown as mean ± standard deviation (SD).

Results

1. *In silico* data

1.1 *TRIB1*, *TRIB2* and *TRIB3* somatic genetic and genomic alterations in *TCGA PanCan Atlas* tumors

The frequency and type of somatic genetic and genomic alterations of *TRIB* genes were explored in the 33 different cancer types included in the *TCGA PanCan Atlas* dataset, by using the cBioPortal web platform. Overall, *TRIB* genes were found to be altered in 9.8% of the tumors (1069/10953). The frequencies of genetic/genomic alterations are 7%, 1.3%, and 1.5% for *TRIB1*, *TRIB2* and *TRIB3*, respectively. The most frequent alteration is gene amplification, while deletions and point mutations are less common (Fig. 1A). We also investigated the distribution of *TRIBs* point mutations (missense and truncating mutations) across protein domains. As shown in Fig. 1B, point mutations are located in different domains of TRIB proteins: they are mostly located in the pseudokinase domain in TRIB1, whereas they are scattered along different domains in TRIB2 and TRIB3. Missense mutations (81.5% for TRIB1, 94.6% for TRIB2, 82.8% for TRIB3) are the most frequent mutation type (Fig. 1B).

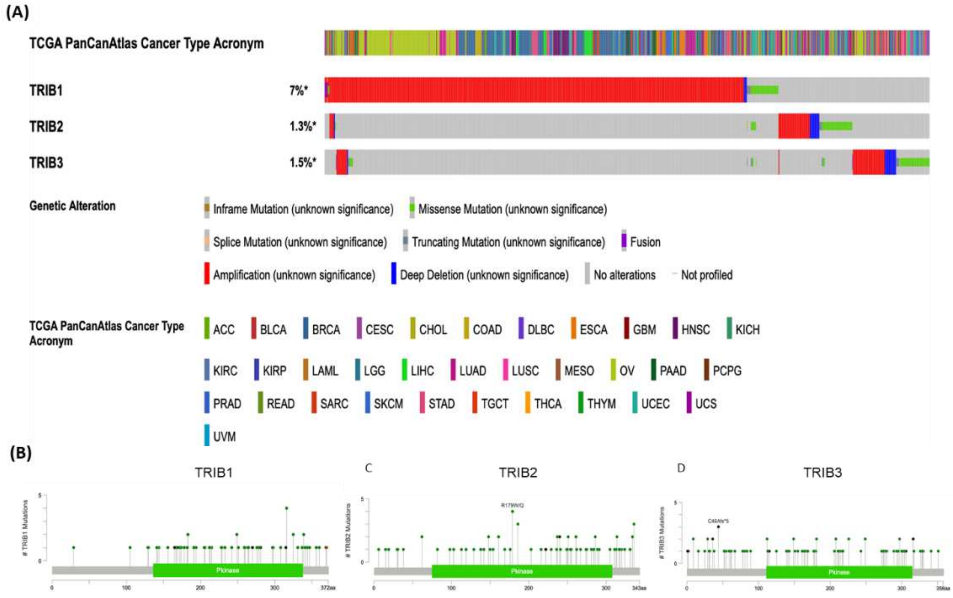

Figure 1. (A) Frequency and types of *TRIB* genetic and genomic alterations in the 33 tumor types from the *TCGA PanCancer Atlas*. "*" next to the percentages indicates overlap between alteration types in the same patient **(B)** Distribution of the point mutations across TRIB protein domains from the Pfam database. Green lollipops indicate missense mutations and black lollipops indicate truncating mutations.

Tumors and corresponding acronyms: ACC (Adrenocortical carcinoma), BLCA (Bladder Urothelial Carcinoma), BRCA (Breast invasive carcinoma), CESC (Cervical squamous cell carcinoma and endocervical adenocarcinoma), CHOL (Cholangiocarcinoma), COAD (Colon adenocarcinoma), DLBC (Lymphoid Neoplasm Diffuse Large B-cell Lymphoma), ESCA (Esophageal carcinoma), GMB (Glioblastoma multiforme), HNSC (Head and Neck squamous cell carcinoma), KICH (Kidney Chromophobe), KIRC (Kidney renal clear cell carcinoma), KIRP (Kidney renal papillary cell carcinoma), AML (Acute Myeloid Leukemia), LGG (Brain Lower Grade Glioma), LIHC (Liver hepatocellular carcinoma), LUAD (Lung adenocarcinoma), LUSC (Lung squamous cell carcinoma), MESO (Mesothelioma), OV (Ovarian serous cystadenocarcinoma), PAAD (Pancreatic adenocarcinoma), PCPG (Pheochromocytoma and Paraganglioma), PRAD (Prostate adenocarcinoma), READ (Rectum adenocarcinoma), SARC (Sarcoma), SKCM (Skin Cutaneous Melanoma), STAD (Stomach adenocarcinoma), TGCT (Testicular Germ Cell Tumors), THCA (Thyroid carcinoma), THYM (Thymoma), UCEC (Uterine Corpus Endometrial Carcinoma), UCS (Uterine Carcinosarcoma), UVM (Uveal Melanoma).

1.2 Frequencies of *TRIB1*, *TRIB2* and *TRIB3* somatic genetic and genomic alterations in *TCGA PanCan Atlas* STomach ADenocarcinoma (STAD) dataset

The frequency and type of genetic and genomic alterations of *TRIB* genes were explored in gastric cancer tumors reported in the *Stomach Adenocarcinoma (STAD) TCGA PanCan Atlas* dataset, using the cBioPortal web platform. In STAD, the total frequency of *TRIB1-2-3* genes was 13.5% (60/440). Specifically, the frequencies of genetic and genomic alterations were 9%, 2% and 2.5% for *TRIB1*, *TRIB*2 and *TRIB3,* respectively (Fig. 2). As observed in our previous analysis in different cancer types, the most frequent alteration in STAD was gene amplifications, while deletions and point mutations were very rare.

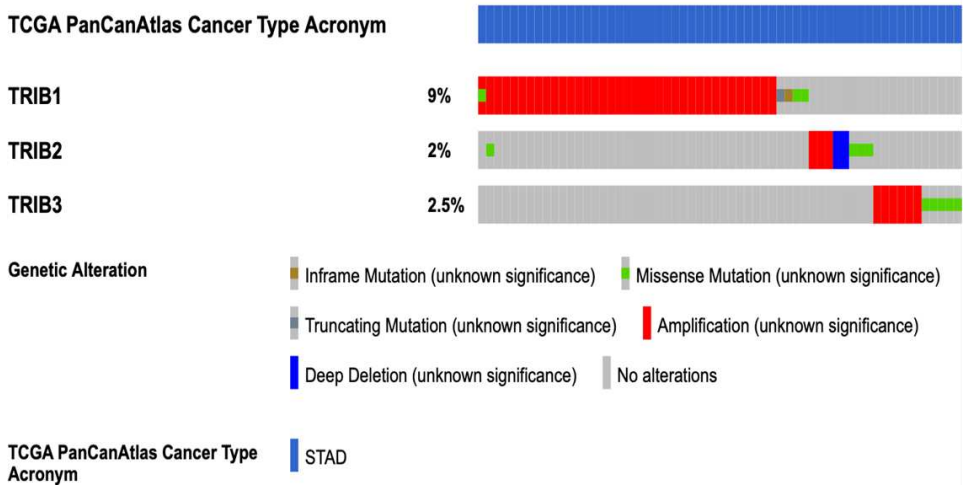

Figure 2. Frequency and types of *TRIB* genetic and genomic alterations in stomach adenocarcinoma (STAD).

1.3 *TRIBs* mRNA expression in gastric cancer cell lines

We next explored the level of *TRIBs* gene expression in the 37 gastric cancer (GC) cell lines reported in the Cancer Cell Line Encyclopedia (CCLE) database. We found that *TRIB1* has a higher expression level in GC cells compared to *TRIB2* and *TRIB3*, while *TRIB2* and *TRIB3* show a wider range of mRNA expression levels compared to *TRIB1* (Fig. 3).

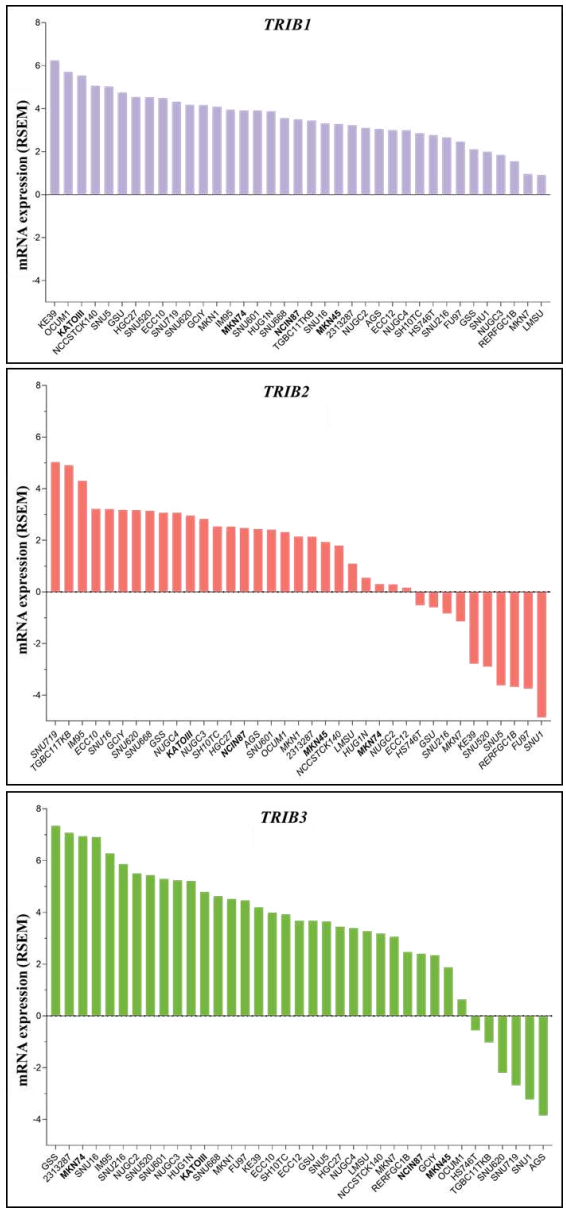

Figure 3. Expression of *TRIB1*, *TRIB2* and *TRIB3* in the 37 GC cell lines reported in the CCLE database. The y-axis shows mRNA levels expressed in RSEM (RNA-Seq by Expectation Maximization).

1.4 *TRIBs* mRNA expression in normal and gastric cancer tissues

To investigate *TRIBs* gene expression in normal and cancer gastric tissues, we performed a data mining of the TCGA STAD dataset available on UALCAN and we compared the mRNA expression level of the *TRIBs* genes in normal (34) and STAD (415) samples. *TRIB1, TRIB2* and *TRIB3* showed a statistically significant higher expression in tumors compared to normal tissue samples (Fig. 4).

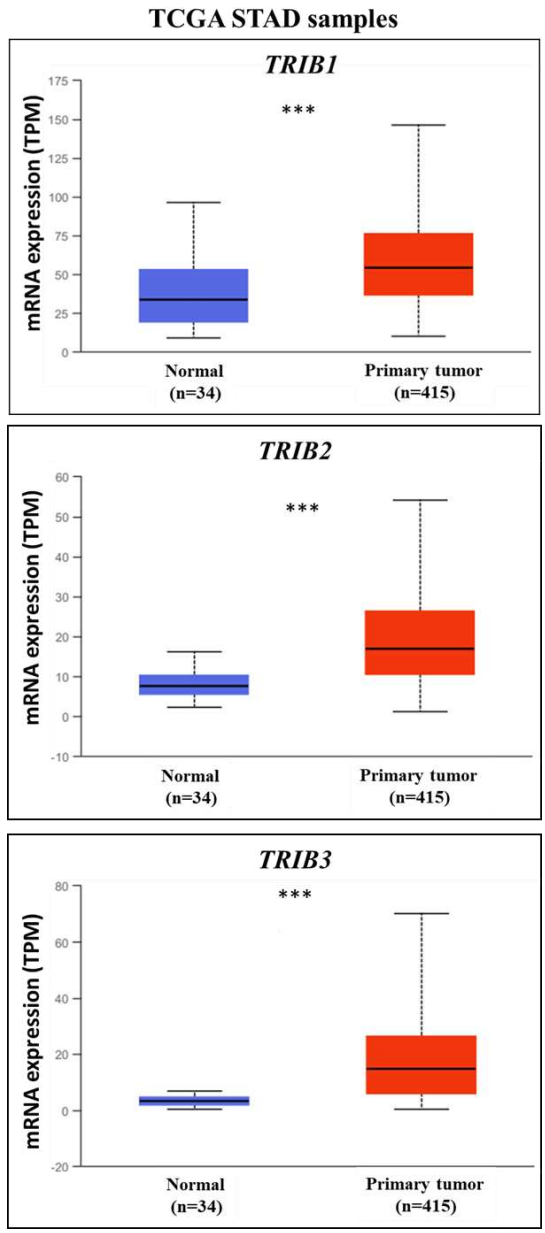

Figure 4: Expression levels of *TRIB1*, *TRIB2* and *TRIB3* genes in normal and cancer (STAD) tissue samples. The y-axis shows mRNA levels expressed in transcripts per million (TPM). Data are shown as mean ± standard deviation (SD); ***P<0.001.

1.5 *TRIBs mRNA* expression in *TCGA PanCan Atlas STAD* dataset

We analyzed the *TRIBs* mRNA distribution profile of the 412 TCGA STAD tumors in cBioPortal, normalized either to all samples or to normal samples.

In line with our results on GC cells, *TRIBs* showed a wide range of mRNA expression levels in STAD (Fig. 5). In addition, we observed a statistically significant difference of expression between "high-25" (highest level of mRNA expression; 103 samples) and "low-25" (lowest level of mRNA expression; 103 samples) subsets, as well as between "high-25" and "others" (low/intermediated levels of mRNA expression; 309 samples) subsets (Fig. 6-7-8).

Identical results were obtained for the mRNA expression normalized to the two reference populations (all samples or normal samples). On this basis, to include the entire STAD dataset (412 samples), our subsequent analyses were conducted by comparing the "high-25" and the "others" subsets and by using the normalization to all samples (unless indicated otherwise, only results obtained using the normalization to all samples are shown).

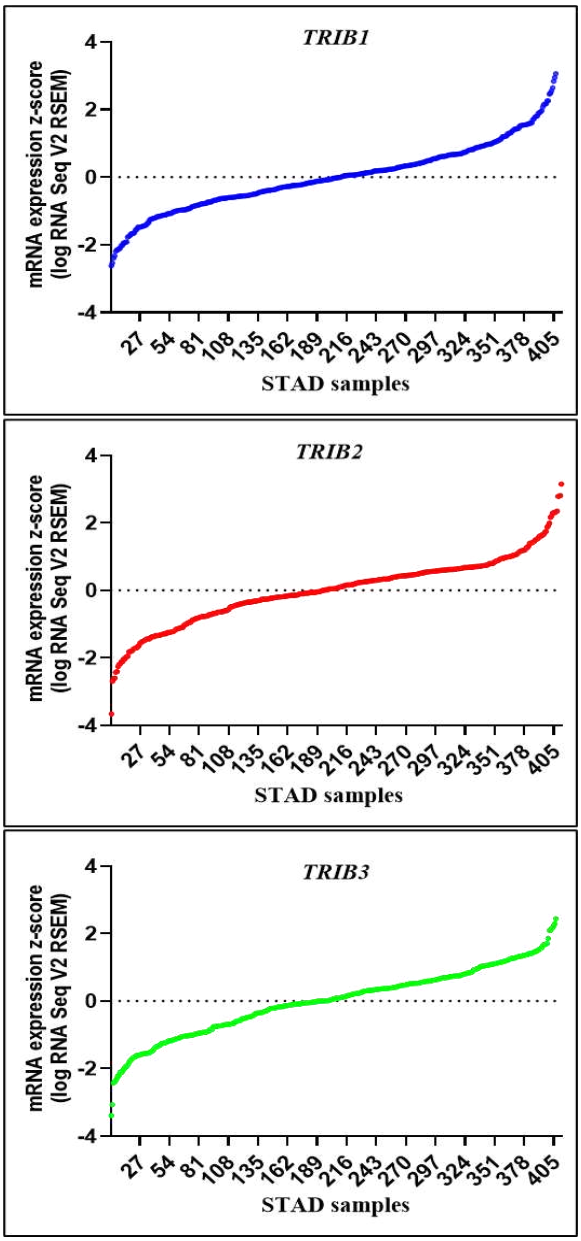

Figure 5. *TRIB1*, *TRIB2* and *TRIB3* mRNA level distribution profile in *TCGA PanCan STAD* dataset. The y-axis shows mRNA levels expressed in z-scores (log RNA Seq V2 RSEM).

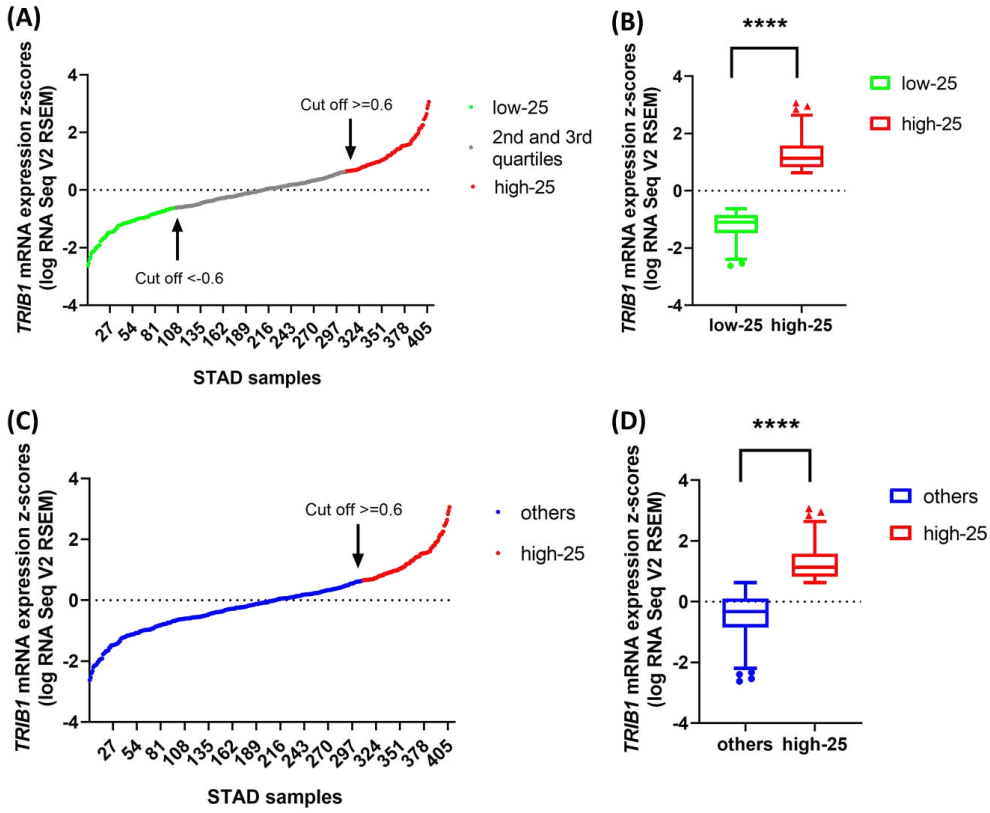

Figure 6. (A-C) *TRIB1* mRNA distribution profile. The black arrows indicate the cut-offs expressed as z-score for the "high-25", "low-25" and "others" subsets. **(B-D)** The box plots show a significant difference of mRNA expression levels between quartiles (**B:** "high-25" *vs.* "low-25", $P < 0.0001$; **D:** "high-25" *vs*. "others", $P < 0.0001$). The y-axis shows mRNA levels expressed in z-scores (log RNA Seq V2 RSEM). Data are shown as mean ± standard deviation (SD); **** $P \leq 0.0001$.

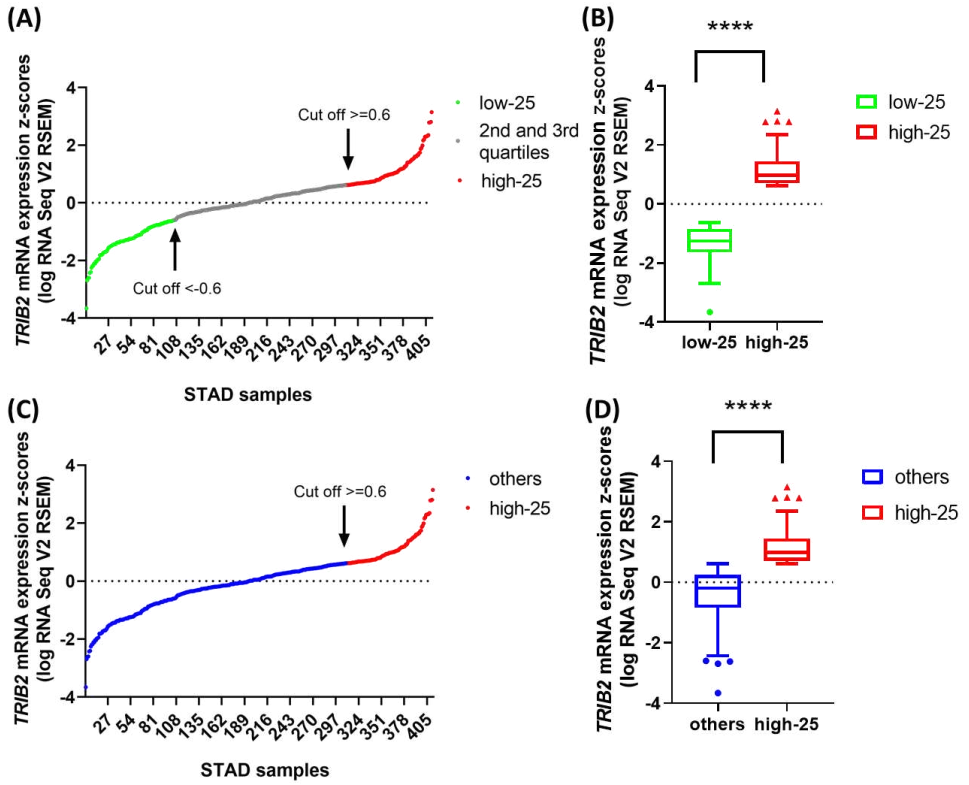

Figure 7. (A-C) *TRIB2* mRNA distribution profile. The black arrows indicate the cut-offs expressed as z-score for the "high-25", "low-25" and "others" subsets. **(B-D)** The box plots show a significant difference of mRNA expression levels between quartiles (**B:** "high-25" *vs.* "low-25", $P < 0.0001$; **D:** "high-25" *vs*. "others", $P < 0.0001$). The y-axis shows mRNA levels expressed in z-scores (log RNA Seq V2 RSEM). Data are shown as mean ± standard deviation (SD); **** $P \leq 0.0001$.

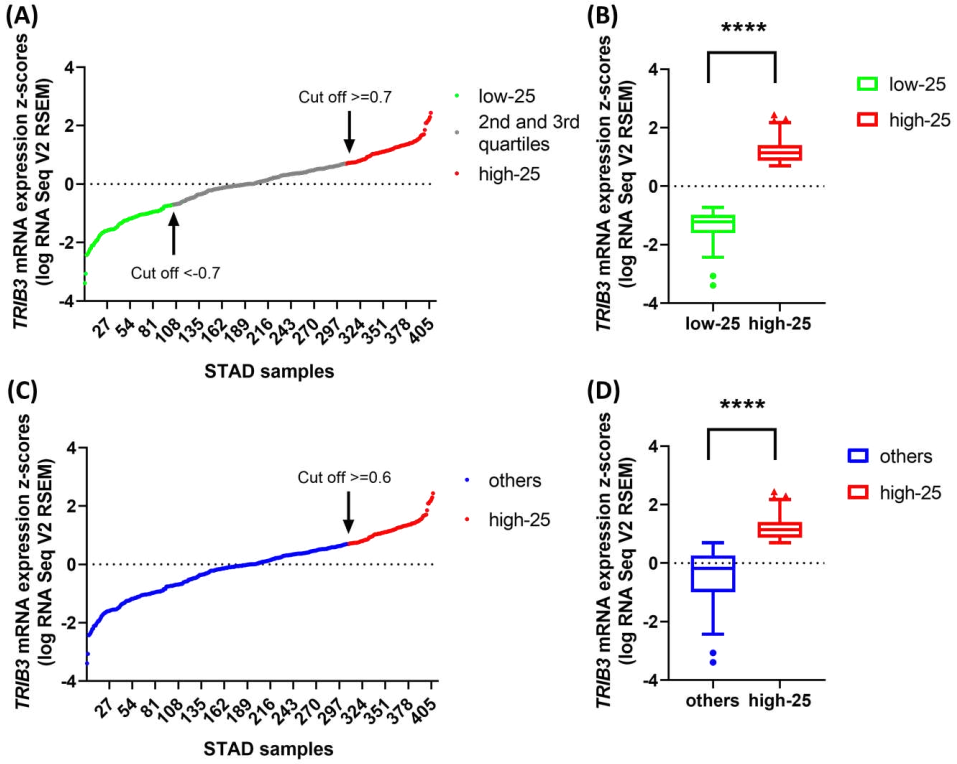

Figure 8. (A-C) *TRIB3* mRNA distribution profile. The black arrows indicate the cut-offs expressed as z-score for the "high-25", "low-25" and "others" subsets. **(B-D)** The box plots show a significant difference of mRNA expression levels between quartiles (**B:** "high-25" *vs.* "low-25", $P < 0.0001$; **D:** "high-25" *vs*. "others", $P < 0.0001$). The y-axis shows mRNA levels expressed in z-scores (log RNA Seq V2 RSEM). Data are shown as mean ± standard deviation (SD); **** $P \leq 0.0001$.

1.6 *TRIBs* mRNA expression in GC molecular subtypes

To evaluate the clinical significance of the *TRIBs* mRNA dysregulation in STAD, we first sorted STAD cases based on their molecular classification, including chromosomal instability (CIN), microsatellite instability (MSI), Epstein-Barr virus (EBV) and genomically stable (GS) subtypes. We then splitted cases into two subsets based on *TRIBs* mRNA expression ("high-25": with the highest expression; "others": with low/intermediate expression). Our analysis demonstrated that

different levels of *TRIBs* expression were not correlated with specific molecular subtypes (Fig. 9).

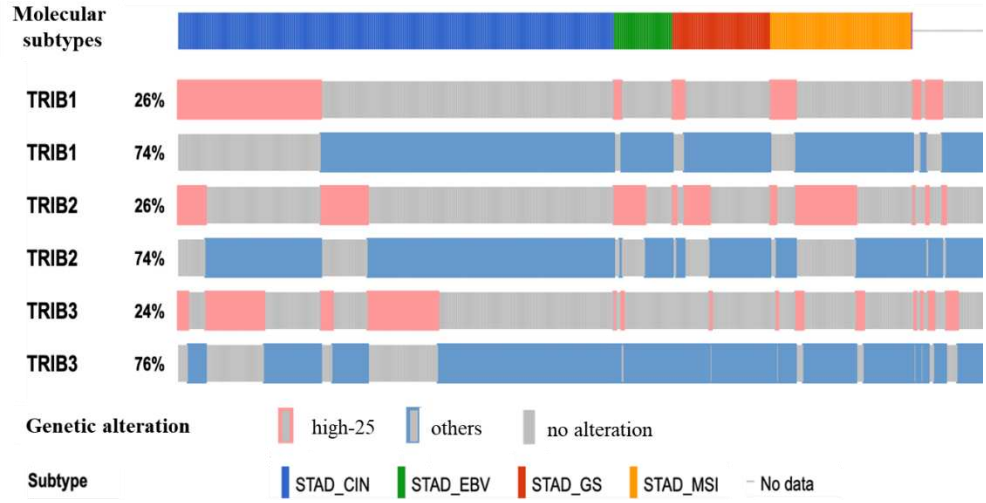

Figure 9. Oncoprint showing the STAD cases sorted by molecular subtypes and *TRIB* genes expression. Cases with highest gene expression ("high-25") are indicated in pink (z-score ≥ 0.6 for *TRIB1-2* and z-score ≥ 0.7 for *TRIB3*), cases with low/intermediate gene expression ("others") are indicated in blue (z-score < -0.6 for *TRIB1-2* and z-score < - 0.7 for *TRIB3*). CIN: chromosomal instability; EBV: Epstein-Barr virus; GS: genomically stable; MSI: microsatellite instability.

Next, we focused on the two most common GC molecular subtypes, *i.e.* tumors with chromosomal instability (CIN: 223 cases) and tumors with microsatellite instability (MSI: 73 cases). We analyzed separately CIN and MSI tumors in relation to *TRIBs* expression normalized to either all tumors or normal samples. No significant association was found between *TRIB1* mRNA expression level and CIN/MSI phenotype (Fig. 10A*vs.*D). On the contrary, a statistically significant lower expression of *TRIB2* was found in CIN compared to MSI tumors (P <0.0001) (Fig. 10B*vs.*E). In addition, we detected a statistically significant higher expression of *TRIB3* in CIN tumors compared to MSI cases (P <0.0001) (Fig. 10C*vs.*F).

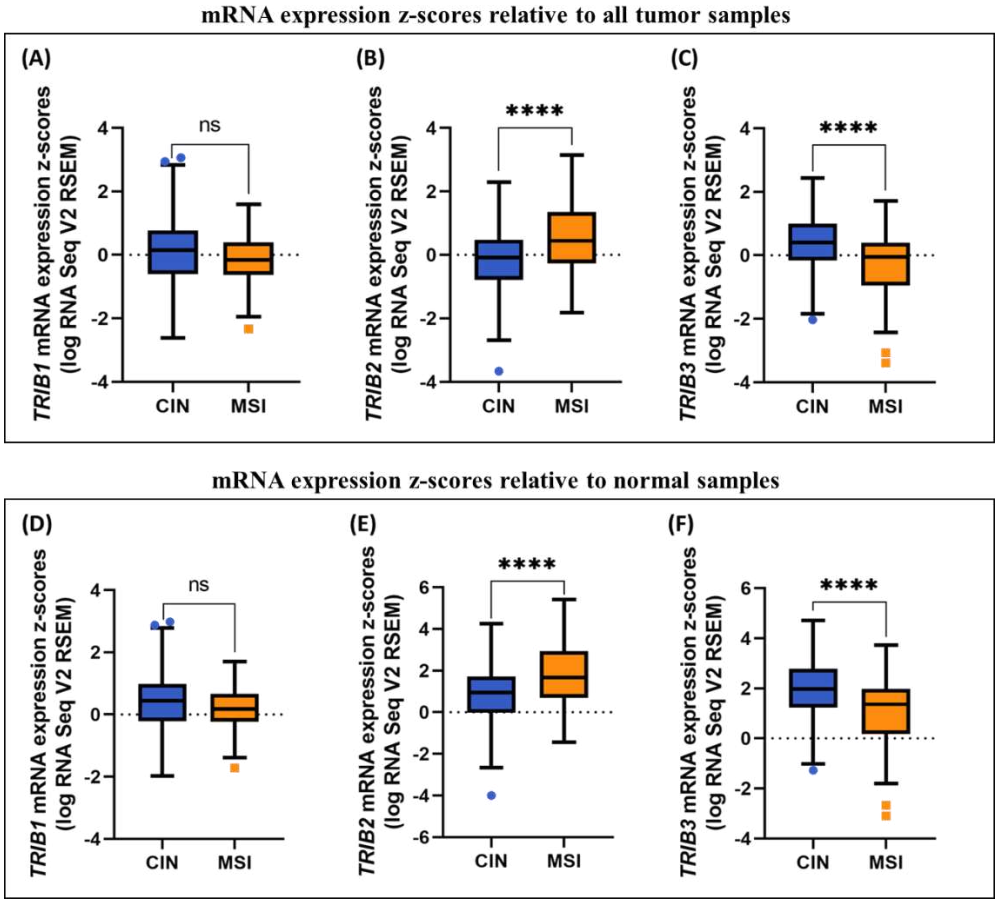

Figure 10: Boxplots showing *TRIB1* **(A-D)**, *TRIB2* **(B-E)** and *TRIB3* **(C-F)** expression normalized to either all tumor samples or normal samples in STAD tumors with CIN or MSI phenotype. The y-axis shows mRNA level expressed in z-scores (log RNA Seq V2 RSEM). CIN: chromosomal instability; MSI: microsatellite instability. Data are shown as mean ± standard deviation (SD); **** $P \leq 0.0001$.

1.7. The clinical significance of *TRIB2* mRNA dysregulation in CIN and MSI tumors

Since no studies have been performed on *TRIB2* in GC, we decided to deeply focus on this gene by investigating the correlation between mRNA levels and clinico-

pathological parameters. We considered CIN (223) and MSI (73) cases and tumors ranked as expressing high ("high-25") or low/intermediate ("others") levels of *TRIB2* mRNA; then, in the four tumor subsets we evaluated the correlation between gene expression and sex, tumor stage, tumor histological grade and patients' survival.

Males and females were equally represented in CIN tumors showing high or low/intermediate *TRIB2* gene expression. In MSI tumors, females were prevalent in the low/intermediate *TRIB2* mRNA expression subset (64.1%, 25/39) compared to males (35.9%, 14/39), while males were prevalent in the highest *TRIB2* mRNA expression subset (61.8%, 21/34) compared to females (38.2%, 13/34) (Fig. 11).

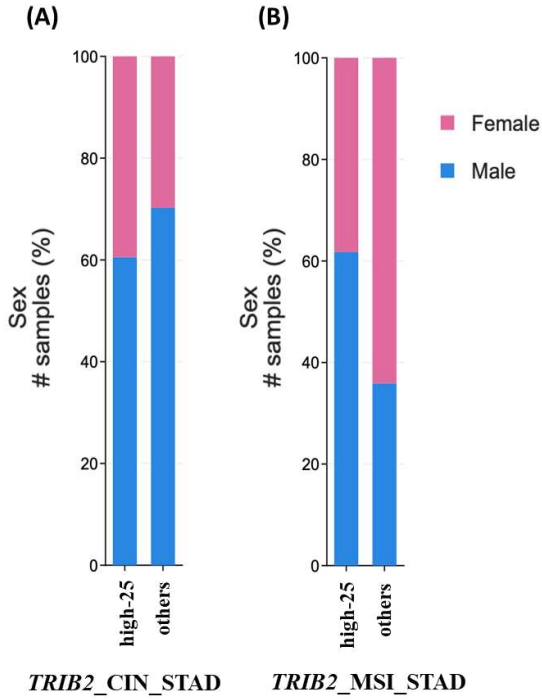

Figure 11: Gender distribution in tumors with CIN **(A)** or MSI **(B)** phenotype and highest ("high-25) or low/intermediate ("others") expression of *TRIB2*.

Regarding tumor stage, *TRIB2* showed highly variable expression levels in both CIN and MSI tumors. Interestingly, in CIN tumors, we found a significant correlation between low/intermediate levels of *TRIB2* expression and a more advanced stage (T4) (P = 0.0374). In contrast, in MSI tumors, we observed a significant correlation between highest levels of *TRIB2* expression and an early stage (T2) (P = 0.0374) (Fig. 12).

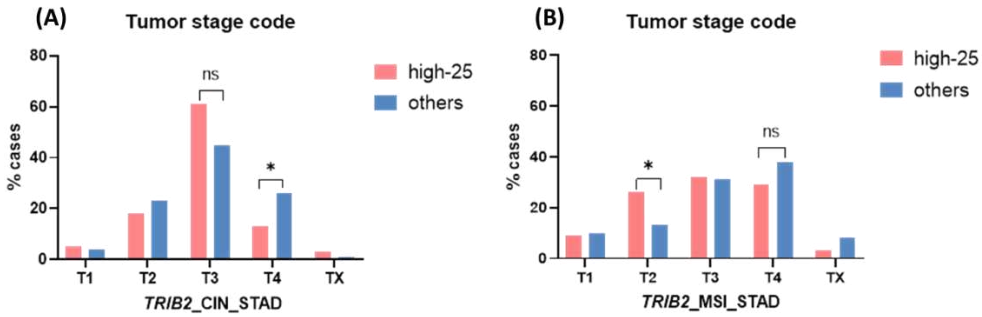

Figure 12: Distribution of CIN **(A)** or MSI **(B)** tumors with different stages and higher ("high-25) or low/intermediate ("others") expression of *TRIB2*. T1 to T4: less advanced to more advanced stage; TX: undetermined stage.

In both CIN and MSI tumors, no significant correlations were observed between *TRIB2* mRNA expression levels and histological grade (Fig. 13) or patients' survival (Fig. 14).

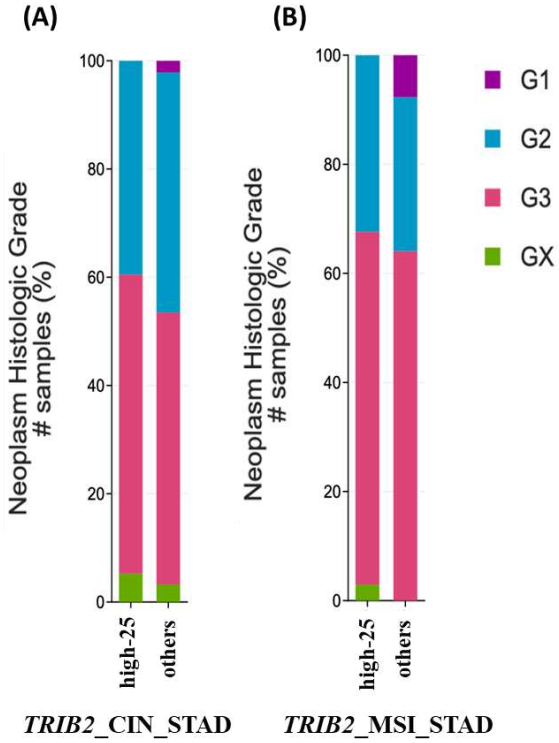

Figure 13: Distribution of CIN **(A)** or MSI **(B)** tumors with different histologic grade and higher ("high-25) or low/intermediate ("others") expression of *TRIB2*. G1 to G3: less aggressive and well differentiated to more aggressive and poorly differentiated. GX: grade not determined.

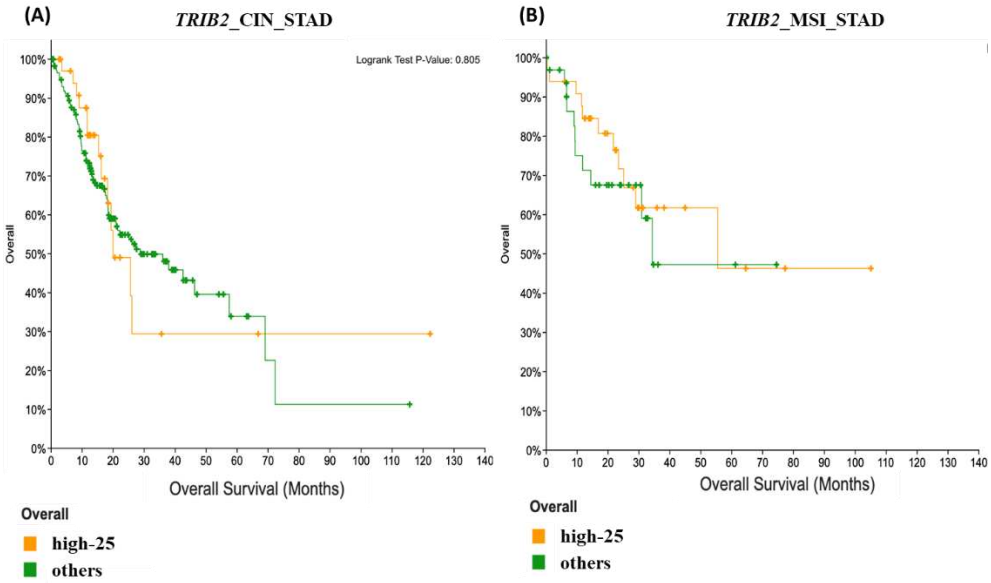

Figure 14: Correlation between *TRIB2* mRNA expression levels and patients' overall survival in CIN **(A)** and MSI **(B)** cases. Patients were divided based on *TRIB2* expression level into two groups indicated as "high-25" and "others".

2. *In vitro* data

Based on *in silico* analysis showing lower levels of *TRIB2* expression in CIN tumors, we decided to generate stable GC cell lines with lentiviral-mediated *TRIB2* overexpression by using four parental cell lines (MKN45, NCI-N87, MKN74 and KATO-III) characterized by CIN phenotype (MSS) and intermediate *TRIB2* mRNA expression level [see our analysis of Cancer Cell Line Encyclopedia (CCLE) database]. The functional effect of TRIB2 overexpression was then analyzed by different assays.

2.1 Endogenous expression levels of TRIB2 in GC cell lines

We evaluated the endogenous expression level of TRIB2 protein in the four selected GC cell lines (MKN74, KATO-III, MKN45 and NCI-N87) by western blot

(WB) analysis. Cell lines showed approximately the same level of TRIB2 expression, accordingly with data reported in CCLE database (Fig. 15).

Figure 15: Western blot analysis of the endogenous expression level of TRIB2 protein in MKN45, KATO-III, MKN74 and NCI-N87 GC cells. A human prostate cancer cell line (PC3) was used as positive control; the α-tubulin expression was used as internal control.

2.2 TRIB2 overexpression in GC cell lines

The four cell lines were infected with the TRIB2-overexpression lentivirus we produced as reported in Materials and Methods. The lentiviral mediated overexpression of TRIB2 was confirmed by WB analysis in the stable GC cell lines. A lentiviral vector for GFP overexpression (pLenti-C-mGFP-P2A-Puro) was used as positive control. As shown in Fig. 16, KATO-III, MKN45, MKN74 and NCI-N87 TRIB2-overexpressing cells showed variable levels of the endogenous protein and very high levels of the TRIB2-GFP fusion protein (Fig. 16).

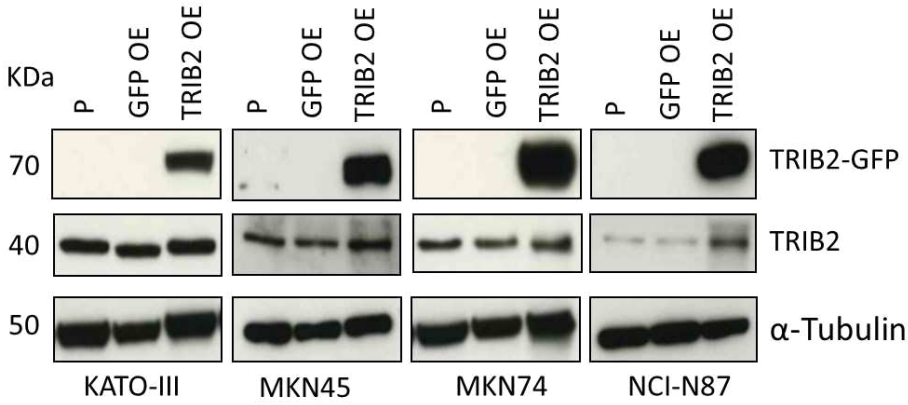

Figure 16: Western blot with anti-TRIB2 antibodies showing endogenous TRIB2 and TRIB2-GFP fusion proteins. KATO-III, MKN45, MKN74 and NCI-N87: parental cells, cells overexpressing the GFP protein (GFP OE), and cells overexpressing the TRIB2-GFP (TRIB2 OE) fusion protein are shown in parallel for each cell line. The α-tubulin expression was utilized as internal control.

2.3 Functional characterization of the TRIB2-overexpressing GC cell lines

To investigate the impact of TRIB2 overexpression, several functional assays were performed aimed at evaluating cell proliferation, cell colony formation, cell cycle and cell migration. We first investigated the effect of TRIB2 overexpression on cell proliferation and we then tested the possible involvement of the mitogen-activated protein kinase (MAPK) pathway. For each cell line, TRIB2-overexpressing (TRIB2 OE) cells were compared to the corresponding GFP-overexpressing (GFP OE) control cells. The results obtained are summarized in Table 1 and described below (Fig. 17-18).

	MKN74 TRIB2 OE	KATO-III TRIB2 OE	MKN45 TRIB2 OE	NCI-N87 TRIB2 OE
Cell proliferation assay	-	-	+	+
MAPK pathway analysis	-	-	-	-

Table 1: Summary of the analysis of TRIB2-overexpressing cell lines: - indicates no differences between GFP-overexpressing cells and TRIB2-overexpressing cells; + indicates a significant effect of TRIB2 overexpression. TRIB2-OE: TRIB2-overexpressing cells.

2.3.1 TRIB2 OE effect on cell proliferation

To investigate the effect of TRIB2 overexpression on cell proliferation, we performed the WST-1 cell viability assay. As shown by the following graphs (Fig. 17), TRIB2 overexpression can significantly inhibit the proliferation of MKN45 and NCI-N87 cells. On the contrary, TRIB2 overexpression does not affect proliferation of MKN74 and KATO-III cell lines.

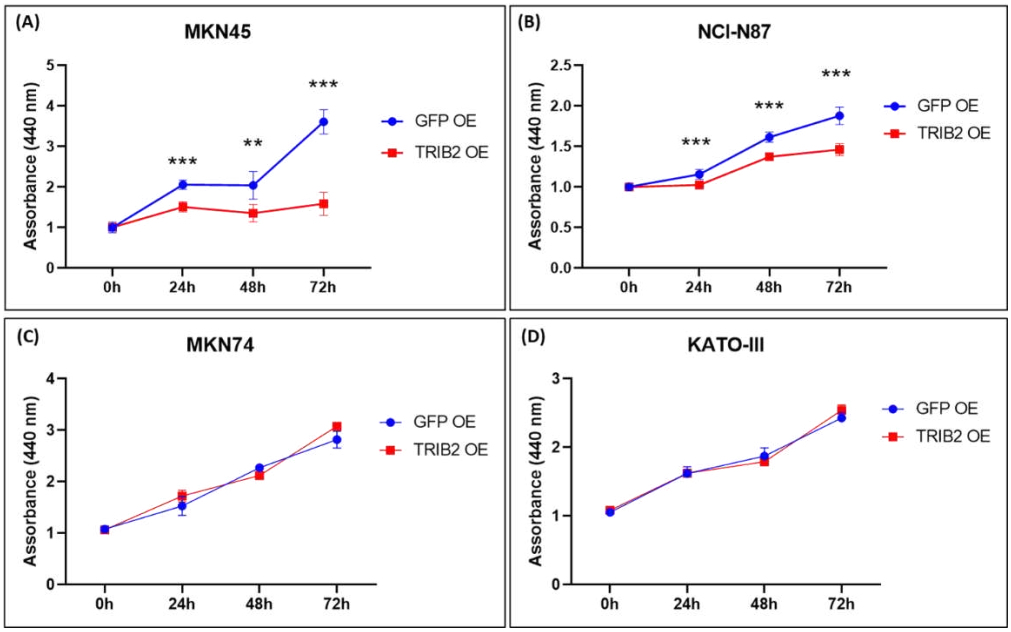

Figure 17: WST-1 assay on MKN45 **(A)**, NCI-N87 **(B)**, MKN74 **(C)** and KATO-III **(D)** TRIB2 OE cells *vs* GFP OE control cells. Data are shown as mean ± standard deviation (SD). *P <0 .05;**P<0.01;***P<0.001. GFP-OE: GFP-overexpressing control cells; TRIB2-OE: TRIB2-overexpressing cells.

2.3.2 Mitogen-activated protein kinase (MAPK) pathway analysis

Tribbles act as adaptors in signalling pathways for crucial cellular processes, including mitogen-activated protein kinase (MAPK) pathway. To investigate the possible involvement of MAPK proteins following the overexpression of TRIB2, we performed WB analysis of TRIB2 OE cells. As shown in Fig. 18, the relative expression levels of the phosphorylated forms of AKT and ERK proteins appeared to be similar in control and TRIB2 OE cells, indicating that the MAPK pathway is unlikely to be affected by TRIB2 overexpression.

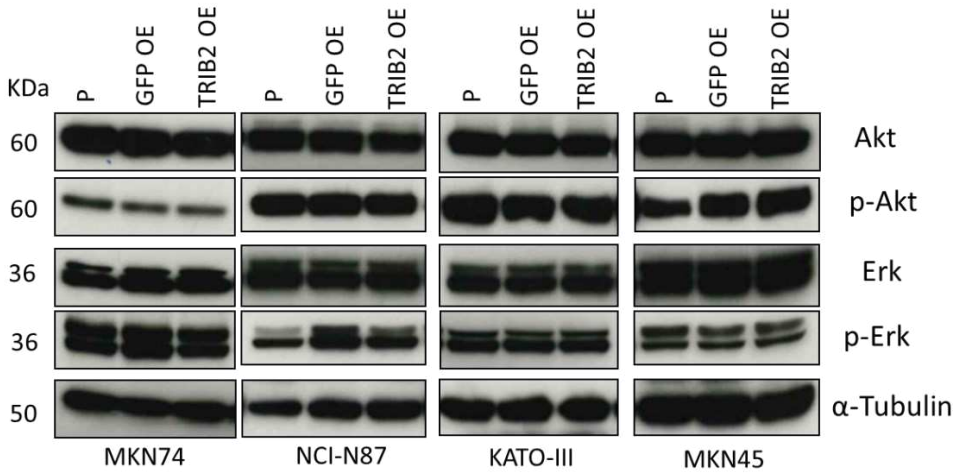

Figure 18: Western blot of MAPK proteins. Total-AKT, phospho-(p)-AKT (Ser473), total-ERK and phospho-(p)-ERK expression levels in GC parental, GFP-OE and TRIB2-OE cell lines. α-tubulin is the internal control. P: parental; GFP-OE: GFP-overexpressing control cells; TRIB2-OE: TRIB2-overexpressing cells.

Based on the proliferation assay, we decided to further investigate the effect of TRIB2 overexpression in MKN45 and NCI-N87, the two cell lines that were found to be affected by TRIB2 overexpression. Therefore, the following results only concern these two cell lines.

2.3.3 TRIB2 OE effect on colony formation ability

The effect of TRIB2 overexpression on cell proliferation was assessed through the colony formation assay. TRIB2 overexpression reduced cell colony formation ability in MKN45 TRIB2 OE cells and showed no effect on NCI-N87 TRIB2 OE cells when compared to GFP-control infected cells (Fig. 19).

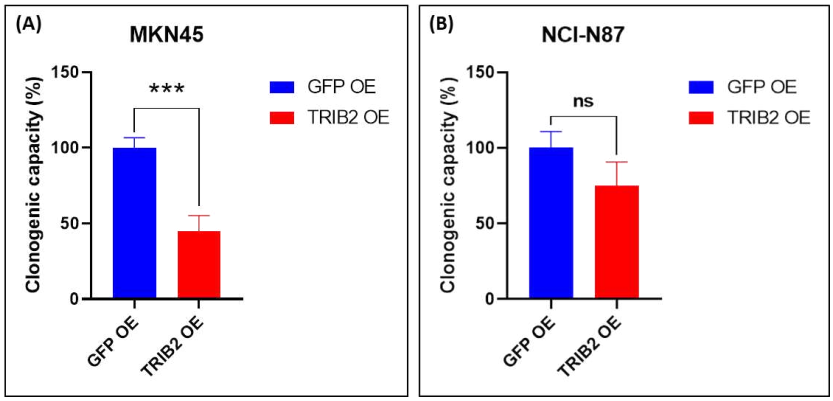

Figure 19: Cell colony formation assay of MKN45 TRIB2 OE **(A)** and NCI-N87 TRIB2 OE **(B)** cells compared to control cells. Data are shown as mean ± standard deviation (SD). *P <0 .05;**P<0.01;***P<0.001. GFP-OE: GFP-overexpressing control cells; TRIB2-OE: TRIB2-overexpressing cells.

2.3.4 TRIB2 OE effect on cell cycle

To test the impact of TRIB2 overexpression on cell proliferation, cell cycle analysis was carried out by comparing parental cells with control cells and with the stably infected cells. The overexpression of TRIB2 proved to affect the cell cycle of MKN45 TRIB2 OE by blocking cells in G2 phase, as evident by comparing MKN45 TRIB2 OE cells with parental and GFP OE control cells (Fig. 20A). On the other side, TRIB2 overexpression did not affect NCI-N87 TRIB2 OE cell cycle compared to the parental and GFP OE cells (Fig. 20B).

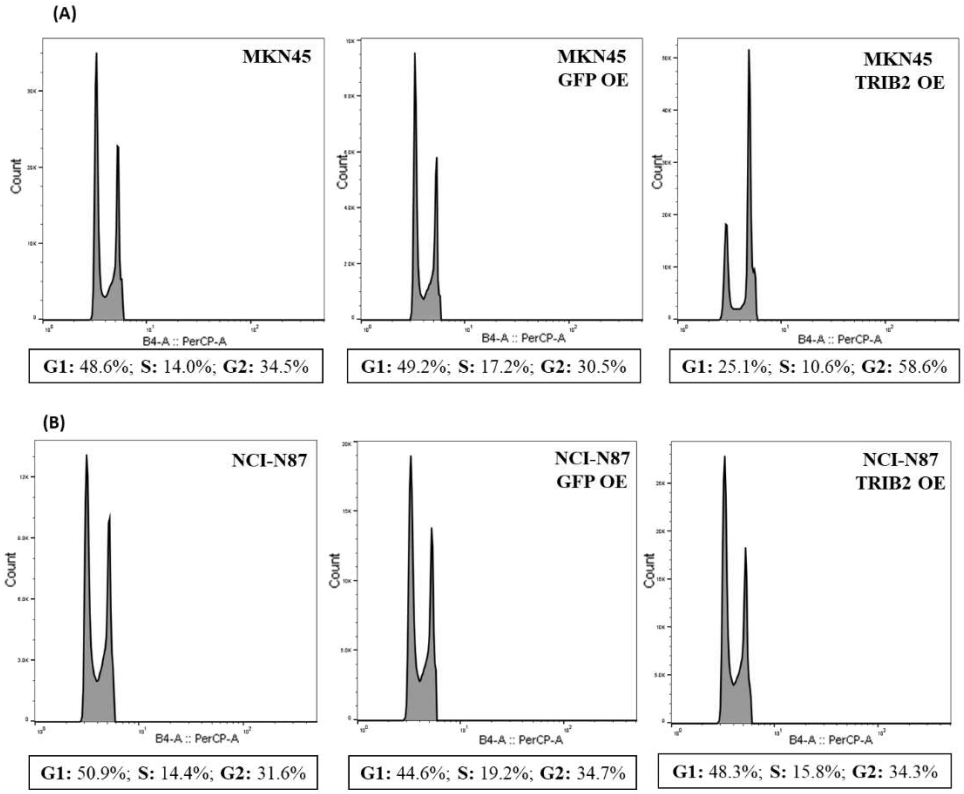

Figure 20: Cell cycle analysis of MKN45 **(A)** and NCI-N87 **(B)**: parental, GFP OE and TRIB2 OE cell lines. GFP-OE: GFP-overexpressing cells; TRIB2-OE: TRIB2-overexpressing cells.

2.3.5 TRIB2 OE effect on cell migration

We evaluate the migration ability of the TRIB2-overexpressing cell lines. TRIB2 overexpression did not affect MKN45 TRIB2 OE cell migration (Fig. 21A), while NCI-N87 TRIB2-OE cells showed reduced migration capacity compared to GFP-control cells (Fig. 21B).

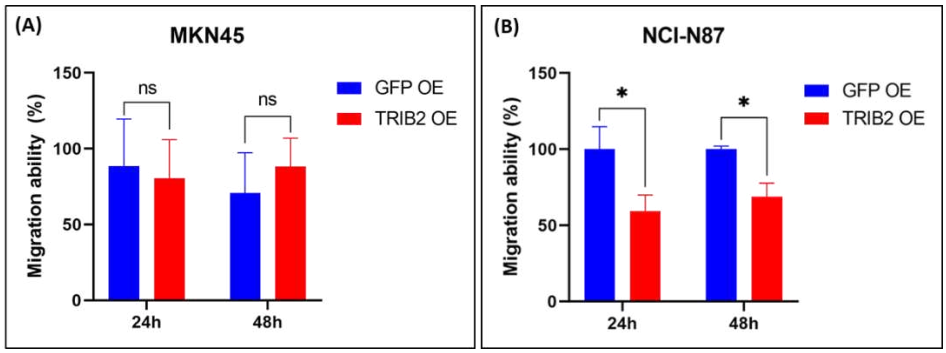

Figure 21: Migration assay of MKN45 TRIB2 OE **(A)** and NCI-N87 TRIB2 OE **(B)** cells compared to control cells. Data are shown as mean ± standard deviation (SD). *P <0 .05;**P<0.01;***P<0.001. GFP-OE: GFP-overexpressing control cells; TRIB2-OE: TRIB2-overexpressing cells.

2.3.6 Drug treatments

Finally, to investigate the possible impact of TRIB2 overexpression on response to drug treatment, we treated TRIB2- and control GFP-overexpressing MKN45 and NCI-N87 cells with different concentrations of two commonly used agents in chemotherapy today, 5-fluorouracyle (5-FU) and doxorubicin. We tested the drugs' effect on the cell viability by WST-1 assay. For both MKN45 and NCI-N87 cell lines, no differences were detected in TRIB2 OE cells treated with the 5-FU or doxorubicin, compared to control cells (Fig. 22).

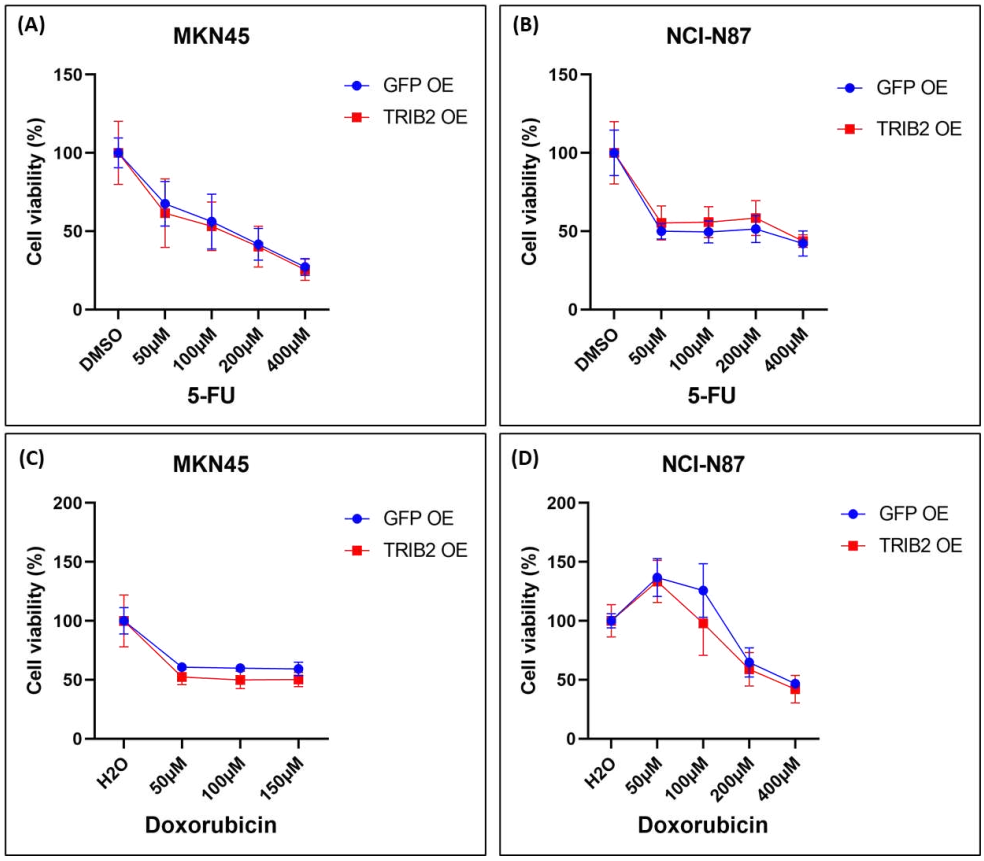

Figure 22: MKN45 and NCI-87 TRIB2 OE and GFP OE cells were treated with different concentration of 5-FU **(A-B)** and doxorubicin **(C-D)** for 72h and cell viability was determined by WST-1. Data are shown as mean ± standard deviation (SD). GFP-OE: GFP-overexpressing control cells; TRIB2-OE: TRIB2-overexpressing cells.

Discussion

Discussion

The purpose of the present study was to investigate the possible significance of TRIB2 in gastric cancer (GC). The Tribbles/TRIBs (TRIB1, TRIB2 and TRIB3) proteins are serine/threonine pseudokinases that act as signalling mediators or scaffold subunits to regulate the degradation of target proteins and to modulate multiple signalling pathways. In particular, through the interaction with the ubiquitin-proteasome degradation system and with the mitogen-activated protein kinase (MAPK) signalling pathways, TRIBs exert their function as regulators of cell cycle, differentiation, cell growth, metabolism, proliferation and cell stress, playing a role in both physiological and pathological conditions (Eyers *et al*., 2017; Lohan & Keeshan, 2013; Yokoyama & Nakamura, 2011). In cancer, TRIBs expression varies among cancer subtypes and current knowledge indicates both oncogenic and tumor suppressive roles, depending on the family member and on the cellular context (Richmond & Keeshan, 2020). Recent studies highlighted the involvement of TRIBs in tumors of the gastrointestinal tract, including colorectal (CRC) and gastric cancers. In this context, the investigated functions mainly concern TRIB3 in colorectal carcinogenesis (review of Ferreira *et al*., 2021). In contrast, the role of TRIBs in GC has been poorly investigated so far and data on TRIB2 protein are extremely scanty.

On this basis, we decided to investigate the possible involvement of TRIBs in gastric carcinogenesis. To this purpose, we performed data mining of the The Cancer Genome Atlas (TCGA) dataset, to evaluate the pattern of genetic and genomic alterations and the mRNA expression profile of *TRIB* genes in STomach ADenocarcinoma (STAD) tumors. We found a very low frequency of genetic and genomic alterations of *TRIBs* (TRIB1: 9%, TRIB2: 2% and TRIB3: 2.5%) in STAD tumors. On the contrary, the analysis of *TRIB* mRNA expression levels produced more interestingly results, in line with literature data which suggest a pathological significance of TRIBs dysregulation in tumors (Richmond & Keeshan, 2020).
By comparing the *TRIB1-2-3* gene expression in normal (34 cases) and STAD (415 cases) tissues from the TCGA dataset available on UALCAN, we found a statistically significant higher expression of *TRIBs* in STAD compared to normal gastric samples. In addition, we detected more variability for *TRIB1-2-3* mRNA expression levels in STAD tissues compared to normal tissues. The same extended variability was observed among the 37 GC cell lines reported in the Cancer Cell

Line Encyclopedia (CCLE) database: *TRIB2* and *TRIB3* showed a wider range of mRNA expression variability compared to *TRIB1* that, in turn, showed a higher level of expression compared to *TRIB2* and *TRIB3*. Likewise, the *TRIBs* mRNA distribution profile of TCGA STAD cases from cBioPortal (412 cases) revealed a wide range of *TRIB1, TRIB2* and *TRIB3* mRNA expression levels in GC patients, including: a subset of patients with very high *TRIBs* expression levels, a subset with very low *TRIBs* expression levels, and a subset with intermediate expression.

Once defined the reference population and the z-score cut-off value required for statistical evaluations, through the above-mentioned web resource, we exploited the possibility to classify the *TRIBs* mRNA expression data of TCGA STAD patients based on the gastric cancer molecular phenotypes. Specifically, we focused our attention on the two most common GC molecular subtypes: tumors with chromosomal instability (CIN) and tumors with microsatellite instability (MSI). We analysed separately the 296 tumors divided into CIN (223 cases) and MSI (73 cases) according to the *TRIBs* expression. Our analysis revealed no significant association between *TRIB1* mRNA expression and the CIN or MSI phenotype. On the contrary, we observed that CIN tumors had a statistically significant lower expression of *TRIB2* ($P<0.0001$) and a statistically significant higher expression of *TRIB3* ($P<0.0001$) compared to the MSI tumors, by using both normalized reference populations (normal stomach or all TCGA tumors). This observation suggests that *TRIB2* may play a role as tumor suppressor in GC with a CIN phenotype compared to GC with MSI phenotype, while *TRIB3* may have a role as oncogene in CIN tumors compared to MSI cases.

While *TRIB3* oncogenic function in GC has been investigated by recent studies (Wu *et al*., 2013; Zhu *et al*., 2017; Dong *et al*., 2016; Wu *et al*., 2017; Sun *et al*., 2020), so far there is one only report indicating that the level of *TRIB2* is downregulated in a GC cell line (MGC-803) following treatment with the anti-cancer agent dioscin (Zhao *et al*., 2016). This is the reason why we decided to focus our attention on this last gene.

We investigated the clinical significance of *TRIB2* by evaluating the different gene expression in CIN and MSI tumors in relation to clinico-patological parameters including sex, tumor stage, histological grade, and patients'survival. CIN tumors showed a statistically significant correlation between lower/intermediate levels of *TRIB2* expression and T4, *i.e.* advanced tumor stage ($P=0.0374$). On the contrary, MSI tumors showed a statistically significant correlation between higher levels of *TRIB2* expression and T2, *i.e.* early tumor stage ($P=0.0374$). These results are in

line with our hypothesis of a tumor suppressor function for *TRIB2* in CIN GCs, suggesting an inactivation of this tumor suppressor gene to allow tumor progression to more advanced stage. However, possibly due to the number of cases, we did not observe a correlation with tumor grade or patients' overall survival. Regarding sex, we found that females were prevalent (64.1%, 25/39) compared to males (35.9%, 14/39) in MSI tumors with low/intermediate *TRIB2* expression, whereas males were prevalent (61.8%, 21/34) compared to females (38.2%, 13/34) in the subset of tumors showing the highest *TRIB2* expression. This observation highlights the correlations between gender and tumor phenotypes. While the importance of gender as modulator of disease biology and treatment outcomes is well considered in other disciplines of medicine, it remains an undervalued issue in oncology where only recently more attention has been paid to sex differences. In general, men are at a higher risk of developing GC than women and this gender disparity has been attributed to the oncogenic role of the androgen receptor in gastric carcinogenesis (Tian *et al*., 2013). Regarding GC molecular phenotypes, it has been reported that the MSI phenotype is associated with the female gender; however, the molecular mechanism linking tumor genetic instability and gender remains totally unknown (Polom *et al*., 2018).

Based on the *in silico* analysis of GC cases, we investigated the role of *TRIB2* as tumor suppressor in a CIN background by using four GC cell lines with CIN phenotype as an *in vitro* model. NCI-N87, MKN74, MKN45 and KATO-III are human GC cell lines derived from tumors with different histotypes and with a microsatellite stable phenotype, corresponding to the CIN molecular subtype. Moreover, these cells show "intermediate" *TRIB2* mRNA expression levels (as we established from the CCLE dataset analysis), are commercially available, are easy to handle and have quick growing capacity. Given that CIN tumors had shown *in silico* a significant low/intermediate *TRIB2* mRNA expression compared to MSI tumors, we decided to test the impact of TRIB2 lentiviral mediated overexpression in the four cell lines. *In vitro* experiments proved that TRIB2 overexpression (OE) can reduce cell proliferation in MKN45 and NCI-N87 cell lines. Accordingly, we decided to deeply investigate TRIB2 OE in MKN45 and NCI-N87 cells. In accordance with the results of the proliferation assay, TRIB2 OE reduced colony formation ability and induced cell cycle arrest in G2/M phase in MKN45 cells. On the other side, TRIB2 OE reduced migration ability in NCI-N87 cells. These results

confirmed the tumor suppressive function of TRIB2 in GC and the involvement of this protein in cell proliferation, cell cycle and cell migration processes.

Several studies demonstrated that TRIB2 regulates different downstream signalling pathways through the C-terminal region, which include two important conserved sequences: the ILDHPWF sequence required for the interaction with the MEK family members, that modules the MAPK signal transduction pathway *via* increased AKT/ERK phosphorylation, and the sequence DQLVPD involved in the interaction with Ubiquitin E3-ligases, that regulates the polyubiquitination of the substrates attached to the TRIB2 pseudokinase domain. Through these interactions TRIB2 plays a key role in cellular processes like cell cycle, proliferation, senescence, protein degradation and cell survival (review of Mayoral-Varo *et al*., 2021). To understand the process behind the tumor suppressor effect we observed in GC cells, we performed MAPK pathway analysis. WB analysis did not showed difference between total-AKT, phospho-(p)-AKT (Ser473), total-ERK and phospho-(p)-ERK expression levels among parental, GFP OE and TRIB2 OE cell lines, indicating that TRIB2 does not exert its tumor suppressor function thought the MAPK pathway. The interactions with proteasome machinery proteins and the degradation of transcription factors are other important TRIB2 signalling mechanisms that could be investigated. For instance, Liang and collaborators (2016) demonstrated that TRIB2 interacts directly with the Cell Division Cycle 25C (CDC25C), a key physiological cell cycle regulator. They demonstrate that TRIB2, controlling CDC25C K48-linked polyubiquitination, regulates its subsequent degradation *via* the proteasome, leading to cell cycle arrest.

Owing to their variable expression, TRIB proteins have been proposed as valuable biomarkers for diagnosis, prognosis, outcome prediction of therapy and clinical strategy in different types of cancer (Richmond & Keeshan, 2020). For instance, TRIB2 is considered an emerging novel biomarker of chemoresistance for blood cancer treatment (O'Connor *et al*., 2018). For GC treatment, chemotherapy is performed in combination with surgery as adjuvant chemotherapy or as elective therapy when surgery is not an option. Moreover, GC is often diagnosed at advanced stages and drug resistance to conventional chemotherapy often occurs, leading to treatment failure. Therefore, the investigation of GC genetic signatures might represent a novel approach to identify new biomarkers and the studies aimed at assessing the role of new genes in GC tumorigenesis might unveil molecular targets for innovative therapies. We investigated if TRIB2 plays a role in response

to drugs by treating TRIB2 OE cell lines with two chemotherapeutic agents commonly utilized for GC, 5-fluorouracyle (5-FU) and doxorubicin. We did not observe difference between TRIB2-overexpressing and control GFP-overexpressing cells treated for 72h with different concentrations of doxorubicin or 5-FU. These observations suggest that TRIB2 does not affect the treatment with these two chemotherapeutic agents.

To the best of our knowledge, this is the first study to evaluate the pattern of genetic and genomic alterations and the mRNA expression profile of *TRIB* genes in TCGA STAD tumors and to investigate the effect of TRIB2 overexpression in GC cell lines. On the whole, our results pinpoint to a tumor suppressor function of TRIB2 in GC with a CIN molecular phenotype. Therefore, TRIB2 may represent a novel putative biomarker in CIN GC cases. Ongoing studies are assessing the expression of TRIB2 protein in human GC samples, with potential implications as biomarker for patients' stratification that may help in the prediction of treatment outcome and for individualized therapy.

References

References

Aime, P., Sun, X., Zareen, N., Rao, A., Berman, Z., Volpicelli-Daley, L., Bernd, P., Crary, J. F., Levy, O. A., & Greene, L. A. (2015). Trib3 Is Elevated in Parkinson's Disease and Mediates Death in Parkinson's Disease Models. J Neurosci, 35(30), 10731-10749. https://doi.org/10.1523/JNEUROSCI.0614-15.2015

Amin MB, Edge SB, American Joint Committee on Cancer. (2017). AJCC Cancer Staging Manual. Springer. International Publishing https://link.springer.com/book/9783319406176

Baj, J., Korona-Glowniak, I., Forma, A., Maani, A., Sitarz, E., Rahnama-Hezavah, M., Radzikowska, E., & Portincasa, P. (2020). Mechanisms of the Epithelial-Mesenchymal Transition and Tumor Microenvironment in Helicobacter pylori-Induced Gastric Cancer. Cells, 9(4). https://doi.org/10.3390/cells9041055

Bao, X. Y., Sun, M., Peng, T. T., & Han, D. M. (2021). TRIB3 promotes proliferation, migration, and invasion of retinoblastoma cells by activating the AKT/mTOR signaling pathway. Cancer Biomark, 31(4), 307-315. https://doi.org/10.3233/CBM-200050

Barretina J, Caponigro G, Stransky N, Venkatesan K, Margolin AA, Kim S, Wilson CJ, Lehár J, Kryukov GV, Sonkin D, Reddy A, Liu M, Murray L, Berger MF, Monahan JE, Morais P, Meltzer J, Korejwa A, Jané-Valbuena J, Mapa FA, Thibault J, Bric-Furlong E, Raman P, Shipway A, Engels IH, Cheng J, Yu GK, Yu J, Aspesi P Jr, de Silva M, Jagtap K, Jones MD, Wang L, Hatton C, Palescandolo E, Gupta S, Mahan S, Sougnez C, Onofrio RC, Liefeld T, MacConaill L, Winckler W, Reich M, Li N, Mesirov JP, Gabriel SB, Getz G, Ardlie K, Chan V, Myer VE, Weber BL, Porter J, Warmuth M, Finan P, Harris JL, Meyerson M, Golub TR, Morrissey MP, Sellers WR, Schlegel R, Garraway LA. (2012). The Cancer Cell Line Encyclopedia enables predictive modelling of anticancer drug sensitivity. Nature. 483(7391):603-7. https://doi.org/10.1038/nature11003

Bauer, R. C., Sasaki, M., Cohen, D. M., Cui, J., Smith, M. A., Yenilmez, B. O., Steger, D. J., & Rader, D. J. (2015). Tribbles-1 regulates hepatic lipogenesis through posttranscriptional regulation of C/EBPalpha. J Clin Invest, 125(10), 3809-3818. https://doi.org/10.1172/JCI77095

Berx, G., Staes, K., van Hengel, J., Molemans, F., Bussemakers, M. J., van Bokhoven, A., & van Roy, F. (1995). Cloning and characterization of the human invasion suppressor gene E-cadherin (CDH1). Genomics, 26(2), 281-289. https://doi.org/10.1016/0888-7543(95)80212-5

Bezy, O., Vernochet, C., Gesta, S., Farmer, S. R., & Kahn, C. R. (2007). TRB3 blocks adipocyte differentiation through the inhibition of C/EBPbeta transcriptional activity. Mol Cell Biol, 27(19), 6818-6831. https://doi.org/10.1128/MCB.00375-07

Bisoffi, M., Klima, I., Gresko, E., Durfee, P. N., Hines, W. C., Griffith, J. K., Studer, U. E., & Thalmann, G. N. (2004). Expression profiles of androgen independent bone metastatic prostate cancer cells indicate up-regulation of the putative serine-threonine kinase GS3955. J Urol, 172(3), 1145-1150. https://doi.org/10.1097/01.ju.0000135117.40086.fa

Boige, V.; Pignon, J.; Saint-Aubert, B.; Lasser, P.; Conroy, T.; Bouché, O.; Segol, P.; Bedenne, L.; Rougier, P.; Ychou, M. (2007). Final results of a randomized trial comparing preoperative 5-fluorouracil (F)/cisplatin (P) to surgery alone in adenocarcinoma of stomach and lower esophagus (ASLE): FNLCC ACCORD07-FFCD 9703 trial. J. Clin. Oncol., 25, 4510

Cancer Genome Atlas Research, N. (2014). Comprehensive molecular characterization of gastric adenocarcinoma. Nature, 513(7517), 202-209. https://doi.org/10.1038/nature13480

Cerami E, Gao J, Dogrusoz U, Gross BE, Sumer SO, Aksoy BA, Jacobsen A, Byrne CJ, Heuer ML, Larsson E, Antipin Y, Reva B, Goldberg AP, Sander C, Schultz N. (2012). The cBio cancer genomics portal: an open platform for exploring multidimensional cancer genomics data. Cancer Discov. 2(5):401-4. https://doi.org/10.1158/2159-8290.CD-12-0095

Chandrashekar DS, Bashel B, Balasubramanya SAH, Creighton CJ, Ponce-Rodriguez I, Chakravarthi BVSK, Varambally S. (2017). UALCAN: A Portal for Facilitating Tumor Subgroup Gene Expression and Survival Analyses. Neoplasia. 19(8):649-658. https://doi.org/10.1016/j.neo.2017.05.002

Correa, P. (1992). Human gastric carcinogenesis: a multistep and multifactorial process--First American Cancer Society Award Lecture on Cancer

Epidemiology and Prevention. Cancer Res, 52(24), 6735-6740. https://www.ncbi.nlm.nih.gov/pubmed/1458460

Cunningham, D., Allum, W. H., Stenning, S. P., Thompson, J. N., Van de Velde, C. J., Nicolson, M., Scarffe, J. H., Lofts, F. J., Falk, S. J., Iveson, T. J., Smith, D. B., Langley, R. E., Verma, M., Weeden, S., Chua, Y. J., & Participants, M. T. (2006). Perioperative chemotherapy versus surgery alone for resectable gastroesophageal cancer. N Engl J Med, 355(1), 11-20. https://doi.org/10.1056/NEJMoa055531

Do, E. K., Park, J. K., Cheon, H. C., Kwon, Y. W., Heo, S. C., Choi, E. J., Seo, J. K., Jang, I. H., Lee, S. C., & Kim, J. H. (2017). Trib2 regulates the pluripotency of embryonic stem cells and enhances reprogramming efficiency. Exp Mol Med, 49(11), e401. https://doi.org/10.1038/emm.2017.191

Dong, S., Xia, J., Wang, H., Sun, L., Wu, Z., Bin, J., Liao, Y., Li, N., & Liao, W. (2016). Overexpression of TRIB3 promotes angiogenesis in human gastric cancer. Oncol Rep, 36(4), 2339-2348. https://doi.org/10.3892/or.2016.5017

Du, K., Herzig, S., Kulkarni, R. N., & Montminy, M. (2003). TRB3: a tribbles homolog that inhibits Akt/PKB activation by insulin in liver. Science, 300(5625), 1574-1577. https://doi.org/10.1126/science.1079817

Eyers, P. A., Keeshan, K., & Kannan, N. (2017). Tribbles in the 21st Century: The Evolving Roles of Tribbles Pseudokinases in Biology and Disease. Trends Cell Biol, 27(4), 284-298. https://doi.org/10.1016/j.tcb.2016.11.002

Ferreira, B. I., Santos, B., Link, W., & De Sousa-Coelho, A. L. (2021). Tribbles Pseudokinases in Colorectal Cancer. Cancers (Basel), 13(11). https://doi.org/10.3390/cancers13112825

Fitzgerald, R. C., Hardwick, R., Huntsman, D., Carneiro, F., Guilford, P., Blair, V., Chung, D. C., Norton, J., Ragunath, K., Van Krieken, J. H., Dwerryhouse, S., Caldas, C., & International Gastric Cancer Linkage, C. (2010). Hereditary diffuse gastric cancer: updated consensus guidelines for clinical management and directions for future research. J Med Genet, 47(7), 436-444. https://doi.org/10.1136/jmg.2009.074237

Flejou, J. F. (2011). [WHO Classification of digestive tumors: the fourth edition]. Ann Pathol, 31(5 Suppl), S27-31.

https://doi.org/10.1016/j.annpat.2011.08.001 (Classification OMS 2010 des tumeurs digestives: la quatrieme edition.)

Forman, D., & Burley, V. J. (2006). Gastric cancer: global pattern of the disease and an overview of environmental risk factors. Best Pract Res Clin Gastroenterol, 20(4), 633-649. https://doi.org/10.1016/j.bpg.2006.04.008

Gao J, Aksoy BA, Dogrusoz U, Dresdner G, Gross B, Sumer SO, Sun Y, Jacobsen A, Sinha R, Larsson E, Cerami E, Sander C, Schultz N. (2013). Integrative analysis of complex cancer genomics and clinical profiles using the cBioPortal. Sci Signal. 6(269):pl1. https://doi.org/10.1126/scisignal.2004088

Gholami, S., Cassidy, M. R., & Strong, V. E. (2017). Minimally Invasive Surgical Approaches to Gastric Resection. Surg Clin North Am, 97(2), 249-264. https://doi.org/10.1016/j.suc.2016.11.003

Grandinetti, K. B., Stevens, T. A., Ha, S., Salamone, R. J., Walker, J. R., Zhang, J., Agarwalla, S., Tenen, D. G., Peters, E. C., & Reddy, V. A. (2011). Overexpression of TRIB2 in human lung cancers contributes to tumorigenesis through downregulation of C/EBPalpha. Oncogene, 30(30), 3328-3335. https://doi.org/10.1038/onc.2011.57

Grosshans, J., & Wieschaus, E. (2000). A genetic link between morphogenesis and cell division during formation of the ventral furrow in Drosophila. Cell, 101(5), 523-531. https://doi.org/10.1016/s0092-8674(00)80862-4

Hansford, S., Kaurah, P., Li-Chang, H., Woo, M., Senz, J., Pinheiro, H., Schrader, K. A., Schaeffer, D. F., Shumansky, K., Zogopoulos, G., Santos, T. A., Claro, I., Carvalho, J., Nielsen, C., Padilla, S., Lum, A., Talhouk, A., Baker-Lange, K., Richardson, S., Lewis, I., Lindor, N. M., Pennell, E., MacMillan, A., Fernandez, B., Keller, G., Lynch, H., Shah, S. P., Guilford, P., Gallinger, S., Corso, G., Roviello, F., Caldas, C., Oliveira, C., Pharoah, P. D., & Huntsman, D. G. (2015). Hereditary Diffuse Gastric Cancer Syndrome: CDH1 Mutations and Beyond. JAMA Oncol, 1(1), 23-32. https://doi.org/10.1001/jamaoncol.2014.168

Hegedus, Z., Czibula, A., & Kiss-Toth, E. (2007). Tribbles: a family of kinase-like proteins with potent signalling regulatory function. Cell Signal, 19(2), 238-250. https://doi.org/10.1016/j.cellsig.2006.06.010

Hill, R., Kalathur, R. K., Colaco, L., Brandao, R., Ugurel, S., Futschik, M., & Link, W. (2015). TRIB2 as a biomarker for diagnosis and progression of melanoma. Carcinogenesis, 36(4), 469-477. https://doi.org/10.1093/carcin/bgv002

Hill, R., Madureira, P. A., Ferreira, B., Baptista, I., Machado, S., Colaco, L., Dos Santos, M., Liu, N., Dopazo, A., Ugurel, S., Adrienn, A., Kiss-Toth, E., Isbilen, M., Gure, A. O., & Link, W. (2017). TRIB2 confers resistance to anti-cancer therapy by activating the serine/threonine protein kinase AKT. Nat Commun, 8, 14687. https://doi.org/10.1038/ncomms14687

Hong, B., Zhou, J., Ma, K., Zhang, J., Xie, H., Zhang, K., Li, L., Cai, L., Zhang, N., Zhang, Z., & Gong, K. (2019). TRIB3 Promotes the Proliferation and Invasion of Renal Cell Carcinoma Cells via Activating MAPK Signaling Pathway. Int J Biol Sci, 15(3), 587-597. https://doi.org/10.7150/ijbs.29737

Hu, B., El Hajj, N., Sittler, S., Lammert, N., Barnes, R., & Meloni-Ehrig, A. (2012). Gastric cancer: Classification, histology and application of molecular pathology. J Gastrointest Oncol, 3(3), 251-261. https://doi.org/10.3978/j.issn.2078-6891.2012.021

Hua, F., Mu, R., Liu, J., Xue, J., Wang, Z., Lin, H., Yang, H., Chen, X., & Hu, Z. (2011). TRB3 interacts with SMAD3 promoting tumor cell migration and invasion. J Cell Sci, 124(Pt 19), 3235-3246. https://doi.org/10.1242/jcs.082875

Hua, F., Shang, S., Yang, Y. W., Zhang, H. Z., Xu, T. L., Yu, J. J., Zhou, D. D., Cui, B., Li, K., Lv, X. X., Zhang, X. W., Liu, S. S., Yu, J. M., Wang, F., Zhang, C., Huang, B., & Hu, Z. W. (2019). TRIB3 Interacts With beta-Catenin and TCF4 to Increase Stem Cell Features of Colorectal Cancer Stem Cells and Tumorigenesis. Gastroenterology, 156(3), 708-721 e715. https://doi.org/10.1053/j.gastro.2018.10.031

Huang, Q. R., & Pan, X. B. (2019). Prognostic lncRNAs, miRNAs, and mRNAs Form a Competing Endogenous RNA Network in Colon Cancer. Front Oncol, 9, 712. https://doi.org/10.3389/fonc.2019.00712

Huo, X., Yuan, K., Shen, Y., Li, M., Wang, Q., Xing, L., & Shi, G. (2014). Clinical value of magnetic resonance imaging in preoperative T staging of gastric cancer and postoperative pathological diagnosis. Oncol Lett, 8(1), 275-280. https://doi.org/10.3892/ol.2014.2135

Imai, S., Koizumi, S., Sugiura, M., Tokunaga, M., Uemura, Y., Yamamoto, N., Tanaka, S., Sato, E., & Osato, T. (1994). Gastric carcinoma: monoclonal epithelial malignant cells expressing Epstein-Barr virus latent infection protein. Proc Natl Acad Sci U S A, 91(19), 9131-9135. https://doi.org/10.1073/pnas.91.19.9131

Imajo, M., & Nishida, E. (2010). Human Tribbles homolog 1 functions as a negative regulator of retinoic acid receptor. Genes Cells, 15(10), 1089-1097. https://doi.org/10.1111/j.1365-2443.2010.01445.x

Johnston, F. M., & Beckman, M. (2019). Updates on Management of Gastric Cancer. Curr Oncol Rep, 21(8), 67. https://doi.org/10.1007/s11912-019-0820-4

Kathiresan, S., Melander, O., Guiducci, C., Surti, A., Burtt, N. P., Rieder, M. J., Cooper, G. M., Roos, C., Voight, B. F., Havulinna, A. S., Wahlstrand, B., Hedner, T., Corella, D., Tai, E. S., Ordovas, J. M., Berglund, G., Vartiainen, E., Jousilahti, P., Hedblad, B., Taskinen, M. R., Newton-Cheh, C., Salomaa, V., Peltonen, L., Groop, L., Altshuler, D. M., & Orho-Melander, M. (2008). Six new loci associated with blood low-density lipoprotein cholesterol, high-density lipoprotein cholesterol or triglycerides in humans. Nat Genet, 40(2), 189-197. https://doi.org/10.1038/ng.75

Keeshan, K., Bailis, W., Dedhia, P. H., Vega, M. E., Shestova, O., Xu, L., Toscano, K., Uljon, S. N., Blacklow, S. C., & Pear, W. S. (2010). Transformation by Tribbles homolog 2 (Trib2) requires both the Trib2 kinase domain and COP1 binding. Blood, 116(23), 4948-4957. https://doi.org/10.1182/blood-2009-10-247361

Keeshan, K., He, Y., Wouters, B. J., Shestova, O., Xu, L., Sai, H., Rodriguez, C. G., Maillard, I., Tobias, J. W., Valk, P., Carroll, M., Aster, J. C., Delwel, R., & Pear, W. S. (2006). Tribbles homolog 2 inactivates C/EBPalpha and causes acute myelogenous leukemia. Cancer Cell, 10(5), 401-411. https://doi.org/10.1016/j.ccr.2006.09.012

Khatoon, J., Rai, R. P., & Prasad, K. N. (2016). Role of Helicobacter pylori in gastric cancer: Updates. World J Gastrointest Oncol, 8(2), 147-158. https://doi.org/10.4251/wjgo.v8.i2.147

Kiss-Toth, E., Wyllie, D. H., Holland, K., Marsden, L., Jozsa, V., Oxley, K. M., Polgar, T., Qwarnstrom, E. E., & Dower, S. K. (2006). Functional mapping

and identification of novel regulators for the Toll/Interleukin-1 signalling network by transcription expression cloning. Cell Signal, 18(2), 202-214. https://doi.org/10.1016/j.cellsig.2005.04.012

Kotzev, A. I., & Draganov, P. V. (2018). Carbohydrate Antigen 19-9, Carcinoembryonic Antigen, and Carbohydrate Antigen 72-4 in Gastric Cancer: Is the Old Band Still Playing? Gastrointest Tumors, 5(1-2), 1-13. https://doi.org/10.1159/000488240

Lauren, P. (1965). The Two Histological Main Types of Gastric Carcinoma: Diffuse and So-Called Intestinal-Type Carcinoma. An Attempt at a Histo-Clinical Classification. Acta Pathol Microbiol Scand, 64, 31-49. https://doi.org/10.1111/apm.1965.64.1.31

Li B, Dewey CN. (2011). RSEM: accurate transcript quantification from RNA-Seq data with or without a reference genome. BMC Bioinformatics. 12:323. https://doi.org/10.1186/1471-2105-12-323

Liang KL, Paredes R, Carmody R, Eyers PA, Meyer S, McCarthy TV, Keeshan K. (2016). Human TRIB2 Oscillates during the Cell Cycle and Promotes Ubiquitination and Degradation of CDC25C. Int J Mol Sci. 17(9):1378 https://doi.org/10.3390/ijms17091378

Lin, Z. Y., Huang, Y. Q., Zhang, Y. Q., Han, Z. D., He, H. C., Ling, X. H., Fu, X., Dai, Q. S., Cai, C., Chen, J. H., Liang, Y. X., Jiang, F. N., Zhong, W. D., Wang, F., & Wu, C. L. (2014). MicroRNA-224 inhibits progression of human prostate cancer by downregulating TRIB1. Int J Cancer, 135(3), 541-550. https://doi.org/10.1002/ijc.28707

Lohan, F., & Keeshan, K. (2013). The functionally diverse roles of tribbles. Biochem Soc Trans, 41(4), 1096-1100. https://doi.org/10.1042/BST20130105

Machlowska, J., Baj, J., Sitarz, M., Maciejewski, R., & Sitarz, R. (2020). Gastric Cancer: Epidemiology, Risk Factors, Classification, Genomic Characteristics and Treatment Strategies. Int J Mol Sci, 21(11). https://doi.org/10.3390/ijms21114012

Majewski IJ, Kluijt I, Cats A, Scerri TS, de Jong D, Kluin RJ, Hansford S, Hogervorst FB, Bosma AJ, Hofland I, Winter M, Huntsman D, Jonkers J, Bahlo M, Bernards R. (2013). An α-E-catenin (CTNNA1) mutation in

hereditary diffuse gastric cancer. J Pathol. 229(4):621-9. https://doi.org/10.1002/path.4152

Makino, S., Takahashi, H., Okuzaki, D., Miyoshi, N., Haraguchi, N., Hata, T., Matsuda, C., Yamamoto, H., Mizushima, T., Mori, M., & Doki, Y. (2020). DCLK1 integrates induction of TRIB3, EMT, drug resistance and poor prognosis in colorectal cancer. Carcinogenesis, 41(3), 303-312. https://doi.org/10.1093/carcin/bgz157

Marin, J. J., Al-Abdulla, R., Lozano, E., Briz, O., Bujanda, L., Banales, J. M., & Macias, R. I. (2016). Mechanisms of Resistance to Chemotherapy in Gastric Cancer. Anticancer Agents Med Chem, 16(3), 318-334. https://doi.org/10.2174/1871520615666150803125121

Mata, J., Curado, S., Ephrussi, A., & Rorth, P. (2000). Tribbles coordinates mitosis and morphogenesis in Drosophila by regulating string/CDC25 proteolysis. Cell, 101(5), 511-522. https://doi.org/10.1016/s0092-8674(00)80861-2

Mayoral-Varo V, Jiménez L, Link W. (2021). The Critical Role of TRIB2 in Cancer and Therapy Resistance. Cancers (Basel). 13(11):2701. https://doi.org/10.3390/cancers1311270

Mayumi-Matsuda, K., Kojima, S., Suzuki, H., & Sakata, T. (1999). Identification of a novel kinase-like gene induced during neuronal cell death. Biochem Biophys Res Commun, 258(2), 260-264. https://doi.org/10.1006/bbrc.1999.0576

Menyhart, O., Kakisaka, T., Pongor, L. S., Uetake, H., Goel, A., & Gyorffy, B. (2019). Uncovering Potential Therapeutic Targets in Colorectal Cancer by Deciphering Mutational Status and Expression of Druggable Oncogenes. Cancers (Basel), 11(7). https://doi.org/10.3390/cancers11070983

Mistry J, Chuguransky S, Williams L, Qureshi M, Salazar GA, Sonnhammer ELL, Tosatto SCE, Paladin L, Raj S, Richardson LJ, Finn RD, Bateman A. (2021). Pfam: The protein families database in 2021. Nucleic Acids Res. 49(D1):D412-D419. https://doi.org/10.1093/nar/gkaa913

Mocellin, S., & Pasquali, S. (2015). Diagnostic accuracy of endoscopic ultrasonography (EUS) for the preoperative locoregional staging of primary gastric cancer. Cochrane Database Syst Rev(2), CD009944. https://doi.org/10.1002/14651858.CD009944.pub2

Nakayama, K., & Iwamoto, S. (2017). An adaptive variant of TRIB2, rs1057001, is associated with higher expression levels of thermogenic genes in human subcutaneous and visceral adipose tissues. J Physiol Anthropol, 36(1), 16. https://doi.org/10.1186/s40101-017-0132-z

Niikura, R., Hirata, Y., Hayakawa, Y., Kawahara, T., Yamada, A., & Koike, K. (2020). Effect of aspirin use on gastric cancer incidence and survival: A systematic review and meta-analysis. JGH Open, 4(2), 117-125. https://doi.org/10.1002/jgh3.12226

O'Connor, C., Yalla, K., Salome, M., Moka, H. A., Castaneda, E. G., Eyers, P. A., & Keeshan, K. (2018). Trib2 expression in granulocyte-monocyte progenitors drives a highly drug resistant acute myeloid leukaemia linked to elevated Bcl2. Oncotarget, 9(19), 14977-14992. https://doi.org/10.18632/oncotarget.24525

Offerhaus, G. J., Tersmette, A. C., Huibregtse, K., van de Stadt, J., Tersmette, K. W., Stijnen, T., Hoedemaeker, P. J., Vandenbroucke, J. P., & Tytgat, G. N. (1988). Mortality caused by stomach cancer after remote partial gastrectomy for benign conditions: 40 years of follow up of an Amsterdam cohort of 2633 postgastrectomy patients. Gut, 29(11), 1588-1590. https://doi.org/10.1136/gut.29.11.1588

Plummer, M., Franceschi, S., Vignat, J., Forman, D., & de Martel, C. (2015). Global burden of gastric cancer attributable to Helicobacter pylori. Int J Cancer, 136(2), 487-490. https://doi.org/10.1002/ijc.28999

Polom K, Marano L, Marrelli D, De Luca R, Roviello G, Savelli V, Tan P, Roviello F. (2018). Meta-analysis of microsatellite instability in relation to clinicopathological characteristics and overall survival in gastric cancer. Br J Surg. 105(3):159-167. https://doi.org/10.1002/bjs.10663

Praud, D., Rota, M., Pelucchi, C., Bertuccio, P., Rosso, T., Galeone, C., Zhang, Z. F., Matsuo, K., Ito, H., Hu, J., Johnson, K. C., Yu, G. P., Palli, D., Ferraroni, M., Muscat, J., Lunet, N., Peleteiro, B., Malekzadeh, R., Ye, W., Song, H., Zaridze, D., Maximovitch, D., Aragones, N., Castano-Vinyals, G., Vioque, J., Navarrete-Munoz, E. M., Pakseresht, M., Pourfarzi, F., Wolk, A., Orsini, N., Bellavia, A., Hakansson, N., Mu, L., Pastorino, R., Kurtz, R. C., Derakhshan, M. H., Lagiou, A., Lagiou, P., Boffetta, P., Boccia, S., Negri, E., & La Vecchia, C. (2018). Cigarette smoking and

gastric cancer in the Stomach Cancer Pooling (StoP) Project. Eur J Cancer Prev, 27(2), 124-133. https://doi.org/10.1097/CEJ.0000000000000290

Prudente, S., Scarpelli, D., Chandalia, M., Zhang, Y. Y., Morini, E., Del Guerra, S., Perticone, F., Li, R., Powers, C., Andreozzi, F., Marchetti, P., Dallapiccola, B., Abate, N., Doria, A., Sesti, G., & Trischitta, V. (2009). The TRIB3 Q84R polymorphism and risk of early-onset type 2 diabetes. J Clin Endocrinol Metab, 94(1), 190-196. https://doi.org/10.1210/jc.2008-1365

Puiffe, M. L., Le Page, C., Filali-Mouhim, A., Zietarska, M., Ouellet, V., Tonin, P. N., Chevrette, M., Provencher, D. M., & Mes-Masson, A. M. (2007). Characterization of ovarian cancer ascites on cell invasion, proliferation, spheroid formation, and gene expression in an in vitro model of epithelial ovarian cancer. Neoplasia, 9(10), 820-829. https://doi.org/10.1593/neo.07472

Puskas, L. G., Juhasz, F., Zarva, A., Hackler, L., Jr., & Farid, N. R. (2005). Gene profiling identifies genes specific for well-differentiated epithelial thyroid tumors. Cell Mol Biol (Noisy-le-grand), 51(2), 177-186. https://www.ncbi.nlm.nih.gov/pubmed/16171553

Qi, L., Heredia, J. E., Altarejos, J. Y., Screaton, R., Goebel, N., Niessen, S., Macleod, I. X., Liew, C. W., Kulkarni, R. N., Bain, J., Newgard, C., Nelson, M., Evans, R. M., Yates, J., & Montminy, M. (2006). TRB3 links the E3 ubiquitin ligase COP1 to lipid metabolism. Science, 312(5781), 1763-1766. https://doi.org/10.1126/science.1123374

Richmond, L., & Keeshan, K. (2020). Pseudokinases: a tribble-edged sword. FEBS J, 287(19), 4170-4182. https://doi.org/10.1111/febs.15096

Rosenbaum, S. J., Stergar, H., Antoch, G., Veit, P., Bockisch, A., & Kuhl, H. (2006). Staging and follow-up of gastrointestinal tumors with PET/CT. Abdom Imaging, 31(1), 25-35. https://doi.org/10.1007/s00261-005-0031-3

Sakai S, Miyajima C, Uchida C, Itoh Y, Hayashi H, Inoue Y. (2016). Tribbles-Related Protein Family Members as Regulators or Substrates of the Ubiquitin-Proteasome System in Cancer Development. Curr Cancer Drug Targets. 16(2):147-56 https://doi.org/10.2174/1568009616666151112122645

Salazar, M., Lorente, M., Garcia-Taboada, E., Perez Gomez, E., Davila, D., Zuniga-Garcia, P., Maria Flores, J., Rodriguez, A., Hegedus, Z., Mosen-Ansorena, D., Aransay, A. M., Hernandez-Tiedra, S., Lopez-Valero, I., Quintanilla, M., Sanchez, C., Iovanna, J. L., Dusetti, N., Guzman, M., Francis, S. E., Carracedo, A., Kiss-Toth, E., & Velasco, G. (2015). Loss of Tribbles pseudokinase-3 promotes Akt-driven tumorigenesis via FOXO inactivation. Cell Death Differ, 22(1), 131-144. https://doi.org/10.1038/cdd.2014.133

Saleem, S., & Biswas, S. C. (2017). Tribbles Pseudokinase 3 Induces Both Apoptosis and Autophagy in Amyloid-beta-induced Neuronal Death. J Biol Chem, 292(7), 2571-2585. https://doi.org/10.1074/jbc.M116.744730

Salome, M., Hopcroft, L., & Keeshan, K. (2018). Inverse and correlative relationships between TRIBBLES genes indicate non-redundant functions during normal and malignant hemopoiesis. Exp Hematol, 66, 63-78 e13. https://doi.org/10.1016/j.exphem.2018.07.005

Scheidbach H, Lippert H, Meyer F. (2010). Gastric carcinoma: when is palliative gastrectomy justified? Oncol Rev. 4(2):127–132. https://doi.org/10.1007/s12156-010-0046-z).

Simoni, L., Delgado, V., Ruer-Laventie, J., Bouis, D., Soley, A., Heyer, V., Robert, I., Gies, V., Martin, T., Korganow, A. S., Reina-San-Martin, B., & Soulas-Sprauel, P. (2018). Trib1 Is Overexpressed in Systemic Lupus Erythematosus, While It Regulates Immunoglobulin Production in Murine B Cells. Front Immunol, 9, 373. https://doi.org/10.3389/fimmu.2018.00373

Singh, P. P., & Singh, S. (2013). Statins are associated with reduced risk of gastric cancer: a systematic review and meta-analysis. Ann Oncol, 24(7), 1721-1730. https://doi.org/10.1093/annonc/mdt150

Sitarz, R., Skierucha, M., Mielko, J., Offerhaus, G. J. A., Maciejewski, R., & Polkowski, W. P. (2018). Gastric cancer: epidemiology, prevention, classification, and treatment. Cancer Manag Res, 10, 239-248. https://doi.org/10.2147/CMAR.S149619

Smyth EC, Nilsson M, Grabsch HI, van Grieken NC, Lordick F. (2020). Gastric cancer. Lancet.396(10251):635-648. https://doi.org/10.1016/S0140-6736(20)31288-5

Sun, M., Qiu, J., Zhai, H., Wang, Y., Ma, P., Li, M., & Chen, B. (2020). Prognostic Implications of Novel Gene Signatures in Gastric Cancer Microenvironment. Med Sci Monit, 26, e924604. https://doi.org/10.12659/MSM.924604

Sung, H. Y., Francis, S. E., Crossman, D. C., & Kiss-Toth, E. (2006). Regulation of expression and signalling modulator function of mammalian tribbles is cell-type specific. Immunol Lett, 104(1-2), 171-177. https://doi.org/10.1016/j.imlet.2005.11.010

Sung, H., Ferlay, J., Siegel, R. L., Laversanne, M., Soerjomataram, I., Jemal, A., & Bray, F. (2021). Global Cancer Statistics 2020: GLOBOCAN Estimates of Incidence and Mortality Worldwide for 36 Cancers in 185 Countries. CA Cancer J Clin, 71(3), 209-249. https://doi.org/10.3322/caac.21660

Takada, K. (2000). Epstein-Barr virus and gastric carcinoma. Mol Pathol, 53(5), 255-261. https://doi.org/10.1136/mp.53.5.255

Tang, B., Wu, W., Zhang, Q., Sun, Y., Cui, Y., Wu, F., Wei, X., Qi, G., Liang, X., Tang, F., Li, Y., & Fan, W. (2015). Inhibition of tribbles protein-1 attenuates radioresistance in human glioma cells. Sci Rep, 5, 15961. https://doi.org/10.1038/srep15961

Tang, K., Finley, R. L., Jr., Nie, D., & Honn, K. V. (2000). Identification of 12-lipoxygenase interaction with cellular proteins by yeast two-hybrid screening. Biochemistry, 39(12), 3185-3191. https://doi.org/10.1021/bi992664v

Thrift, A. P., & Nguyen, T. H. (2021). Gastric Cancer Epidemiology. Gastrointest Endosc Clin N Am, 31(3), 425-439. https://doi.org/10.1016/j.giec.2021.03.001

Tian Y, Wan H, Lin Y, Xie X, Li Z, Tan G. (2013). Androgen receptor may be responsible for gender disparity in gastric cancer. Med Hypotheses. 80(5):672-4. https://doi.org/10.1016/j.mehy.2013.01.023

Wang, J., Park, J. S., Wei, Y., Rajurkar, M., Cotton, J. L., Fan, Q., Lewis, B. C., Ji, H., & Mao, J. (2013). TRIB2 acts downstream of Wnt/TCF in liver cancer cells to regulate YAP and C/EBPalpha function. Mol Cell, 51(2), 211-225. https://doi.org/10.1016/j.molcel.2013.05.013

Wang, J., Zuo, J., Wahafu, A., Wang, M. D., Li, R. C., & Xie, W. F. (2020). Combined elevation of TRIB2 and MAP3K1 indicates poor prognosis and chemoresistance to temozolomide in glioblastoma. CNS Neurosci Ther, 26(3), 297-308. https://doi.org/10.1111/cns.13197

Wang, K., Yuen, S. T., Xu, J., Lee, S. P., Yan, H. H., Shi, S. T., Siu, H. C., Deng, S., Chu, K. M., Law, S., Chan, K. H., Chan, A. S., Tsui, W. Y., Ho, S. L., Chan, A. K., Man, J. L., Foglizzo, V., Ng, M. K., Chan, A. S., Ching, Y. P., Cheng, G. H., Xie, T., Fernandez, J., Li, V. S., Clevers, H., Rejto, P. A., Mao, M., & Leung, S. Y. (2014). Whole-genome sequencing and comprehensive molecular profiling identify new driver mutations in gastric cancer. Nat Genet, 46(6), 573-582. https://doi.org/10.1038/ng.2983

Wang, P. L., Xiao, F. T., Gong, B. C., & Liu, F. N. (2017). Alcohol drinking and gastric cancer risk: a meta-analysis of observational studies. Oncotarget, 8(58), 99013-99023. https://doi.org/10.18632/oncotarget.20918

Wang, S., Wang, C., Li, X., Hu, Y., Gou, R., Guo, Q., Nie, X., Liu, J., Zhu, L., & Lin, B. (2020). Down-regulation of TRIB3 inhibits the progression of ovarian cancer via MEK/ERK signaling pathway. Cancer Cell Int, 20, 418. https://doi.org/10.1186/s12935-020-01509-z

Wang, X. J., Li, F. F., Zhang, Y. J., Jiang, M., & Ren, W. H. (2020). TRIB3 promotes hepatocellular carcinoma growth and predicts poor prognosis. Cancer Biomark, 29(3), 307-315. https://doi.org/10.3233/CBM-201577

Warren, J. R., & Marshall, B. (1983). Unidentified curved bacilli on gastric epithelium in active chronic gastritis. Lancet, 1(8336), 1273-1275. https://www.ncbi.nlm.nih.gov/pubmed/6134060

Wei, S. C., Rosenberg, I. M., Cao, Z., Huett, A. S., Xavier, R. J., & Podolsky, D. K. (2012). Tribbles 2 (Trib2) is a novel regulator of toll-like receptor 5 signaling. Inflamm Bowel Dis, 18(5), 877-888. https://doi.org/10.1002/ibd.22883

Wennemers, M., Bussink, J., Scheijen, B., Nagtegaal, I. D., van Laarhoven, H. W., Raleigh, J. A., Varia, M. A., Heuvel, J. J., Rouschop, K. M., Sweep, F. C., & Span, P. N. (2011). Tribbles homolog 3 denotes a poor prognosis in breast cancer and is involved in hypoxia response. Breast Cancer Res, 13(4), R82. https://doi.org/10.1186/bcr2934

Wilkin, F., Suarez-Huerta, N., Robaye, B., Peetermans, J., Libert, F., Dumont, J. E., & Maenhaut, C. (1997). Characterization of a phosphoprotein whose mRNA is regulated by the mitogenic pathways in dog thyroid cells. Eur J Biochem, 248(3), 660-668. https://doi.org/10.1111/j.1432-1033.1997.t01-1-00660.x

Willer, C. J., Sanna, S., Jackson, A. U., Scuteri, A., Bonnycastle, L. L., Clarke, R., Heath, S. C., Timpson, N. J., Najjar, S. S., Stringham, H. M., Strait, J., Duren, W. L., Maschio, A., Busonero, F., Mulas, A., Albai, G., Swift, A. J., Morken, M. A., Narisu, N., Bennett, D., Parish, S., Shen, H., Galan, P., Meneton, P., Hercberg, S., Zelenika, D., Chen, W. M., Li, Y., Scott, L. J., Scheet, P. A., Sundvall, J., Watanabe, R. M., Nagaraja, R., Ebrahim, S., Lawlor, D. A., Ben-Shlomo, Y., Davey-Smith, G., Shuldiner, A. R., Collins, R., Bergman, R. N., Uda, M., Tuomilehto, J., Cao, A., Collins, F. S., Lakatta, E., Lathrop, G. M., Boehnke, M., Schlessinger, D., Mohlke, K. L., & Abecasis, G. R. (2008). Newly identified loci that influence lipid concentrations and risk of coronary artery disease. Nat Genet, 40(2), 161-169. https://doi.org/10.1038/ng.76

Wu, H. L., Duan, Z. T., Jiang, Z. D., Cao, W. J., Wang, Z. B., Hu, K. W., Gao, X., Wang, S. K., He, B. S., Zhang, Z. Y., & Xie, H. G. (2013). Increased endoplasmic reticulum stress response is involved in clopidogrel-induced apoptosis of gastric epithelial cells. PLoS One, 8(9), e74381. https://doi.org/10.1371/journal.pone.0074381

Wu, I. J., Lin, R. J., Wang, H. C., Yuan, T. M., & Chuang, S. M. (2017). TRIB3 downregulation enhances doxorubicin-induced cytotoxicity in gastric cancer cells. Arch Biochem Biophys, 622, 26-35. https://doi.org/10.1016/j.abb.2017.04.008

Wu, M., Xu, L. G., Zhai, Z., & Shu, H. B. (2003). SINK is a p65-interacting negative regulator of NF-kappaB-dependent transcription. J Biol Chem, 278(29), 27072-27079. https://doi.org/10.1074/jbc.M209814200

Yang, H., Jin, W., Liu, H., Gan, D., Cui, C., Han, C., & Wang, Z. (2020). Immune-Related Prognostic Model in Colon Cancer: A Gene Expression-Based Study. Front Genet, 11, 401. https://doi.org/10.3389/fgene.2020.00401

Yokoyama, T., & Nakamura, T. (2011). Tribbles in disease: Signaling pathways important for cellular function and neoplastic transformation. Cancer Sci, 102(6), 1115-1122. https://doi.org/10.1111/j.1349-7006.2011.01914.x

Yokoyama, T., Kanno, Y., Yamazaki, Y., Takahara, T., Miyata, S., & Nakamura, T. (2010). Trib1 links the MEK1/ERK pathway in myeloid leukemogenesis. Blood, 116(15), 2768-2775. https://doi.org/10.1182/blood-2009-10-246264

Zhang, Y., Davis, J. L., & Li, W. (2005). Identification of tribbles homolog 2 as an autoantigen in autoimmune uveitis by phage display. Mol Immunol, 42(11), 1275-1281. https://doi.org/10.1016/j.molimm.2004.11.020

Zhao, X., Xu, L., Zheng, L., Yin, L., Qi, Y., Han, X., Xu, Y., & Peng, J. (2016). Potent effects of dioscin against gastric cancer in vitro and in vivo. Phytomedicine, 23(3), 274-282. https://doi.org/10.1016/j.phymed.2016.01.012

Zhou, H., Luo, Y., Chen, J. H., Hu, J., Luo, Y. Z., Wang, W., Zeng, Y., & Xiao, L. (2013). Knockdown of TRB3 induces apoptosis in human lung adenocarcinoma cells through regulation of Notch 1 expression. Mol Med Rep, 8(1), 47-52. https://doi.org/10.3892/mmr.2013.1453

Zhu, P., Xue, J., Zhang, Z. J., Jia, Y. P., Tong, Y. N., Han, D., Li, Q., Xiang, Y., Mao, X. H., & Tang, B. (2017). Helicobacter pylori VacA induces autophagic cell death in gastric epithelial cells via the endoplasmic reticulum stress pathway. Cell Death Dis, 8(12), 3207. https://doi.org/10.1038/s41419-017-0011-x

List of original manuscripts

- Mohr H, **Foscarini A**, Steiger K, Ballke S, Rischpler C, Schilling F, Pellegata NS. Imaging pheochromocytoma in small animals: preclinical models to improve diagnosis and treatment. EJNMMI Res. 2021 Dec 11;11(1):121. doi: 10.1186/s13550-021-00855-x. PMID: 34894301. *Pdf of this paper is included.*

- Gulde S, **Foscarini A**, April-Monn SL, Toledo R, Schrader J, Schiavo Lena M, Partelli S, Perren A, Marinoni I, Pellegata NS. Targeting PI3K and CDK4/6 shows synergistic antitumor effects in pancreatic neuroendocrine tumors. *In preparation*.

- **Foscarini A**, Tricarico R, De Martino D, Mohr H, Gentile F, Gulde S, Vanoli A, Ranzani GN*, Pellegata NS*. Functional characterization of *TRIB2* pseudokinase points to a tumor suppressor role in gastric cancer. *Co-corresponding authors. *In preparation*.

Acknowledgements

I would like to thank Prof. G. Nadia Ranzani, who always supported me since I was a master student and who gave me the opportunity to pursue my PhD under her supervision. She taught me to think as a researcher and I will always be grateful to her for this.

An equal weight of gratitude goes to Prof. Natalia S. Pellegata, who welcomed me in her laboratory, and to the members of the NET group. In the same way she supported and encouraged me during these three years.

Another big thank you is for Dr. Rossella Tricarico, who helped me with the experiment and the thesis, with her example she taught me to never give up.

EJNMMI Research

REVIEW

Open Access

Imaging pheochromocytoma in small animals: preclinical models to improve diagnosis and treatment

Hermine Mohr[1,2], Alessia Foscarini[1], Katja Steiger[3], Simone Ballke[3], Christoph Rischpler[4], Franz Schilling[4] and Natalia S. Pellegata[1,2,5*]

Abstract

Pheochromocytomas (PCCs) and paragangliomas (PGLs), together referred to as PPGLs, are rare chromaffin cell-derived tumors. They require timely diagnosis as this is the only way to achieve a cure through surgery and because of the potentially serious cardiovascular complications and sometimes life-threatening comorbidities that can occur if left untreated. The biochemical diagnosis of PPGLs has improved over the last decades, and the knowledge of the underlying genetics has dramatically increased. In addition to conventional anatomical imaging by CT and MRI for PPGL detection, new functional imaging modalities have emerged as very useful for patient surveillance and stratification for therapy. The availability of validated and predictive animal models of cancer is essential for translating molecular, imaging and therapy response findings from the bench to the bedside. This is especially true for rare tumors, such as PPGLs, for which access to large cohorts of patients is limited. There are few animal models of PPGLs that have been instrumental in refining imaging modalities for early tumor detection, as well as in identifying and evaluating novel imaging tracers holding promise for the detection and/or treatment of human PPGLs. The in vivo PPGL models mainly include xenografts/allografts generated by engrafting rat or mouse cell lines, as no representative human cell line is available. In addition, there is a model of endogenous PCCs (i.e., MENX rats) that was characterized in our laboratory. In this review, we will summarize the contribution that various representative models of PPGL have given to the visualization of these tumors in vivo and we present an example of a tracer first evaluated in MENX rats, and then translated to the detection of these tumors in human patients. In addition, we will illustrate briefly the potential of ex vivo biological imaging of intact adrenal glands in MENX rats.

Keywords: Positron emission tomography, Paraganglioma, ^{18}F-LMI1195, ^{68}GA-DOTATATE, Xenograft, MSOT, Norepinephrine transporter, MENX-affected rats

Background

Pheochromocytomas (PCCs) and paragangliomas (PGLs) are catecholamine-secreting tumors arising from the transformation of neural crest-derived chromaffin cells located in the adrenal medulla or in paravertebral autonomic ganglia, respectively. These tumors are together referred to as PPGLs. The first-line and sole curative treatment for PPGLs is surgery, but subsequent recurrence or metastatic spread always remains possible. For inoperable metastatic disease, there is no approved medical therapy in Europe, although molecular targeted therapies are currently being investigated. For slow-progressing PPGLs, radionuclide therapy using [^{177}Lu]-1,4,7,10-tetraazacyclododecane-tetraacetic acid (DOTA)-Tyr3-octreotide (DOTATATE) or [^{131}I]-Meta-iodobenzylguanidine (MIBG) is the preferred first-line therapy, with the latter being the only approved

*Correspondence: natalia.pellegata@helmholtz-muenchen.de
[1] Institute for Diabetes and Cancer, Helmholtz Zentrum München, Ingolstaedter Landstrasse 1, 85764 Neuherberg, Germany
Full list of author information is available at the end of the article

therapy in the USA [1]. However, the former treatment only works if tumors express somatostatin receptor 2 (SSTR2), and the latter has variable efficacy as outlines below. For rapidly progressing metastatic PPGLs, chemotherapy is the recommended first-line option but has shown limited success.

PPGLs cause unspecific symptoms in patients, and this can hamper their timely diagnosis. Hypertension, headaches, palpitation and diaphoresis are most often reported [2]. However, patients can also present with anxiety, nausea, new onset of diabetes, weakness, pallor, flushing, abdominal chest pains or orthostatic hypotension. Yet, none of these symptoms alone clearly points to the presence of PPGLs, hence, this disease gained the title "the great mimic" [3]. The lack of specific symptoms, combined with the fact that these tumors are uncommon, makes it difficult for clinicians to suspect PPGLS as the underlying cause. Given the severe comorbidities associated with undiagnosed/untreated PPGLs, it is important to develop sensitive and specific tools for their early diagnosis.

Chromaffin cells naturally produce norepinephrine, epinephrine and dopamine. In PPGL patients, the levels of these catecholamines are, with some exceptions, strongly enhanced. Based on recent guidelines, PPGLs are initially diagnosed by the assessment of elevated levels of catecholamines or their metabolites (metanephrines), being the measurement of plasma-free or urinary fractioned metanephrines the most reliable method [4]. While norepinephrine- and epinephrine-overproducing tumors can be reliably identified by the detection of metanephrines, the much rarer dopamine-producing PPGLs need an additional test assessing the increase in circulating levels of methoxytyramine, the O-methylated metabolite of dopamine [5]. A positive biochemical diagnosis of PPGL is usually followed by localization of the tumor using imaging techniques, such as computed tomography (CT), T2-weighted magnetic resonance imaging (MRI), [^{123}I]-MIBG scintigraphy and, more recently, by functional positron emission tomography (PET) imaging [6] (see below).

Subtypes of PPGL

Over 30–40% of PPGL patients carry germline mutations in at least 25 cancer susceptibility genes, and additional 35–40% of cases associate with somatic driver mutations, so that about 70% of PPGLs is genetically defined. The underlying mutations associate with specific gene expression signatures. Based on these signatures, PPGLs were classified into three main subtypeswere classified into three main subtypes: a pseudohypoxic, a kinase signaling and a Wnt-altered cluster. These clusters are associated with specific genetic mutations, catecholamine secretion profiles and a variable risk of metastases [7]. The pseudohypoxic cluster comprises tumors having mutations in, e.g., *SDHA*, *SDHB*, *SDHD*, *VHL* and *EPAS1* genes, and typically consists of norepinephrine- and dopamine-producing tumors. PPGLs of the pseudohypoxic cluster have a higher risk to metastasize than those belonging to the other clusters. Mutations in, e.g., *NF1*, *RET*, *TMEM127* and *HRAS* cause PPGLs belonging to the kinase signaling cluster and having mostly an adrenergic biochemical phenotype. PPGLs of this subtype are usually benign, but show a high degree of recurrence and tumor multiplicity [8]. The most recently identified subcluster is the Wnt-altered one, for which only sporadic mutations in *CSED1* and *MAML3* have been described as the underlying genetic cause. The Wnt-altered cluster displays a mixed biochemical profile, having both adrenergic and noradrenergic phenotypes. Based on the TCGA study on the molecular characterization of PPGLs, the most extensive to date, pseudohypoxic tumors account for over 30% of cases, those with a kinase activation profile for over 20% and those in the Wnt subcluster for less than 10% [7].

Diagnosis of PPGL by anatomical and functional imaging

While it has been estimated that PPGLs are the underlying cause in 0.1 to 1% of all hypertensive patients, about 25% of all PPGL are incidentally discovered during imaging studies for unrelated disorders [9]. Moreover, in 0.05–0.1% of autopsy examinations, PPGLs were detected that were not diagnosed during the lifetime of the diseased persons [10]. It needs to be considered that undiagnosed PPGLs can carry relevant morbidity, can cause significant comorbidities, may lead to fatal complications during anesthesia (preformed to treat other disorders) or can cause the fatal shock syndrome. In contrast, the prognosis for PPGLs that are detected at an early stage is very good, thereby supporting the need for tools that allow a timely diagnosis and accurate staging of these tumors.

Although biochemical tests have high predictive value for the presence of PPGLs, so that subtype, size and even tumor location (adrenal, extra-adrenal) of the primary tumor may be inferred from these data [5], further validation by imaging modalities is recommended [11]. Anatomical imaging, such as CT or MRI, should be considered as the first choice to identify the location of the tumor, as indicated in the recent European Association of Nuclear Medicine (EANM) guidelines for imaging PPGLs [12]. Precise knowledge of the tumor location is necessary to guide surgery, the only curative treatment for most PPGLs. However, the diagnosis of PPGLs by anatomical imaging can be very challenging. Indeed, benign pathological changes in the adrenal glands may be misdiagnosed as tumors [13]. Substantial improvements in the diagnosis of PPGLs could be obtained by

combining anatomical with functional imaging, hence several modalities have been developed that take advantage of the expression of specific receptors or transport systems in chromaffin cells. Depending on genetic risk factors, molecular cluster, size and location of the original tumor, additional functional imaging scans or postsurgical follow-up screens are recommended [4]. The current functional imaging tracers available for PPGLs can be grouped in four major classes depending on the targeted processes/molecules: (1) catecholamine metabolism/norepinephrine transporter expression; (2) somatostatin receptors (SSTRs); (3) glucose uptake; and (4) amino acid uptake (Fig. 1). Up to recently, the gold standard imaging approach to detect PPGLs was scintigraphy with [^{123}I]-MIBG a norepinephrine analog, which is taken up by chromaffin cells via the norepinephrine transport (NET) system [14]. Comparison among tumors belonging to the various clusters, as well as of benign *versus* metastatic PPGLs, revealed varying sensitivities toward the individual tracers [15]. Therefore, beyond localization, the imaging signature obtained by functional imaging can help in cluster-specific patients stratification in view of subsequent intervention by targeted therapy or radionuclide therapy [16]. Given that the various PPGL subtypes show different sensitivities to the various radionuclides depending on their characteristics (mutations, location, aggressiveness), an algorithm has been proposed for the use of nuclear imaging of these tumors [12]. Being SDHx-associated PPGLs more prone to metastasize than other molecular subtypes, the identification of sensitive and specific tracers for these pseudohypoxic tumors would be clinically relevant.

Reliable detection of small primary tumors, of metastases, and prediction of tumor characteristics are urgently needed to improve prognosis and to achieve tailored treatments for PPGL patients. Animal models of cancer are crucial for the evaluation and development of novel imaging modalities. This is especially true for rare tumors for which access to large cohorts of patients to evaluate novel medical imaging or treatment approaches is highly limited. In this review, we will present the contribution that studies on animal models have provided to PPGL detection. We will focus on the different imaging tools that have been tested with the aim of validating the suitability of the animal model, of improving tumor detection and monitoring therapy response, of assessing imaging

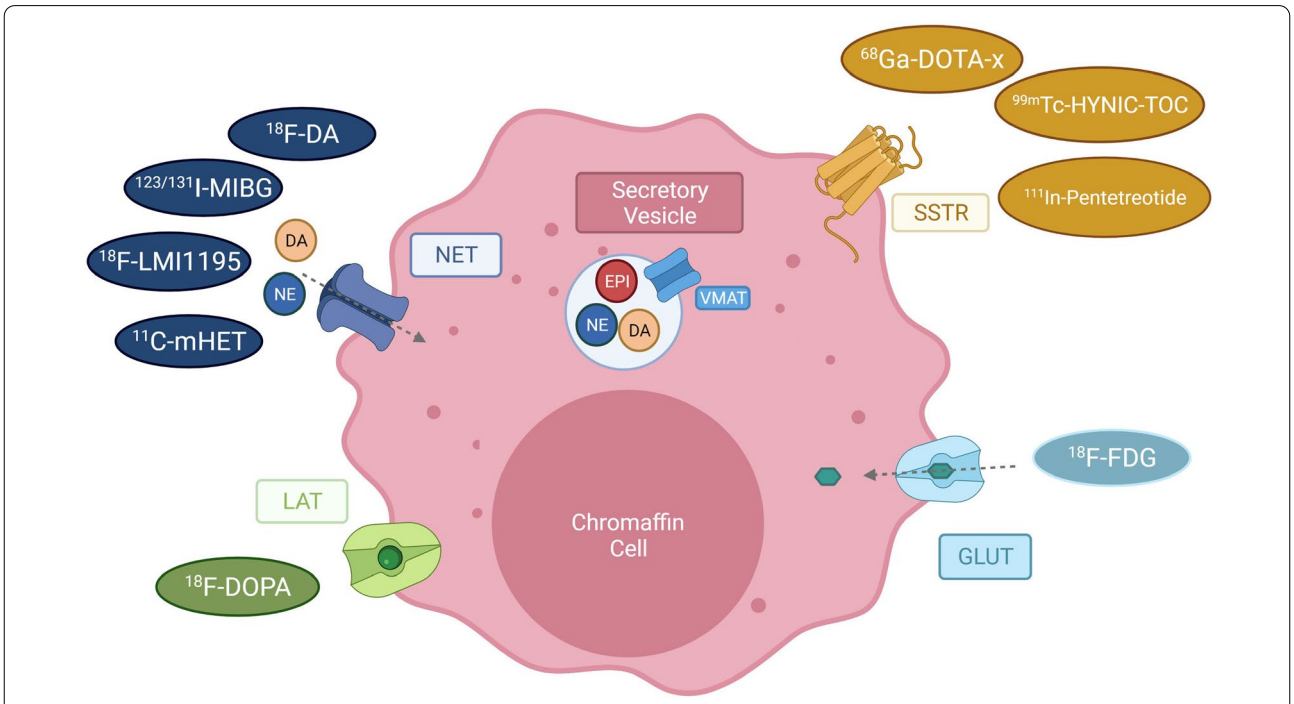

Fig. 1 Available PET tracers for imaging of pheochromocytoma and paraganglioma. Depicted are receptors of chromaffin cells used as targets for PET imaging (*LAT* large amino acid transporter, *NET* Norepinephrine transporter, *SSTR* Somatostatin receptor, GLUT = glucose transporter) and their tracers ([^{18}F]-DOPA = [^{18}F]-dihydroxyphenylalanine; [^{68}Ga]-DOTA-X = derivatives of [^{68}Ga]1,4,7,10-tetraazacyclododecane-tetraacetic acid, e.g., DOTATATE, DOTA-NOC, DOTA-TOC, [^{99m}Tc] -HYNIC-TOC = [^{99m}Tc]-hydrazinonicotinyl-Tyr3-octreotide, [^{18}F]-FDG =, [^{18}F]-Fluordesoxyglucose). The vesicular monoamine transporter (VMAT) transports catecholamines as norepinephrine (NE), epinephrine (EPI) and dopamine (DA) into secretory vesicles, from where they are released into the extracellular matrix. Reuptake or norepinephrine is mediated via the NET transporter. (Adapted from Blanchet et al., 2011 [82])

tracer distribution as well as improving or developing image-guided therapy for PPGLs (Fig. 2).

Imaging of xenograft and allograft PPGL models

Owing to the paucity of genetically engineered mouse strains that reproduce the human disease [17], most in vivo studies so far conducted relied on the injection of PPGLs cell lines into immunocompromised mice. Given that establishing human tumor cell lines has proved to be an arduous task, there is currently none available that represents a functional catecholamine-secreting PPGL. The few sporadically reported human PPGL cell lines were never distributed to the research community or display a progenitor cell phenotype. The most commonly used rodent cell lines are PC12 and MPC cells. PC12 is a clonal line originating from PCC cells derived from the tumor of an irradiated rat [18], which were further passaged subcutaneously in rats [19]. PC12 cells are noradrenergic, synthesizing and storing dopamine and norepinephrine [19]. PC12 represent an extensively used model in neuroscience research as these cells differentiate into neurons when exposed to nerve growth factor (NGF) [20]. MPC (mouse pheochromocytoma cells) cells, and their aggressive derivative MTT (mouse tumor tissue) cells, were derived from a PCC that developed in a *Nf1* knockout mouse [21, 22]. MPC cells mainly secrete epinephrine and strongly express the receptor tyrosine kinase, Ret and the GDNF receptor, GFRalpha1 [23], indicating a progenitor-like genetic signature.

Xenografts/allograft models have been generated by engrafting these rodent PPGL cell lines into mice. PC12-derived xenografts were used to study the efficacy of both [^{131}I]-MIBG radionuclide therapy [24] and the receptor tyrosine kinase inhibitors sunitinib and sorafenib [25]. Despite being effective against this tumor model, neither ^{131}IMIBG [26] nor sunitinib [27] therapy caused the clinical benefits expected based on the outcomes in these preclinical studies, indicating that more clinically relevant models should be employed. Allografts generated by injecting MPC cells have proved to be a very valuable experimental tool to evaluate novel imaging modalities for PPGL diagnosis and theranostic approaches. Studies with patient-derived xenografts (PDXs) aimed at propagating this precious material in vivo are still at their early stages, and the groups attempting to establish these models have reported low engraftment rates [28, 29]. Therefore, the potential of PDXs to contribute to PPGL research is still to be determined.

Anatomical imaging

Anatomical imaging gathers information about the basic physical structure and the composition of a tissue by measuring characteristics such as electron density for CT or proton density for MRI. CT was the first imaging modality to offer detailed 3D imaging of internal anatomy [30] using serial radiographic projections of X-rays to create a cross-sectional image. In the practical clinical guidelines of the endocrine society on the "Diagnosis and

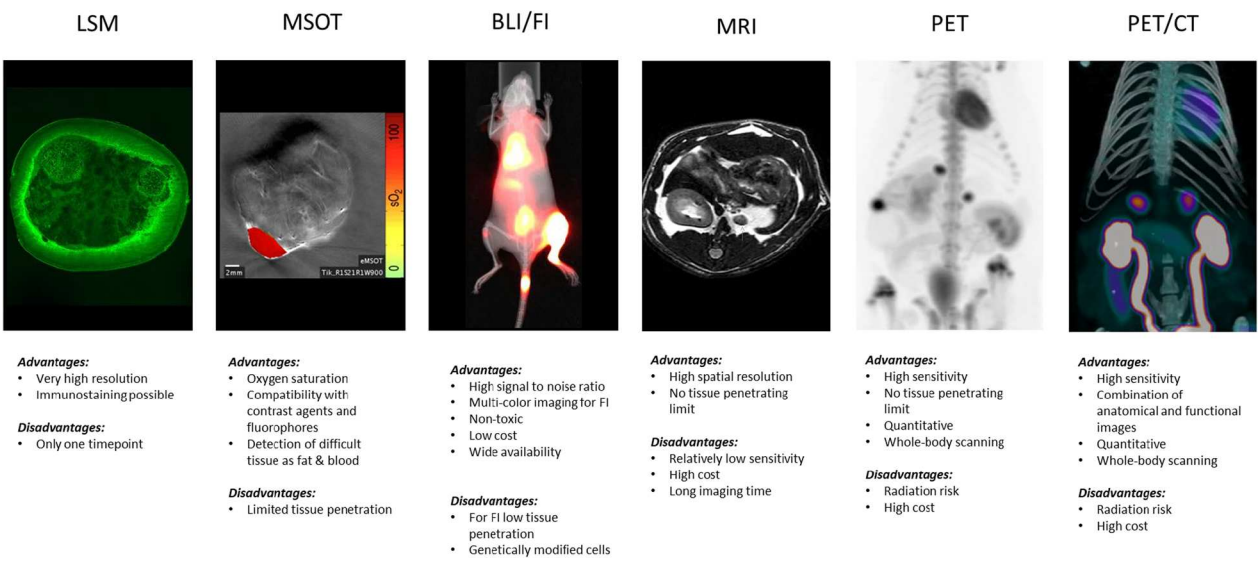

Fig. 2 Image modalities used for PPGL research in small animals. *LSM* Light sheet microscopy (PCC from a mut/mut MENX rat), *MSOT* multispectral optoacoustic tomography (MENX PCC senograft), *BLI/FI* bioluminescence/fluorescence imaging (metastasized MPC-luc cells in an allograft model, kindly provided by Martin Ullrich), *PET* positron emission tomography (MENX rat with [^{18}F]-LMI1195), *PET/CT* combined picture of PET and computed tomography (MENX rat with [^{18}F]-LMI1195 and CT). Advantages and disadvantage of each modality are listed

Treatment of Pheochromocytoma and Paraganglioma," CT is recommended as initial imaging modality [11]. In case the tumor is located in the adrenal gland, anatomical imaging can be considered sufficient for the initial diagnosis, for extra-adrenal PPGL additional functional imaging is recommended by the EANM Guidelines [12].

MicroCT in PPGL research

As the detection of metastatic PPGLs is a highly clinically relevant issue, studies have focused on the identification of sensitive imaging modalities allowing to visualize metastases in animal models. Megapixel charge-coupled device detectors and significant increases in computer memory and speed, allowed to adapt traditional clinical CT to small animals, a technique called microCT, which offers high spatial resolution [31]. The first PPGL metastatic model was established in 2006 by Ohta et al. by injecting MPC intravenously into the tail vein of nude mice [32]. The cells were able to colonize the body and form liver tumors, but only rarely in other organs (lungs, bone, adrenal glands). Given that the liver is among the preferred sites of PPGL metastases, this model might give useful information in view of clinical translation. MicroCT using the hepatobiliary-specific contrast agent glycery1-2-oley-1,3-bis-[7-(3-amino-2,4,6-triiodophenyl)-heptanoate] (DHOG) allowed detection of tumors as small as 0.35 mm, thereby establishing this imaging modality as a promising technique to visualize small metastases in live animals. A caveat of this model is the fast growth of the tumors and the rapidly deteriorating health of the mice.

MRI for PPGL research

CT is more often used in clinical practice to detect and locate PPGLs due to lower costs, higher availability and better spatial resolution. However, MRI reaches higher sensitivity for detection of PGLs or metastasized PPGLs, and being free of ionizing radiation is therefore better suited for pregnant women, children or patients with adverse reactions to an iodinated contrast medium [33]. Moreover, it has been suggested that MRI is superior to CT in characterizing human adrenal masses [34]. A study in mice compared the use of the contrast-enhanced microCT technique versus non-enhanced MRI for the detection of metastasizing MPC cells [35]. Herein, both methods were equally suited to detect liver lesions. MRI was superior to microCT in detecting lesions at other organs (lung, adrenal, ovarian and renal), whereas neither modality detected early bone lesions. The authors suggested that it might be more suitable to use MRI instead of CT to lower the radiation burden to the animals.

Functional imaging

Scintigraphy with [$^{123/131}$I]-MIBG and derivatives

[^{123}I]-MIBG was the first tracer to be developed for PPGLs, and until recently planar [^{123}I]-MIBG scintigraphy was the gold standard in PPGL imaging [36], although it has now been replaced by single-photon emission computer tomography (SPECT) allowing more accurate anatomical localization. MIBG is a structural analogue of norepinephrine, and it is taken up by the NET present on the chromaffin cells' membrane (uptake 1) and stored inside the secretory vesicles (Fig. 1). The signal of the tracer is proportional to vesicular granules density inside the tumor cells [37]. Given that MIBG uptake scanning enables whole-body imaging, thereby allowing the detection of extra-adrenal tumors and metastatic deposits, it is often the preferred initial screening modality. MIBG can be labeled with either ^{131}I or ^{123}I, the latter being more suitable for imaging (especially when using SPECT), whereas the former is the tracer of choice for MIBG therapy. [^{123}I]-MIBG scintigraphy has a sensitivity of 77–90% and a specificity of 95–100% in the detection of PPGLs [15]. The highly diverse sensitivity can partially be explained by the variable expression of the NET depending on the differentiation and the genetics of the tumors, and on the use of planar scintigraphy *versus* SPECT (more sensitive). Mechanistically, it has been demonstrated that in SDHx-mutated tumors, which are more often metastatic, the accumulation of oncometabolites inhibiting ten–eleven translocation (TET) methylcytosine dioxygenases induces hypermethylation and suppression of gene expression [38]. Among the genes downregulated in these tumors is *SLC6A2*, encoding the NET. The Cancer Genome Atlas (TCGA) PPGL dataset confirmed that there are some patients of the pseudohypoxic cluster showing low levels of *SLC6A2* (Fig. 3). Although for these patients imaging targeting the NET might not be effective, for the majority of PPGL patients such approach should be appropriate. Noteworthy, therapy using the electron emitting radionuclide [^{131}I-MIBG] is the only currently approved therapy for unresectable/metastatic PPGLs with MIBG-positive lesions.

One of the drawbacks of [^{123}I]-MIBG scintigraphy is the limitation in staging and restaging of hereditary and metastatic PPGLs [15], with an especially poor performance in detecting SDHx-mutated tumors. Therefore, novel approaches aimed developing PET tracers, or at increasing the therapeutic radioactive dose, have been tested in small animal models.

A new synthesis method has allowed to produce [^{18}F]-(for diagnosis) or [^{131}I]-labeled (for therapy) (4-fluoro-3-iodobenzyl)guanidine (FIBG), a derivative of MIBG [39]. To evaluate this novel tracer, biodistribution studies,

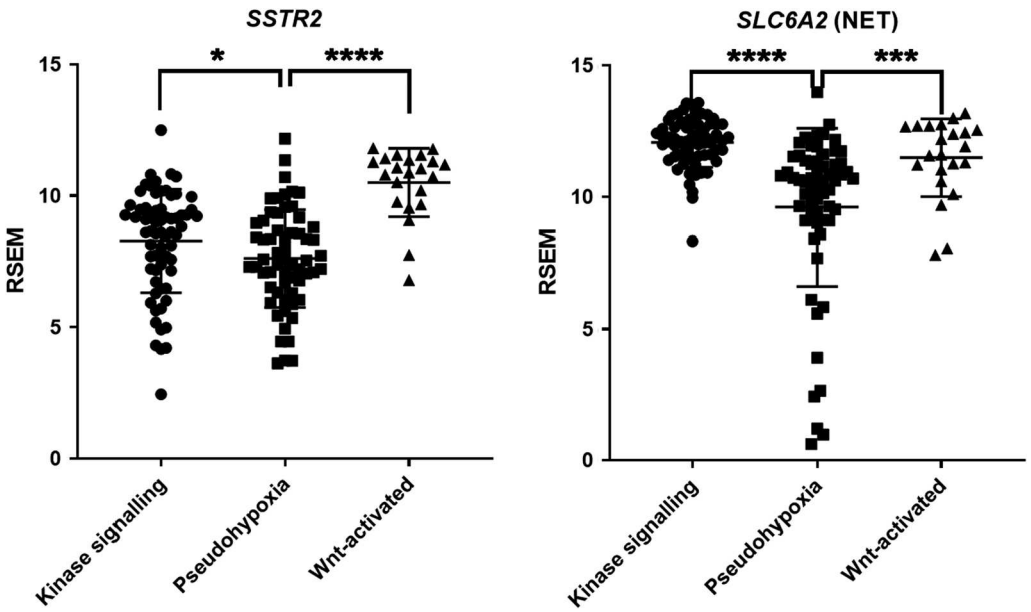

Fig. 3 Expression of Somatostatin and NET transporter in TCGA database. Expression levels of the *SSTR2* and *SLC6A2* (encoding for NET) in the PPGL TCGA dataset RSEM-normalized, exported via www.cbioportal.org (patient stratification into clusters according to Fishbein et al. [6]. Low level of SSTR2 expression in some patients belonging to the pseudohypoxia cluster

PET imaging and a therapeutic study were performed on PC12-derived mouse xenografts. [^{18}F]-FIBG showed good tumor-to-background ratio, with lower incubations times than the original [^{131}I]-MIBG. [^{131}I]-FIBG was retained in higher amounts and for longer time in the tumors when compared with MIBG, and this was associated with a stronger inhibition of tumor growth following a therapeutic dose of [^{131}I]-FIBG versus [^{131}I]-MIBG. Interestingly, the uptake of [^{18}F]-FIBG in the xenografts was proportional to the therapeutic effect of [^{131}I]-FIBG. Thus, this tracer could be used in a theranostic approach, both for the detection ([^{18}F]- labeled) and for the therapy ([^{131}I]- labeled) of PPGLs.

Positron emission tomography (PET)

Nuclear medicine uses radiotracers, radioactively labeled ligands at very low (picomolar to nanomolar) concentrations, to visualize functional processes. Several radiotracers have been developed for PPGLS, which take advantage of the expression of specific receptors and transport systems on the membrane of chromaffin cells (Fig. 1).

Imaging the NET with meta-[^{18}F]fluorobenzylguanidine ([^{18}F]-MFBG)

As outlined above, [^{123}I]-MIBG only allows for planar and SPECT imaging, which has a lower sensitivity and poorer spatial resolution compared with PET. Other disadvantages include the need for a 2-day protocol and thyroid blockade. ^{18}F-meta-fluorobenzylguanidine ([^{18}F]-MFBG) is a promising alternative for [^{123}I]-MIBG that offers one-day, high-resolution PET/MR imaging. In pilot trials of patients with neural crest tumors (including PPGL), [^{18}F]-MFBG imaging was safe, had favorable biodistribution and kinetics with good targeting of lesions [40]. In preclinical studies on neuroblastoma xenografts, [^{18}F]-MFBG showed a slightly lower lesion uptake compared with [^{123}I]-MIBG, but had significantly faster blood clearance thus enabling high-contrast visualization of lesions already 1 h after injection [41]. This tracer has yet to be evaluated in PPGL models.

Imaging the NET with [^{18}F]-6-fluoro-dopamine ([^{18}F-FDA])

Among the agents available to localize PPGLs is [^{18}F]-6-fluoro-dopamine ([^{18}F-FDA]), which is also internalized into chromaffin cells by NET. In the study of Martiniova and colleagues mentioned above, a comparison of [^{18}F]-DOPA and [^{18}F]-FDA was done in parallel in the MPC metastatic model. [^{18}F]-FDA showed a lower uptake compared to [^{18}F]-DOPA and detected fewer metastatic lesions. A few years later, the same group compared [^{18}F]-DOPA and [^{18}F]-FDA for the detection of subcutaneous or metastatic MPC-derived tumors in mice [42]. They observed a lower accumulation of [^{18}F]-FDA compared to [^{18}F]-DOPA in large liver lesions, presumably due to a decrease in NET expression following tumor dedifferentiation. Interestingly, when MPC cells were injected subcutaneously, only [^{18}F]-DOPA PET, but not

[^{18}F]-FDA could detect the tumors and this may reflect the expression of VMAT 1 and VMAT2 in the tumor cells (Fig. 1) [42]. This data is in conflict with the results obtained in human patients, where [^{18}F]-DOPA had indeed a high sensitivity (81%-100%) in detecting non-metastatic PPGLs [43]. Yet, the sensitivity in metastatic cases was as low as 45% and even lower in SDHB-related cases. In contrast, [^{18}F]-FDA PET/CT showed equally good sensitivity for localizing primary and metastatic PPGLs (77% versus 76%), also in patients with metastatic SDHB-mutated tumors [43]. Thus, the MPC metastatic model may not precisely mimic the situation observed in the patients. Yet, studying the differences in uptake of these two radiopharmaceuticals in these models may shed light into the molecular mechanisms leading to the differences in functional imaging outputs observed in clinical imaging of the various human PPGL subtypes. Moreover, the direct comparison of different tracers would be highly relevant in xenograft/allograft models of genetically modified PPGL cells belonging to other subclusters, given that MPC cells harboring an Nf1 mutation represent the kinase-signaling cluster.

Imaging the LAT Transporter with [^{18}F]-dihydroxyphenylalanine ([^{18}F]-DOPA)

One of the ligands that can be used to target chromaffin cells is dihydroxyphenylalanine (DOPA), which is transported into catecholamine-secreting tumors by the large amino acid transporter (LAT). Once internalized, DOPA is converted to dopamine by the aromatic amino acid decarboxylase and stored in vesicular granules (Fig. 1). The tracer [^{18}F]-DOPA has been widely used for the detection of human PPGLs by PET imaging [44] and shows 84–100% sensitivity and 88–100% specificity [33]. One limitation is, however, that PPGLs with a non-secretory phenotype might not express the LAT transporter, thereby leading to a limited [^{18}F]-DOPA accumulation [45].

By combining MRI and [^{18}F]-DOPA, further improvements to the imaging of both the subcutaneous and the metastatic MPC-derived mouse models (see above) were achieved. Indeed, Martiniova and colleagues showed that tumor lesions in several organs could be readily detected by [^{18}F]-DOPA PET/MRI [22]. In a subsequent study on human PPGL patients, the combination of [^{18}F]-DOPA PET with MRI was found to be superior to MRI-alone and also able to achieve a higher diagnostic confidence than [^{18}F]-DOPA PET/CT [46].

Somatostatin receptor imaging

Somatostatin is a neurotransmitter regulating the release of hormones by various target organs including the pituitary gland (growth hormone), pancreas (insulin, glucagon) and the gastrointestinal tract (gastrin). It demonstrates anti-proliferative and anti-angiogenic effects on cells expressing somatostatin receptors (SSTRs). The broad expression of SSTRs in neuroendocrine tumors led to the development of several somatostatin analogs (SSAs) for diagnosis and therapy. There are five SSTR subtypes (SSTR1-5) with variable expression levels according to the tissue type and having different affinities to the clinically available SSAs. PPGLs express mostly SSTR2 and SSTR3 at a lower level, while SSTR1, SSTR4 and SSTR5 are usually absent, as an immunohistochemical study on 151 PPGL patients revealed [47].

Among the most common imaging modality to visualize neuroendocrine tumors is [^{111}In]-pentetreotide scintigraphy (Octreoscan). This tracer has the highest affinity for SSTR2. In clinical practice, emission data (SPECT) are fused with CT data to improve diagnostic accuracy. Due to suboptimal image quality and relatively high effective doses, a derivative of Octreoscan was created using ^{99m}Tc, resulting in the tracer [^{99m}Tc]-HYNIC-TOC (Fig. 1). Introducing the positron emitter ^{68}Ga to label SSAs allowed the application of these tracers to PET imaging. Among the available radiolabeled SSAs, three should be especially emphasized: [^{68}Ga]-DOTATATE and [^{68}Ga]-DOTA-TOC (^{68}Ga-DOTA-d-Phe1-Tyr3-octreotide), [^{68}Ga]-DOTA-NOC: DOTA-1-Nal3-octreotide (for more information on SSTR-directed imaging read Patel et al. [48]). The minor chemical modifications on the SSAs affect their affinity to the different SSTR subtypes (illustrated in Table 1), thereby allowing to select the imaging tracer according to the relative levels of the various SSTRs in the tumors. [^{68}Ga]-SSA PET can overcome the low resolution of both scintigraphy and conventional SPECT imaging, and is especially useful for the detection of extra-adrenal PPGLs, where it shows higher sensitivity than [^{123}I]-MIBG [12]. Noteworthy, [^{68}Ga]-SSA PET has superior sensitivity at detecting SDHx-mutated PPGLs than [18F]-FDG-PET [49].

Additionally, replacement of ^{68}Ga with the radioisotopes ^{177}Lu or ^{90}Y allows to use these SSAs for targeted peptide receptor radionuclide therapy (PRRT). PRRT represents the current approved indication in Europe and in the USA or patients with advanced (metastatic) and/or

Table 1 Specificity of the SSA ligands toward the SSTR receptors. Depicted are in vitro affinity profiles (50% inhibitory concentration (IC50) in nM ± standard[52]

	SSTR1	SSTR2	SSTR3	SSTR4	SSTR5
^{68} Ga-DOTATATE	> 10,000	*0.2 ± 0.04*	*> 1000*	300 ± 140	377 ± 18
^{68} Ga-DOTA-TOC	> 10,000	*2.5 ± 0.5*	*613 ± 140*	> 1000	73 ± 12
^{68} Ga-DOTA-NOC	> 10,000	*1.9 ± 0.4*	*40 ± 5.8*	260 ± 74	7.2 ± 1.6

progressive neuroendocrine tumors positive on somatostatin receptor imaging, who cannot undergo surgery and whose symptoms do not respond to other medical therapies. [^{177}Lu]-DOTATATE-based PRRT has been evaluated in patients with unresectable, locally advanced or metastatic PPGL and has emerged as a viable alternative to [^{131}I]-MIBG [50, 51].

Both [^{68}Ga]-DOTATATE and [^{68}Ga]-DOTA-TOC tracers were used in a preclinical study from Ullrich et al. 2018, to detect MPC cells labeled with firefly luciferase (luc) and engrafted in various immunocompromised mouse strains [53]. Besides demonstrating that SCID/beige and SKH1 mice are the best suited host strains for MPC-derived metastases studies, the authors also showed that *Sstr2* expression was maintained in MPC cells-derived metastases and could be well detected by using the two radiolabeled SSAs. Unfortunately, a direct comparison of the SSAs in the same animals was not performed. These studies established Sstr-directed imaging as a modality suitable to monitor the response of this metastatic PPGL allograft model to therapies.

Imaging glucose metabolism with [^{18}F]-fluoro-D-glucose ([^{18}F]$^{-}$FDG)-PET

[^{18}F]-FDG represents the most often applied PET imaging tracer and is widely used in many cancer entities. It is based on the high demand of nutrients by cancer cells to support their growth. Uptake of radiolabeled glucose is therefore higher in metabolically active cells, including tumor cells. [^{18}F]-FDG uptake is variable in PPGLs depending on their genetic background, degree of differentiation and malignancy [54, 55]. [^{18}F]-FDG is particularly recommended for patients with known metastatic PPGLs or with mutations in SDHB (at higher risk for metastases) [43]. Indeed, a hallmark of pseudohypoxic PPGLs (often associated with SDHx mutations) is their shift from oxidative phosphorylation to aerobic glycolysis (the so-called Warburg effect). Consequently, these tumors show a rapid glucose turnover. Therefore, [^{18}F]-FDG PET may be used to obtain an in vivo metabolic tumor profiling in patients with PPGLs belonging to the pseudohypoxic cluster [56]. Additionally, and in agreement with what has been reported for other solid tumors, [^{18}F]-FDG PET could be of value in monitoring early treatment response, as tumor cell metabolism adapts much faster than any other parameter detected by standard tumor markers (i.e., cell growth, cell death, tumor vascularization) [57].

[^{18}F-FDG] PET was recently evaluated by Facchin et al., 2020, as part of a novel trimodal imaging system that combined anatomical imaging with X-ray CT, metabolic imaging with [^{18}F]-FDG PET and ultrafast ultrasound imaging (UII) [58]. This imaging sequence referred to as PETRUS (PET Registered Ultrafast Sonography). Ultrasound is usually not recommended for diagnosis of PPGLs, however it was included in the PETRUS sequence in order to image vascular network changes. Specifically, PETRUS was employed to follow the response to the multikinase inhibitor sunitinib of an allograft model obtained by injecting immortalized mouse *Sdhb*-/- cells. This drug inhibits the vascular endothelial growth factor receptor (VEGFR), RET and other kinases. VEGFA is the most important pro-angiogenic factor and as such is upregulated in many tumors. PPGLs are highly vascularized and have a high expression of VEGFA especially in malignant and large tumors. Thus, they are expected to be sensitive to inhibitors of VEGFRs. Therefore, sunitinib was tested on patients with progressive PPGLs in a Phase II clinical study, which was recently completed [27]. In contrast to the expectations, the overall effect of sunitinib in this clinical study was low. Although sunitinib treatment is not beneficial in most PPGL patients, it could be effective in a subset of them, i.e., those showing pseudohypoxic features, known to induce neoangiogenesis, or patients with RET mutations, another receptor kinase targeted by sunitinib. The PETRUS imaging scheme could beautifully monitor the response to sunitinib in the *Sdhb*-/- PPGL allograft model. Although ultrasound is generally only used for the detection of PPGL if CT scans cannot be performed, the authors used it to measure several parameters related to vascularization. Interestingly, following an initial response, the *Sdhb*-/- PPGL allografts developed resistance to sunitinib treatment after a few weeks. The mechanism of resistance might be interesting to follow up on as it could shed light on the low efficacy of this drug against human PPGLs. The PETRUS imaging approach appears to be an interesting imaging modality, suitable to monitor the response of PPGLs to drugs targeting tumor vascularization.

Usage of radiosensitizers to improve radionucleotide therapy and imaging

Radiosensitizers are highly relevant in the cancer field given their ability to enhance the efficacy of radiation therapy. Current radiosensitizers increase the lethal effect of radiotherapy on tumor cells by inhibiting the radiation-induced DNA damage response or improve the local uptake of radionuclides by upregulating the expression of the corresponding target receptors on the cancer cells. The latter strategy could be suitable to improve imaging of malignant, dedifferentiated PPGLs with downregulated expression of NET. Histone deacetylase (HDAC) inhibitors act as epigenetic modulators as well as post-transcriptional regulators of acetylated proteins and were found to restore chromatin accessibility and thereby gene expression. In the MPC-derived metastatic mouse

model of PPGLs, [^{123}I]-MIBG and [^{18}F]-FDA uptake by the tumors could be enhanced by a pretreatment with the HDAC inhibitor romidepsin or trichostatin A thanks to enhanced receptor expression and retention of the radioisotopes [59]. As also suggested by the authors, radiosensitization might profit significantly from further preclinical studies analyzing biodistribution and kinetics of receptor expression, to then infer the optimal timepoint for drug administration. Various animal models able to recapitulate the features of dedifferentiated tumors (of the different subclusters) would be extremely helpful to tackle the problem of the imaging sensitivity drop observed in the most aggressive cases.

Bioluminescence and fluorescence imaging

Bioluminescence and fluorescence imaging are highly sensitive methods with a long history in tumor imaging in small animals. They rely on the use of genetically modified (labeled) cell lines engrafted into mice. In order to follow PPGL progression longitudinally in live animals, Ullrich et al. subcutaneously injected mCherry-labeled MPC cells into nude mice and performed whole-body fluorescence imaging to monitor tumor development [60]. Tumors in this allograft model could be easily detected and quantified by combining fluorescence and MRI imaging approaches. Additional measurements of urinary free monoamines allowed the correlation of fluorescence signal intensities with a functional tumor marker [60]. As tumor growth (by caliper measurements) had a positive linear relationship with fluorescence intensity and monoamine secretion, these parameters emerged as useful markers to follow tumor progression, and hold promise as readouts to monitor the response of PPGL allografts to drug treatment in vivo.

Preclinical studies with novel tracers

Fluorescence imaging of Cox-2 tracer

The greatest strength of animal models is the possibility to test novel imaging techniques that, if promising, might then be translated to the patients. A potential novel target for the detection of PPGLs is the enzyme Cox-2, which is involved in the synthesis of prostaglandin. Cox-2 expression is upregulated in several tumors, and its activity associates with promotion of angiogenesis, invasion of tumor cells and resistance to chemotherapy [61]. Cox-2 inhibitors have been shown to improve sensitivity of tumor cells to radiation [62]. Several studies found an increased expression of Cox-2 in aggressive PPGLs and suggested this enzyme as a marker to discriminate benign from malignant tumors [63–65]. As MPC-luc cells used to generate the preclinical allograft PPGL model described above [60] also express Cox-2, a fluorescently labeled Cox-2 tracer was evaluated in this model and the results compared to bioluminescence imaging [66]. The XenoLight RediJect COX-2 probe accumulated in the tumors (yet, a strong and unspecific tracer accumulation at injection site was also detectable). Thus, a Cox-2-directed tracer might be valuable in assessing the expression level of the enzyme in view of treatment with Cox-2 inhibitors to trigger PPGLs radiosensitization. A Cox-2-targeting tracer for PET imaging has been developed and tested in a colorectal cancer xenograft model [67], but has not yet been applied to PPGLs.

Imaging of endogenously developing PCCs in animal models—examples of MENX-associated PCCs

The previously mentioned imaging studies used allograft or xenograft models of PPGL cell lines to monitor tumor growth, as well as to detect lesions in live animals. However, there are some limitations: subcutaneous tumor models do not reproduce the tumor microenvironment of PPGLs; and metastatic MPC-derived models (by intravenous injection) have very high tumor multiplicity, and the aggressiveness of the disease leads to termination of the studies after only few weeks.

Among the few available animal models of endogenous PPGLs is the MENX rat strain. Tumor formation in this model is caused by a spontaneous frameshift mutation in *Cdkn1b*, encoding the cell cycle regulator p27kip1 (p27). This mutation associates with a loss of function of p27 and with uncontrolled cell proliferation [68]. Homozygous mutant rats develop bilateral PCC (frequency 100%) with a clear progression from hyperplasia (age 4–5 months) to full-blown PCCs (age 8–10 months). They also present with abdominal PGLs (frequency 10–20%)[69]. Recently, we showed that rat PCCs show pseudohypoxic features [70]. These studies established MENX rats as the only currently available model of spontaneous, endogenous pseudohypoxic PCCs. The kinetics of tumor development in this model allow the analysis of the various stages of progression, in contrast to the fast-growing cell lines used to generate xenograft/allograft models. Endogenous tumors in MENX rats are therefore highly valuable to evaluate imaging modalities and to perform preclinical therapy studies in view of a clinical translation. With this in mind, several imaging modalities used to visualize PPGLs in patients were tested in MENX rats to demonstrate whether this model resembles the human disease concerning the uptake of specific tracers (see also Fig. 2).

Comparison of [^{11}C]-HED and [^{68}Ga]-DOTATOC

The uptake of ^{11}C-hydroxyephedrine ([^{11}C]-HED), targeting the NET, and [^{68}Ga-DOTATOC, targeting SSTR receptors, were compared side by side in 8–10-month-old MENX rats (bearing histologically confirmed tumors)

and control unaffected rats [71]. Tracer uptake was correlated with the expression of *Sstr* genes and of *Slc6a2* encoding the NET. Both tracers showed a stronger uptake in the adrenal glands of mutant rats compared with unaffected adrenals of wild-type animals. However, ^{11}C-HED/PET provided better signal-to-noise ratio compared to ^{68}Ga-DOTATOC. While *Sstr2* mRNA levels were significantly upregulated in rat PCCs *versus* normal adrenal, the expression of *Slc6a2* was, on average, not differentially regulated (although some individual tumors exhibited a higher expression). The superior performance of ^{11}C-HED/PET suggests that there could be a different post-transcriptional regulation of *Slc6a2* in tumor versus normal medullary cells leading to higher expression of the NET in the former. Furthermore, by using ^{68}Ga-DOTATOC, there was a high background signal originating from the kidneys that made the detection of the adrenal glands difficult. In a retrospective study of 134 PPGL patients imaged with ^{11}C-HED/PET and PET/CT, a sensitivity of 91% and a specificity of 100% of the former could be revealed. Interestingly, ^{11}C-HED/PET imaging was less sensitive in MEN2 patients [72]. Although, ^{11}C-HED provides excellent results in the detection of PCC, it is rarely used in human patients: the 20-min half-life of the tracer requires on-site synthesis, which is available only in few specialized centers.

Comparison of ^{18}F-LMI1195 and ^{123}I-MIBG

In 2013, we showed that the catecholamine analog, [^{18}F]-LMI1195 (also known as [^{18}F]-Flubrobenguane) is a promising novel PET tracer for the detection of PCCs in MENX-affected rats [73]. This tracer is a structural analog of [^{123}I]-MIBG and targets the NET encoded by *Slc6a2*. Imaging by [^{18}F]-PET has the advantage of higher spatial and temporal resolution along with better attenuation correction, absolute quantification and shorter acquisition times than [^{123}I]-based SPECT/CT [74]. [^{18}F] offers the same benefits as [^{11}C] without the disadvantage of its short half-life. In comparison with its predecessor [^{18}F]-FIBG, [^{18}F]-LMI1195 offers the advantage that it is not degraded by monoamine oxidase, and it can be more easily synthesized than [^{18}F]-FDA [74]. When [^{18}F]-LMI1195 was injected into wildtype rats the maximum signal peak in adrenals could be observed after 1 min but a high signal was kept over 60 min, when other background signal in other organs had already washed out [73]. The adrenals of PCC-bearing MENX rats showed much higher standardized uptake value (SUV) compared to normal adrenals of wildtype rats, despite having a similar background noise signal in other organs. The [^{18}F]-LMI1195 signal could be blocked by despiramine, a selective norepinephrine reuptake inhibitor (Fig. 4). Noteworthy, in this study, [^{123}I]-MIBG and [^{18}F]-LMI1195 were directly compared against each other in the same MENX rats. While the signal of both tracers was equally good at detecting tumor-bearing adrenals, the background signal was lower for [^{18}F]-LMI1195 in organs such as liver, lung, small intestine and bone, a feature that could be relevant for the imaging of PPGL metastases or small primary tumors.

After this preclinical proof-of-concept study in the MENX rats and a phase I study in healthy humans assessing human safety, whole-organ biodistribution and radiation dosimetry [75], [^{18}F]-LMI1195 was evaluated in a retrospective study of 24 patients with suspected PPGLs. Patients scans were performed between 2016 and 2018, and the data were recently published [76]. The highest SUV could be observed in thyroid, pancreas and tumor lesions, with unaffected adrenal glands and liver parenchyma having significantly lower SUV compared to the tumors. The intense accumulation of [^{18}F]-LMI1195 in thyroid and pancreas is not unexpected, given these organs have extensive sympathetic innervation where NET is expressed. Surgery and subsequent histological analysis of 13 patients revealed that 11 of them were correctly diagnosed: 9 with PCC and 2 with suspected PGL. The hybrid detection of [^{18}F]-LMI1195 PET and CT/MRI detected more and smaller lesions than conventional imaging, but this did not reach statistical significance probably due to the low patient number. However, diagnosis confidence and detection size was better in [^{18}F]-LMI1195 PET/CT/MRI than CT/MRI alone [76]. The data strongly speaks for further evaluation of this tracer in larger patient cohorts and a comparison with the gold standard MIBG SPECT/CT.

While targeting NET has its limitations for PPGL imaging, which also applies to [^{18}F]-LMI1195, namely the loss of receptor expression in some PPGL tumors, this novel tracer has the potential to be superior to the standard clinical practice. This study represents a prime example of how diagnosis of PPGL patients could be improved by using novel tracers originally tested in a suitable preclinical animal model.

Multispectral optoacoustic tomography

An emerging optical imaging method is multispectral optoacoustic tomography (MSOT) where fast tunable lasers excite tissues with short light impulses of multiple wavelengths. The resulting thermal tissue expansion induces a photoecho, ultrasound waves that can be subsequently measured. This technique provides noninvasive, high-resolution tomographic images of absorbers such as oxygenated and deoxygenated hemoglobin, lipids and melanin [77]. As such, MSOT is particularly indicated to image tissue vascularization in vivo without the need of contrast agents. Furthermore, MSOT can be also

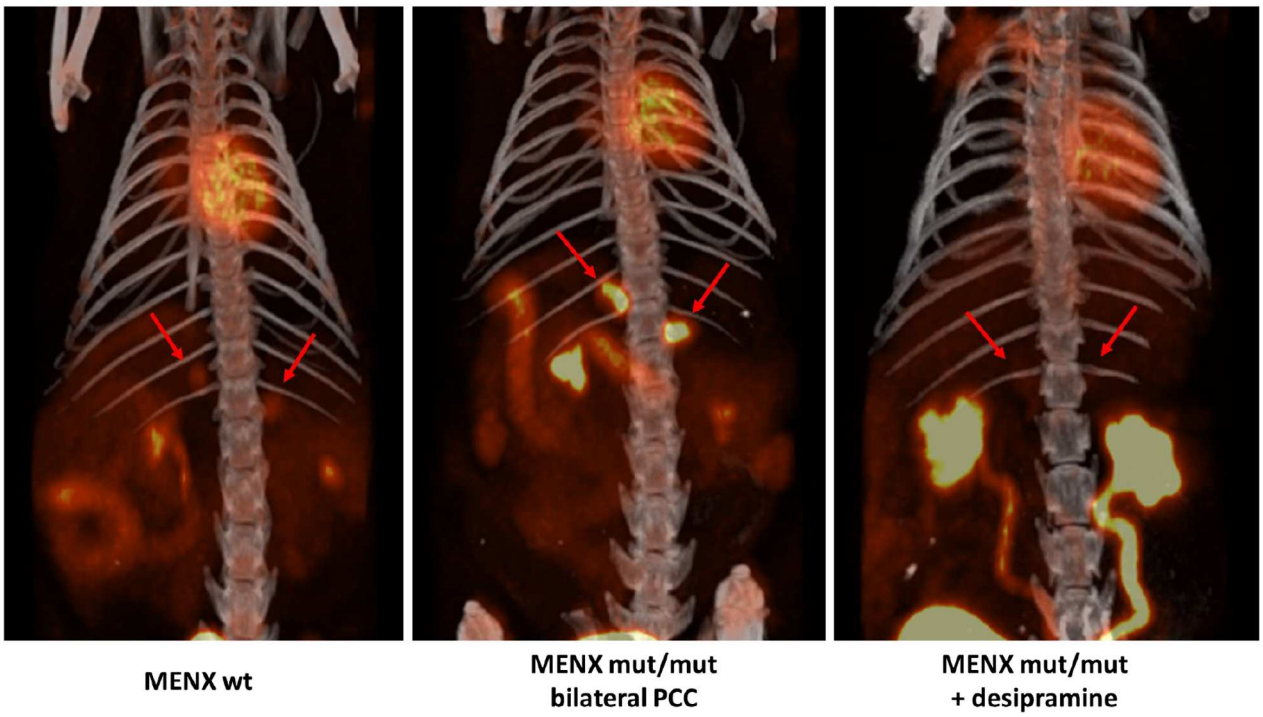

Fig. 4 PCC imaging with [^{18}F]-LMI1195 PET/CT in MENX rats. Exemplary pictures of [18F]-LMI1195 composite PET/CT images. While in normal adrenal glands of a MENX wild-type rat, there is only a moderate accumulation of the tracer (left). An intense tracer accumulation is however observed in adrenal glands of PCC-bearing mut/mut rat (middle). Despiramine, which blocks the uptake of norepinephrine via the NET transporter, reduces also the uptake of the tracer in the PCCs (right)

combined with imaging probes, as quantum dots, GFP or gold particles to visualize biomolecules and their tissue distribution [78]. The maximum penetration depth of 2–3 cm in tissues limits at the moment its application to the diagnosis of PPGLs, but it may be highly suitable to image the progression of xenograft tumors.

As mentioned earlier, PPGLs, especially those with high HIF expression (pseudohypoxic cluster), are highly vascularized tumors, with chaotic vessel architecture [79]. In a proof-of-principle study, we investigated whether MSOT might be used to study PPGL vascularization in vivo. Unfortunately, the size of the rats does not allow direct imaging using the preclinical MSOT scanner. Therefore, as experimental model, we used xenografts of primary rat PCC cells. These cells represent a more physiological system than established cell lines. Moreover, rat primary cells derive from pseudohypoxic tumors (in humans, the most aggressive cluster), whereas MPC cells used for the allograft studies have a kinase activation profile. Primary rat PCCs were successfully engrafted subcutaneously in nude mice, and oxygen saturation was longitudinally monitored by MSOT imaging during tumor growth [70]. The results showed that the tumor grafts derived from the rat PCC cells have high levels of oxygenated hemoglobin (Fig. 2). Thus, this approach might be exploited in the future to monitor the response of pseudohypoxic PCC cells to anti-angiogenic drugs in vivo. Recent studies have demonstrated the high quality of the vessel resolution by MSOT in breast cancer and its suitability to monitor drug treatment response [80], thereby suggesting that this modality might be applicable to preclinical PPGL research as well.

Ex vivo biological imaging of intact PCC vasculature

Recent advances in sample preparation techniques to increase optical transparency of tissue specimens have boosted the use of biological imaging using of light sheet fluorescence microscope systems (LSFM) and broadened its applicability in biological research. An important application of LSFM is the visualization of whole vascular networks in intact organs or tumors in model organisms. While this technique does not allow to follow neoangiogenesis over time, it provides images of intact organs with the highest possible resolution. To investigate the vasculature architecture of rat PCCs, MENX rats endothelial cells were labeled using a fluorescent T-lectin

probe and the adrenal glands collected and cleared for LSFM analysis ex vivo. The results revealed the high vessel density and chaotic vessel formation in MENX PCCs (Fig. 2) [70].

Further improvements, such as the novel deep learning-based metastasize analysis in cleared tissues (DeepMACT), should allow the most precise detection of metastasis in animal models at single cell level [81]. While the resolution of DeepMACT is unbeatable, it does not allow to monitor therapy response over time. For this, PET/CT, using tracers that have a high specificity and a good signal-to-noise ratio in order to discriminate tumor from normal tissue, is still the preferred method.

Conclusion

Accurate diagnosis of PPGLs is essential given the comorbidities associated with undiagnosed/untreated tumors. Moreover, their functional characterization may guide targeted therapies and radionuclide therapy. Medical imaging plays a critical role in both these aspects. Preclinical imaging studies with animal models of PPGLs helped assessing their faithfulness as models of the cognate human tumors. Several imaging modalities, from microCT to functional PET, led to high-resolution detection of PPGLs in xenograft/allograft and in endogenous rodent models. For example, MPC-derived metastases in allograft models could be detected with microCT and [^{68}Ga]-SSA PET. The possibility to detect PPGLs and their metastases with high sensitivity in preclinical settings is a prerequisite to exploit these models for therapy studies. Along these lines, the multimodal PETRUS sequence used by Facchin et al. [58] proved to be suitable to monitor the response of PPGL allografts to anti-angiogenic drugs and could be translated in clinical practice. As a prototypical example of the translational value of in vivo PPGL models, the initial evaluation of a novel PET tracer in MENX rats set the basis for the application of LMI1195/Flubrobenguane in patients with suspected PPGLs. This tracer emerged as useful tool for the staging of PPGLs and now awaits validation in larger patient cohorts.

Abbreviations

CT: Computed tomography; MRI: Magnetic resonance imaging; MTT: Mouse tumor tissue cell line; NET: Norepinephrine transporter; PCC: Pheochromocytoma; PDX: Patient-derived xenograft; PET: Positron emission tomography; PPGL: Pheochromocytoma and paraganglioma; SPECT: Single-photon positron emission tomography.

Acknowledgements

We thank Martin Ullrich for providing us with unpublished pictures of MPC-luc engrafted mice. Figure 1 is created with BioRender.com

Authors' contributions

All authors had contributed equally in writing of the manuscript.

Funding

This research was funded by the Deutsche Forschungsgemeinschaft (DFG) within the SFB824 "Imaging for Selection, Monitoring and Individualization of Cancer Therapies," subprojects: B8 (NSP); Z02 (KS); Z03 (FS), and within the CRC/Transregio 205/1: "The Adrenal: Central Relay in Health and Disease," subproject B11 (NSP).

Declarations

Ethics approval and consent to participate

Not applicable.

Consent for publication

Not applicable.

Availability of data and materials

All data generated or analyzed during this study are included in this published article.

Competing interests

The authors declare that they have no competing interests.

Author details

[1]Institute for Diabetes and Cancer, Helmholtz Zentrum München, Ingolstaedter Landstrasse 1, 85764 Neuherberg, Germany. [2]Joint Heidelberg-IDC Translational Diabetes Program, Heidelberg University Hospital, Heidelberg, Germany. [3]Institute of Pathology, School of Medicine, Technical University of Munich, Munich, Germany. [4]Department of Nuclear Medicine, School of Medicine, Technical University of Munich, Munich, Germany. [5]Department of Biology and Biotechnology "L. Spallanzani", University of Pavia, Pavia, Italy.

Received: 22 June 2021 Accepted: 19 September 2021
Published online: 11 December 2021

References

1. Nolting S, Ullrich M, Pietzsch J, Ziegler CG, Eisenhofer G, Grossman A, Pacak K. Current management of pheochromocytoma/paraganglioma: a guide for the practicing clinician in the era of precision medicine. Cancers (Basel) 2019;11(10).
2. Soltani A, Pourian M, Davani BM. Correction to: Does this patient have Pheochromocytoma? a systematic review of clinical signs and symptoms. J Diabetes Metab Disord. 2017;16:42.
3. Fauci A, Braunwald E, Kasper D, Hauser S, Longo D, Jameson J, Loscalzo J. Harrison's principles of internal medicine. 17th ed. Mcgraw-hill; 2008.
4. Lenders JWM, Kerstens MN, Amar L, Prejbisz A, Robledo M, Taieb D, Pacak K, Crona J, Zelinka T, Mannelli M, et al. Genetics, diagnosis, management and future directions of research of phaeochromocytoma and paraganglioma: a position statement and consensus of the Working Group on Endocrine Hypertension of the European Society of Hypertension. J Hypertens. 2020;38(8):1443–56.
5. Eisenhofer G, Lenders JW, Goldstein DS, Mannelli M, Csako G, Walther MM, Brouwers FM, Pacak K. Pheochromocytoma catecholamine phenotypes and prediction of tumor size and location by use of plasma free metanephrines. Clin Chem. 2005;51(4):735–44.
6. Adjalle R, Plouin PF, Pacak K, Lehnert H. Treatment of malignant pheochromocytoma. Horm Metab Res. 2009;41(9):687–96.
7. Fishbein L, Leshchiner I, Walter V, Danilova L, Robertson AG, Johnson AR, Lichtenberg TM, Murray BA, Ghayee HK, Else T, et al. Comprehensive molecular characterization of pheochromocytoma and paraganglioma. Cancer Cell. 2017;31(2):181–93.
8. Antonio K, Valdez MMN, Mercado-Asis L, Taieb D, Pacak K. Pheochromocytoma/paraganglioma: recent updates in genetics, biochemistry, immunohistochemistry, metabolomics, imaging and therapeutic options. Gland Surg. 2020;9(1):105–23.
9. Lenders JW, Eisenhofer G, Mannelli M, Pacak K. Phaeochromocytoma. Lancet. 2005;366(9486):665–75.
10. Lo CY, Lam KY, Wat MS, Lam KS. Adrenal pheochromocytoma remains a frequently overlooked diagnosis. Am J Surg. 2000;179(3):212–5.

11. Lenders JW, Duh QY, Eisenhofer G, Gimenez-Roqueplo AP, Grebe SK, Murad MH, Naruse M, Pacak K, Young WF Jr, Endocrine S. Pheochromocytoma and paraganglioma: an endocrine society clinical practice guideline. J Clin Endocrinol Metab. 2014;99(6):1915–42.
12. Taieb D, Hicks RJ, Hindie E, Guillet BA, Avram A, Ghedini P, Timmers HJ, Scott AT, Elojeimy S, Rubello D, et al. European Association of Nuclear Medicine Practice Guideline/Society of Nuclear Medicine and Molecular Imaging Procedure Standard 2019 for radionuclide imaging of phaeochromocytoma and paraganglioma. Eur J Nucl Med Mol Imaging. 2019;46(10):2112–37.
13. Blake MA, Kalra MK, Maher MM, Sahani DV, Sweeney AT, Mueller PR, Hahn PF, Boland GW. Pheochromocytoma: an imaging chameleon. Radiographics. 2004;24(Suppl 1):S87-99.
14. Vallabhajosula S, Nikolopoulou A. Radioiodinated metaiodobenzylguanidine (MIBG): radiochemistry, biology, and pharmacology. Semin Nucl Med. 2011;41(5):324–33.
15. Castinetti F, Kroiss A, Kumar R, Pacak K, Taieb D. 15 YEARS OF PARAGANGLIOMA: imaging and imaging-based treatment of pheochromocytoma and paraganglioma. Endocr Relat Cancer. 2015;22(4):T135-145.
16. Crona J, Taieb D, Pacak K. New perspectives on pheochromocytoma and paraganglioma: toward a molecular classification. Endocr Rev. 2017;38(6):489–515.
17. Lepoutre-Lussey C, Thibault C, Buffet A, Morin A, Badoual C, Benit P, Rustin P, Ottolenghi C, Janin M, Castro-Vega LJ, et al. From Nf1 to Sdhb knockout: Successes and failures in the quest for animal models of pheochromocytoma. Mol Cell Endocrinol. 2016;421:40–8.
18. Warren S, Chute RN. Pheochromocytoma. Cancer. 1972;29(2):327–31.
19. Greene LA, Tischler AS. Establishment of a noradrenergic clonal line of rat adrenal pheochromocytoma cells which respond to nerve growth factor. Proc Natl Acad Sci U S A. 1976;73(7):2424–8.
20. Tischler AS, Perlman RL, Nunnemacher G, Morse GM, DeLellis RA, Wolfe HJ, Sheard BE. Long-term effects of dexamethasone and nerve growth factor on adrenal medullary cells cultured from young adult rats. Cell Tissue Res. 1982;225(3):525–42.
21. Powers JF, Evinger MJ, Tsokas P, Bedri S, Alroy J, Shahsavari M, Tischler AS. Pheochromocytoma cell lines from heterozygous neurofibromatosis knockout mice. Cell Tissue Res. 2000;302(3):309–20.
22. Martiniova L, Lai EW, Thomasson D, Kiesewetter DO, Seidel J, Merino MJ, Kvetnansky R, Pacak K. Animal model of metastatic pheochromocytoma: evaluation by MRI and PET. Endocr Regul. 2009;43(2):59–64.
23. Powers JF, Schelling KH, Brachold JM, Tischler AS. Plasticity of pheochromocytoma cell lines from neurofibromatosis knockout mice. Ann N Y Acad Sci. 2002;971:371–8.
24. Rutgers M, Buitenhuis CK, van der Valk MA, Hoefnagel CA, Voute PA, Smets LA. [(131)I] and [(125)I] metaiodobenzylguanidine therapy in macroscopic and microscopic tumors: a comparative study in SK-N-SH human neuroblastoma and PC12 rat pheochromocytoma xenografts. Int J Cancer. 2000;90(6):312–25.
25. Denorme M, Yon L, Roux C, Gonzalez BJ, Baudin E, Anouar Y, Dubessy C. Both sunitinib and sorafenib are effective treatments for pheochromocytoma in a xenograft model. Cancer Lett. 2014;352(2):236–44.
26. Pryma DA, Chin BB, Noto RB, Dillon JS, Perkins S, Solnes L, Kostakoglu L, Serafini AN, Pampaloni MH, Jensen J, et al. Efficacy and safety of high-specific-activity (131)I-MIBG therapy in patients with advanced pheochromocytoma or paraganglioma. J Nucl Med. 2019;60(5):623–30.
27. O'Kane GM, Ezzat S, Joshua AM, Bourdeau I, Leibowitz-Amit R, Olney HJ, Krzyzanowska M, Reuther D, Chin S, Wang L, et al. A phase 2 trial of sunitinib in patients with progressive paraganglioma or pheochromocytoma: the SNIPP trial. Br J Cancer. 2019;120(12):1113–9.
28. Powers JF, Pacak K, Tischler AS. Pathology of human pheochromocytoma and paraganglioma xenografts in NSG mice. Endocr Pathol. 2017;28(1):2–6.
29. Verginelli F, Perconti S, Vespa S, Schiavi F, Prasad SC, Lanuti P, Cama A, Tramontana L, Esposito DL, Guarnieri S, et al. Paragangliomas arise through an autonomous vasculo-angio-neurogenic program inhibited by imatinib. Acta Neuropathol. 2018;135(5):779–98.
30. Evans PM. Anatomical imaging for radiotherapy. Phys Med Biol. 2008;53(12):R151-191.
31. Holdsworth DW, Thornton MM. Micro-CT in small animal and specimen imaging. Trends Biotechnol. 2002;20(8):S34–9.
32. Ohta S, Lai EW, Morris JC, Bakan DA, Klaunberg B, Cleary S, Powers JF, Tischler AS, Abu-Asab M, Schimel D, et al. MicroCT for high-resolution imaging of ectopic pheochromocytoma tumors in the liver of nude mice. Int J Cancer. 2006;119(9):2236–41.
33. Alrezk R, Suarez A, Tena I, Pacak K. Update of pheochromocytoma syndromes: genetics, biochemical evaluation, and imaging. Front Endocrinol (Lausanne). 2018;9:515.
34. Honigschnabl S, Gallo S, Niederle B, Prager G, Kaserer K, Lechner G, Heinz-Peer G. How accurate is MR imaging in characterisation of adrenal masses: update of a long-term study. Eur J Radiol. 2002;41(2):113–22.
35. Martiniova L, Kotys MS, Thomasson D, Schimel D, Lai EW, Bernardo M, Merino MJ, Powers JF, Ruzicka J, Kvetnansky R, et al. Noninvasive monitoring of a murine model of metastatic pheochromocytoma: a comparison of contrast-enhanced microCT and nonenhanced MRI. J Magn Reson Imaging. 2009;29(3):685–91.
36. Sisson JC, Frager MS, Valk TW, Gross MD, Swanson DP, Wieland DM, Tobes MC, Beierwaltes WH, Thompson NW. Scintigraphic localization of pheochromocytoma. N Engl J Med. 1981;305(1):12–7.
37. Havekes B, Lai EW, Corssmit EP, Romijn JA, Timmers HJ, Pacak K. Detection and treatment of pheochromocytomas and paragangliomas: current standing of MIBG scintigraphy and future role of PET imaging. Q J Nucl Med Mol Imaging. 2008;52(4):419–29.
38. Letouze E, Martinelli C, Loriot C, Burnichon N, Abermil N, Ottolenghi C, Janin M, Menara M, Nguyen AT, Benit P, et al. SDH mutations establish a hypermethylator phenotype in paraganglioma. Cancer Cell. 2013;23(6):739–52.
39. Yamaguchi A, Hanaoka H, Higuchi T, Tsushima Y. Radiolabeled (4-Fluoro-3-Iodobenzyl)Guanidine improves imaging and targeted radionuclide therapy of norepinephrine transporter-expressing tumors. J Nucl Med. 2018;59(5):815–21.
40. Pandit-Taskar N, Zanzonico P, Staton KD, Carrasquillo JA, Reidy-Lagunes D, Lyashchenko S, Burnazi E, Zhang H, Lewis JS, Blasberg R, et al. Biodistribution and dosimetry of (18)F-meta-fluorobenzylguanidine: a first-in-human PET/CT imaging study of patients with neuroendocrine malignancies. J Nucl Med. 2018;59(1):147–53.
41. Zhang H, Huang R, Cheung NK, Guo H, Zanzonico PB, Thaler HT, Lewis JS, Blasberg RG. Imaging the norepinephrine transporter in neuroblastoma: a comparison of [18F]-MFBG and 123I-MIBG. Clin Cancer Res. 2014;20(8):2182–91.
42. Martiniova L, Cleary S, Lai EW, Kiesewetter DO, Seidel J, Dawson LF, Phillips JK, Thomasson D, Chen X, Eisenhofer G, et al. Usefulness of [18F]-DA and [18F]-DOPA for PET imaging in a mouse model of pheochromocytoma. Nucl Med Biol. 2012;39(2):215–26.
43. Timmers HJ, Taieb D, Pacak K. Current and future anatomical and functional imaging approaches to pheochromocytoma and paraganglioma. Horm Metab Res. 2012;44(5):367–72.
44. Treglia G, Cocciolillo F, de Waure C, Di Nardo F, Gualano MR, Castaldi P, Rufini V, Giordano A. Diagnostic performance of 18F-dihydroxyphenylalanine positron emission tomography in patients with paraganglioma: a meta-analysis. Eur J Nucl Med Mol Imaging. 2012;39(7):1144–53.
45. Noordzij W, Glaudemans A, Schaafsma M, van der Horst-Schrivers ANA, Slart R, van Beek AP, Kerstens MN. Adrenal tracer uptake by (18)F-FDOPA PET/CT in patients with pheochromocytoma and controls. Eur J Nucl Med Mol Imaging. 2019;46(7):1560–6.
46. Magnaldi S, Mayerhoefer ME, Khameneh A, Schuetz M, Javor D, Mitterhauser M, Dudczak R, Hacker M, Karanikas G. (18)F-DOPA PET/CT and MRI: description of 12 histologically-verified pheochromocytomas. Anticancer Res. 2014;34(2):791–5.
47. Leijon H, Remes S, Hagstrom J, Louhimo J, Maenpaa H, Schalin-Jantti C, Miettinen M, Haglund C, Arola J. Variable somatostatin receptor subtype expression in 151 primary pheochromocytomas and paragangliomas. Hum Pathol. 2019;86:66–75.
48. Patel M, Tena I, Jha A, Taieb D, Pacak K. Somatostatin receptors and analogs in pheochromocytoma and paraganglioma: old players in a new precision medicine world. Front Endocrinol (Lausanne). 2021;12:625312.
49. Kan Y, Zhang S, Wang W, Liu J, Yang J, Wang Z. (68)Ga-somatostatin receptor analogs and (18)F-FDG PET/CT in the localization of metastatic pheochromocytomas and paragangliomas with germline mutations: a meta-analysis. Acta Radiol. 2018;59(12):1466–74.
50. Satapathy S, Mittal BR, Bhansali A. Peptide receptor radionuclide therapy in the management of advanced pheochromocytoma and

paraganglioma: a systematic review and meta-analysis. Clin Endocrinol (Oxf). 2019;91(6):718–27.
51. Taieb D, Jha A, Treglia G, Pacak K. Molecular imaging and radionuclide therapy of pheochromocytoma and paraganglioma in the era of genomic characterization of disease subgroups. Endocr Relat Cancer. 2019;26(11):R627–52.
52. Pauwels E, Cleeren F, Bormans G, Deroose CM. Somatostatin receptor PET ligands—the next generation for clinical practice. Am J Nucl Med Mol Imaging. 2018;8(5):311–31.
53. Ullrich M, Liers J, Peitzsch M, Feldmann A, Bergmann R, Sommer U, Richter S, Bornstein SR, Bachmann M, Eisenhofer G, et al. Strain-specific metastatic phenotypes in pheochromocytoma allograft mice. Endocr Relat Cancer. 2018;25(12):993–1004.
54. Ctvrtlik F, Koranda P, Schovanek J, Skarda J, Hartmann I, Tudos Z. Current diagnostic imaging of pheochromocytomas and implications for therapeutic strategy. Exp Ther Med. 2018;15(4):3151–60.
55. Taieb D, Sebag F, Barlier A, Tessonnier L, Palazzo FF, Morange I, Niccoli-Sire P, Fakhry N, De Micco C, Cammilleri S, et al. 18F-FDG avidity of pheochromocytomas and paragangliomas: a new molecular imaging signature? J Nucl Med. 2009;50(5):711–7.
56. van Berkel A, Vriens D, Visser EP, Janssen MJR, Gotthardt M, Hermus A, Geus-Oei LF, Timmers H. Metabolic subtyping of pheochromocytoma and paraganglioma by (18)F-FDG pharmacokinetics using dynamic PET/CT scanning. J Nucl Med. 2019;60(6):745–51.
57. Ben-Haim S, Ell P. 18F-FDG PET and PET/CT in the evaluation of cancer treatment response. J Nucl Med. 2009;50(1):88–99.
58. Facchin C, Perez-Liva M, Garofalakis A, Viel T, Certain A, Balvay D, Yoganathan T, Woszczyk J, De Sousa K, Sourdon J, et al. Concurrent imaging of vascularization and metabolism in a mouse model of paraganglioma under anti-angiogenic treatment. Theranostics. 2020;10(8):3518–32.
59. Martiniova L, Perera SM, Brouwers FM, Alesci S, Abu-Asab M, Marvelle AF, Kiesewetter DO, Thomasson D, Morris JC, Kvetnansky R, et al. Increased uptake of [(1)(2)(3)I]meta-iodobenzylguanidine, [(1)(8)F]fluorodopamine, and [(3)H]norepinephrine in mouse pheochromocytoma cells and tumors after treatment with the histone deacetylase inhibitors. Endocr Relat Cancer. 2011;18(1):143–57.
60. Ullrich M, Bergmann R, Peitzsch M, Cartellieri M, Qin N, Ehrhart-Bornstein M, Block NL, Schally AV, Pietzsch J, Eisenhofer G, et al. In vivo fluorescence imaging and urinary monoamines as surrogate biomarkers of disease progression in a mouse model of pheochromocytoma. Endocrinology. 2014;155(11):4149–56.
61. Liu B, Qu L, Yan S. Cyclooxygenase-2 promotes tumor growth and suppresses tumor immunity. Cancer Cell Int. 2015;15:106.
62. Saha D, Pyo H, Choy H. COX-2 inhibitor as a radiation enhancer: new strategies for the treatment of lung cancer. Am J Clin Oncol. 2003;26(4):S70-74.
63. Cadden IS, Atkinson AB, Johnston BT, Pogue K, Connolly R, McCance D, Ardill JE, Russell CF, McGinty A. Cyclooxygenase-2 expression correlates with phaeochromocytoma malignancy: evidence for a Bcl-2-dependent mechanism. Histopathology. 2007;51(6):743–51.
64. Zhu Y, He HC, Yuan F, Zhang J, Rui WB, Zhao JP, Shen ZJ, Ning G. Heparanase-1 and Cyclooxygenase-2: prognostic indicators of malignancy in pheochromocytomas. Endocrine. 2010;38(1):93–9.
65. Feng F, Zhu Y, Wang X, Wu Y, Zhou W, Jin X, Zhang R, Sun F, Kasoma Z, Shen Z. Predictive factors for malignant pheochromocytoma: analysis of 136 patients. J Urol. 2011;185(5):1583–90.
66. Ullrich M, Richter S, Seifert V, Hauser S, Calsina B, Martinez-Montes AM, Ter Laak M, Ziegler CG, Timmers H, Eisenhofer G et al. Targeting cyclooxygenase-2 in pheochromocytoma and paraganglioma: focus on genetic background. Cancers (Basel) 2019;11(6).
67. Tietz O, Wuest M, Marshall A, Glubrecht D, Hamann I, Wang M, Bergman C, Way JD, Wuest F. PET imaging of cyclooxygenase-2 (COX-2) in a preclinical colorectal cancer model. EJNMMI Res. 2016;6(1):37.
68. Pellegata NS, Quintanilla-Martinez L, Siggelkow H, Samson E, Bink K, Hofler H, Fend F, Graw J, Atkinson MJ. Germ-line mutations in p27Kip1 cause a multiple endocrine neoplasia syndrome in rats and humans. Proc Natl Acad Sci U S A. 2006;103(42):15558–63.
69. Fritz A, Walch A, Piotrowska K, Rosemann M, Schaffer E, Weber K, Timper A, Wildner G, Graw J, Hofler H, et al. Recessive transmission of a multiple endocrine neoplasia syndrome in the rat. Cancer Res. 2002;62(11):3048–51.
70. Mohr H, Ballke S, Bechmann N, Gulde S, Malekzadeh-Najafabadi J, Peitzsch M, Ntziachristos V, Steiger K, Wiedemann T, Pellegata NS. Mutation of the cell cycle regulator p27kip1 drives pseudohypoxic pheochromocytoma development. Cancers (Basel) 2021;13(1).
71. Miederer M, Molatore S, Marinoni I, Perren A, Spitzweg C, Reder S, Wester HJ, Buck AK, Schwaiger M, Pellegata NS. Functional imaging of pheochromocytoma with Ga-DOTATOC and C-HED in a genetically defined rat model of multiple endocrine neoplasia. Int J Mol Imaging. 2011;2011:175352.
72. Yamamoto S, Hellman P, Wassberg C, Sundin A. 11C-hydroxyephedrine positron emission tomography imaging of pheochromocytoma: a single center experience over 11 years. J Clin Endocrinol Metab. 2012;97(7):2423–32.
73. Gaertner FC, Wiedemann T, Yousefi BH, Lee M, Repokis I, Higuchi T, Nekolla SG, Yu M, Robinson S, Schwaiger M, et al. Preclinical evaluation of 18F-LMI1195 for in vivo imaging of pheochromocytoma in the MENX tumor model. J Nucl Med. 2013;54(12):2111–7.
74. Yu M, Nekolla SG, Schwaiger M, Robinson SP. The next generation of cardiac positron emission tomography imaging agents: discovery of flurpiridaz F-18 for detection of coronary disease. Semin Nucl Med. 2011;41(4):305–13.
75. Sinusas AJ, Lazewatsky J, Brunetti J, Heller G, Srivastava A, Liu YH, Sparks R, Puretskiy A, Lin SF, Crane P, et al. Biodistribution and radiation dosimetry of LMI1195: first-in-human study of a novel 18F-labeled tracer for imaging myocardial innervation. J Nucl Med. 2014;55(9):1445–51.
76. Kessler L, Schlitter AM, Kronke M, von Werder A, Tauber R, Maurer T, Robinson S, Orlandi C, Herz M, Yousefi BH, et al. First experience using (18) F-Flubrobenguane PET imaging in patients with suspected pheochromocytoma or paraganglioma. J Nucl Med. 2021;62(4):479–85.
77. Taruttis A, van Dam GM, Ntziachristos V. Mesoscopic and macroscopic optoacoustic imaging of cancer. Cancer Res. 2015;75(8):1548–59.
78. Gujrati V, Mishra A, Ntziachristos V. Molecular imaging probes for multi-spectral optoacoustic tomography. Chem Commun (Camb). 2017;53(34):4653–72.
79. Favier J, Plouin PF, Corvol P, Gasc JM. Angiogenesis and vascular architecture in pheochromocytomas: distinctive traits in malignant tumors. Am J Pathol. 2002;161(4):1235–46.
80. Liapis E, Klemm U, Karlas A, Reber J, Ntziachristos V. Resolution of spatial and temporal heterogeneity in bevacizumab-treated breast tumors by eigenspectra multispectral optoacoustic tomography. Cancer Res. 2020;80(23):5291–304.
81. Pan C, Schoppe O, Parra-Damas A, Cai R, Todorov MI, Gondi G, von Neubeck B, Bogurcu-Seidel N, Seidel S, Sleiman K, et al. Deep learning reveals cancer metastasis and therapeutic antibody targeting in the entire body. Cell. 2019;179(7):1661-1676 e1619.
82. Blanchet EM, Martucci V, Pacak K. Pheochromocytoma and paraganglioma: current functional and future molecular imaging. Front Oncol. 2011;1:58.

Publisher's Note